الجمهورية الجزائرية الديمقراطية الشعبية

République Algérienne Démocratique et Populaire

Ministère de L'Enseignement Supérieur et de la Recherche Scientifique

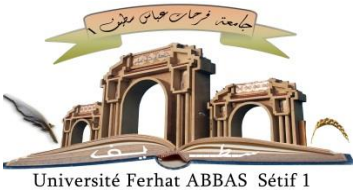

UNIVERSITÉ FERHAT ABBAS - SETIF1

FACULTÉ DE TECHNOLOGIE

THÈSE

Présentée au Département D'électrotechnique

Pour l'obtention du diplôme de

DOCTORAT

Domaine : Sciences et Technologie

Filière: Electrotechnique **Option: Réseaux électriques et haute tension**

Par

KOUADRI Ramzi

THÈME

Contribution à l'optimisation de l'intégration des énergies renouvelables au réseau électrique en présence des dispositifs FACTS-HVDC

Soutenue le 25 / 07 / 2021 devant le Jury:

GHERBI Ahmed	**Professeur**	**Univ. Ferhat Abbas - Sétif 1**	**Président**
SLIMANI Linda	**Professeur**	**Univ. Ferhat Abbas - Sétif 1**	**Directeur de thèse**
MUSIRIN Ismail	**Professeur**	**Univ. Teknologi MARA - Malaysia**	**Co-Directeur**
NOURI Hamou	**Professeur**	**Univ. Ferhat Abbas - Sétif 1**	**Examinateur**
BETKA Achour	**Professeur**	**Univ. Mohamed Khider - Biskra**	**Examinateur**

الجمهورية الجزائرية الديمقراطية الشعبية

People's Democratic Republic of Algeria

Ministry of Higher Education and Research

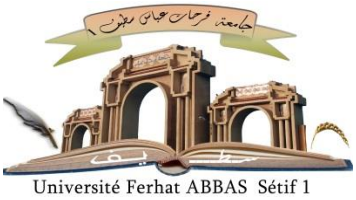

UNIVERSITY FERHAT ABBAS - SETIF1

FACULTY OF TECHNOLOGY

THESIS

A thesis presented to the Department of Electrical Engineering

in fulfilment of the requirement for the degree of

DOCTORAT

Field : Science and Technology

Faculty: Electrotechnique **Option: Electrical networks and high voltage**

By

KOUADRI Ramzi

THESIS TITLE

Contribution to the optimization of renewable energies integration in electrical network considering FACTS-HVDC devices

Defended on 25 / 07 / 2021 approved by:

GHERBI Ahmed	**Professor**	**Univ. Ferhat Abbas - Setif 1**	**Chair of committee**
SLIMANI Linda	**Professor**	**Univ. Ferhat Abbas – Setif 1**	**Supervisor**
MUSIRIN Ismail	**Professor**	**Univ. Teknologi MARA - Malaysia**	**Co-Supervisor**
NOURI Hamou	**Professor**	**Univ. Ferhat Abbas - Setif 1**	**Examiner**
BETKA Achour	**Professor**	**Univ. Mohamed Khider - Biskra**	**Examiner**

Dedication

I dedicate this thesis to:

My loving Mother

In memory of my Father

My Wife and my Son Ghaith

In memory of my Professor BOUKTIR Tarek

To my Brother and my Sisters

To all my Friends, all my Teachers

And to everyone who compels this humble work

Kouadri Ramzi

Acknowledgments

*Firstly, I wish to thank **God ALLAH** for giving me the opportunity to embark on my Ph.D. and for completing this long and challenging journey successfully.*

*My gratitude and thanks go to my supervisor **Professor. SLIMANI Linda** for offering me the theme of this thesis and for directing it in collaboration with **Professor. BOUKTIR Tarek (رحمه الله)** and **Professor. MUSIRIN Ismail**. Thanks to their wise advice, their invaluable help, and their support and incessant encouragement during my research work, I succeeded in carrying out this work.*

*I'd like also to thank again my co-supervisor, **Professor Ismail Musirin** for giving me a great opportunity to do a scholarship at the center for Electrical Power Engineering Studies (CEPES), Universiti Teknologi MARA (UiTM), 40450 Shah Alam, Selangor, Malaysia (s). It was a great honor for me to work with him.*

I'm particularly grateful to all staff members of the Department of Electrical Engineering, University of Ferhat Abbas Setif 1, Algeria, and to staff members of the Department of Electrical Engineering, Universiti Teknologi MARA (UiTM), and UiTM Office of International Affairs for their invaluable assistance during my stay at the UiTM.

*I also thank all the members of the jury: **Professor**.**GHERBI Ahmed, Professor. HAMOU Nouri** and **Professor. BETKA Achour**, for the interest they have shown in my work and for taking the time to revise my thesis. I am thankful that in the midst of all their activities, they accepted to be members of the reading committee.*

Finally, our thanks also go to all of our comrades and friends for their support and encouragement during my study.

Kouadri Ramzi

Table of Contents

List of figures

List of Tables

List of Acronyms and Symbols

Acronyms

G-S	Gauss-Seidel
N-R	Newton–Raphson
FACTS	Flexible Alternatives Current Transmission Systems
SVC	Static Var Compensator
STATCOM	Static Synchronous Compensator
TCSC	Thyristor Controlled Series Capacitor
TSSC	Thyristor switched series capacitor
AC	Alternative Current
DC	Direct Current
TCR	Thyristor Controlled Reactor
TSC	Thyristor Switched Capacitor
HVDC	High Voltage Direct Current
MTDC	Multi-Terminal Direct Current
VSC	Voltage Source Converter
LCC	Line Commutated Converters
CSC	Current Source Converter
IGBT	Insulated Gate Bipolar Transistor
PWM	Pulse Width Modulation
PF	Power Flow
OPF	Optimal Power Flow
SMA	Slime Mould Algorithm
ALO	Ant Lion Optimizer
RESs	Renewable Energy Sources
PV	Photovoltaic
CSP	Concentrated Solar Power
WTs	Wind Turbines
HAWTs	Horizontal Axis Wind Turbines
VAWTs	Vertical Axis Wind Turbines
WECS	Wind Energy Conversion System
DFIG	Doubly Fed Induction Generator

WFs	Wind farms
OWFs	Offshore wind farms
TGC	Total Generation Cost
THGC	Thermal Generation Cost
WGC	Wind Generation Cost
PDF	Probability Density Function

Acronyms

F_i	Objective function
h	Vector of equality constraints
g	Vector of inequality constraints
x	Vector of the state variables
u	Vector of the control variables
a_i, b_i, c_i	Cost coefficients of ith generator
P_{loss}	Active power transmission losses
P_{Gi}	Active power generated
Q_{Gi}	Reactive power generated
P_{Di}	Active power demand
Q_{Di}	Reactive power demand
P_{WSi}	Active wind power output
Q_{WSi}	Reactive wind power output
TVD	Total voltage deviation
w_{VD}	Suitable weighting factor
V_i	The nominal value of voltage (1.0 p.u)
PV	Generator bus
PQ	Load bus
Ref	Slack bus
V_G	Generator voltage
V_L	Voltage magnitude at the load bus
Q_C	Reactive power injected by the shunts compensator
T	Tap setting of transformers
S_l	Apparent power flow

NG	Number of available generators
NC	Number of shunts compensators
NT	Number of regulating transformers
N_L	Total number of load buses
N_l	Total number of transmission lines
NW	Number of wind turbine
δ_{ij}	Phase angle
rand	randomly generated number into [0,1]
dim	dimension
popsize	Size of population
$Iter$	Current iteration
P_i^{max}	Maximum active power generated
P_i^{min}	Minimum active power generated
X_{SVC}	Impedance of SVC
B_{SVC}	Susceptance of SVC
Y_{SVC}	admittance of SVC
Q_{SVC}	Reactive power of SVC
P_{Perte}	Losses of the converter station AC/DC
a, b, c_{rec}, c_{inv}	loss coefficients in the converters
$NHVDC$	Number of HVDC line
V_{min}	Minimum of voltage
X_{tr}	Reactance of transformer
R_{tr}	Resistance of transformer
B_f	Susceptance of filter
R_{dc}	The resistance of the HVDC line
C_p	Power coefficient of the turbine
λ	Tip-speed ratio
Ω	The rotation speed of the slow shaft of the wind turbine
f_V	Weibull probability density function for wind speed
v	Wind speed
$C_{p.wr}$	The cost associated with wind power shortage (overestimation)
$C_{r.wr}$	The cost associated with wind power surplus (underestimation)

Chapter 01: Introduction

1.1. Overview of the Study

In the last decade, energy consumption has been increased significantly especially in developing and highly populated countries. This large consumption has led grid operators to search sources to cover this consumption and guarantee continuity of customer service at all times. For this reason, the managers of the electric grid have thought of introducing renewable energy sources (RESs). RESs is known as green energy or clean energy and is considered one of the best solutions to the problem of the increasing electricity demand. The RESs comes from natural resources such as wind, sunlight, tides, rain, and geothermal heat or comes from processes that are constantly replenished [1], even if their availability depends on weather and weather conditions, and whose exploitation causes the least possible ecological damage, does not cause toxic waste and does not cause damage to the environment. They are cleaner, more environmentally friendly than fossil fuels and fissile energies, environmentally friendly, available in large quantities around the world.

Nowadays, the RESs (i.e., solar, wind, hydropower, etc.) into the electrical grid is experiencing a rapid increase. Among the various RESs, wind energy considered is one of the most desirable sources in recent years that keeps developing thanks to the technological advances made in the field of wind power generators to reduce the cost of system installations. Renewable energy farms such as large-scale onshore and offshore wind farms are usually separated from loading centers in many developed countries. Therefore, the energy provided by these farms needs to be transmitted continuously over a long distance to the load area or the power grid by the technology of high voltage direct current (HVDC). This technology has the advantage of high capacity and long-distance transmission over high voltage alternating current (HVAC) transmission. In addition, the investigates flexible AC transmission systems (FACTS) controllers such as static VAR compensators (SVC) devices is a technically feasible and economical solution to improve power system stability in case of significant electricity demand.

In this thesis, the study focuses on the impact of the insertion of wind energy and FACTS-HVDC technology in the electric grid. The biggest challenge with the integration of wind power in the power system is its intermittent nature. In general, the problem with wind power is the stochastic nature of wind speed. For this reason, it is necessary to confront the stochastic nature of this source for analysis of the planning and operation of modern power systems in order to obtain much more precise results. Thus, the introduction of optimal power flow (OPF) becomes necessary for the

economic integration of stochastic wind energy. In this context. The OPF problem considering stochastic wind energy will be solved by two advanced metaheuristic optimization techniques i.e., slime mould algorithm (SMA) and ant lion optimization (ALO).

1.2. A brief view at the growth of renewable energy generation

Today's world has seen a fundamental transformation in the field of power generation systems, which is the deregulation of the electricity market. The reasons for this deregulation are varied and multiple depending on the country. However, one of the consequences is the appearance of new means of production called renewable energies within the existing electricity networks.

Nowadays, the integration of renewable energy sources (RESs) into the electrical grid is experiencing a rapid increase. The high penetration of RESs could present a significant impact on the grid. Figure 1.1 presents the growth of renewable energy generation worldwide from 1965 to 2018. In this figure: “Other renewables” refers to RES including geothermal, biomass, waste, wave, and tidal. Traditional biomass is not included.

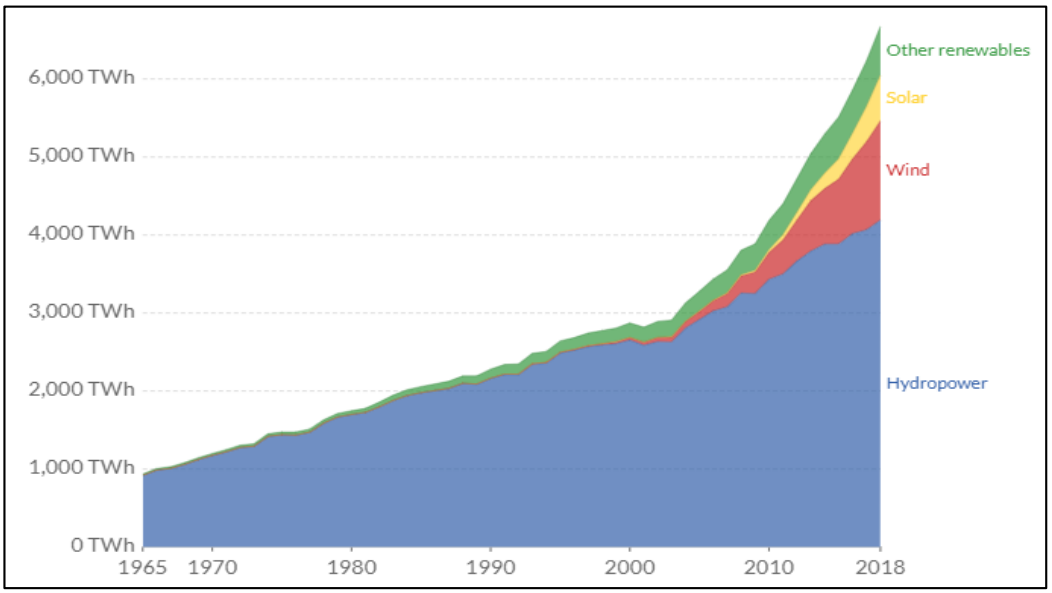

Figure 1.1 Growth of renewable energy generation worldwide from 1965 to 2018 [2]

The deployment of renewable energy has accelerated since 2010, reaching record levels in many regions, especially in Europe, China, India, and the USA (Fig. 1.2). RESs are gaining more attention nowadays in power sectors due to efforts to reduce the usage of fossil fuels to produce electricity. Renewable energy technologies are poised to become an important component of the electricity supply mix. According to the global trends in renewable energy investment (GTRENI) 2019 report, renewable energy made up 12.9% of the global share of electricity generation in 2018,

up from 11.6% in 2017 with not including hydroelectric power (if included, bumps the current renewable share to 26.3 percent of total electricity produced) [3]. Renewable energy sources' contribution is expected to be an approach to 51 % of the total generation mix by 2040, compared to 22 % today [4].

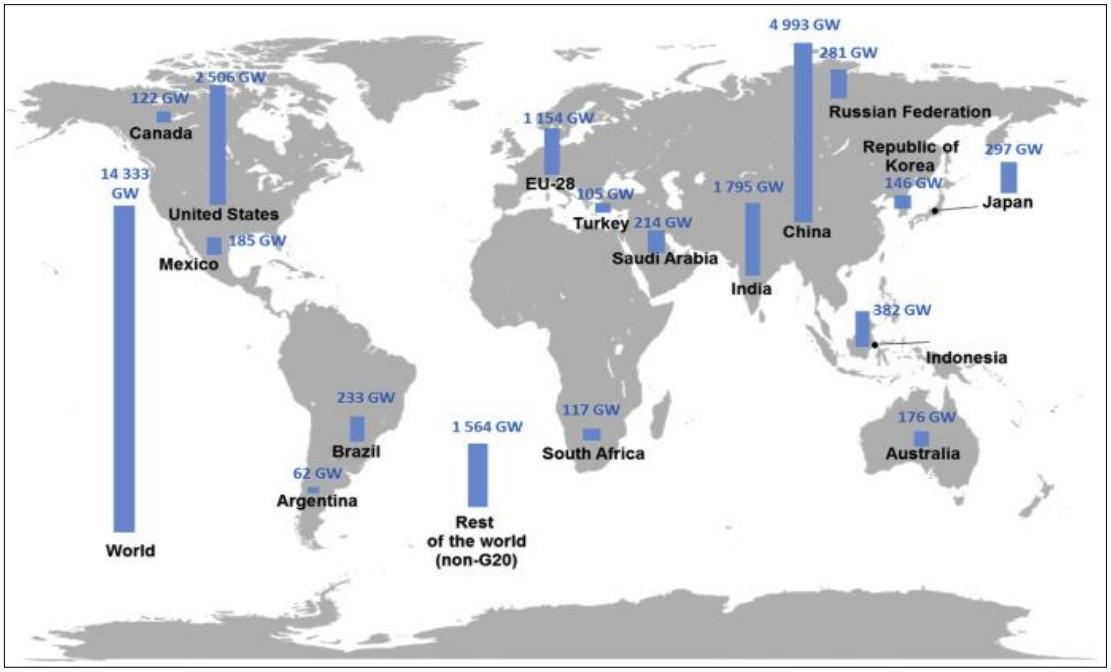

Figure 1.2 Geographical breakdown of renewable energy capacity additions 2018–2050 [5]

According to [6], global investment in renewable energy in 2020 reached $303.5 billion for new projects and small systems, up 2% from 2019, despite the Covid-19 pandemic. Moreover, the global investment in renewable energy was a total of $2.6 trillion in the years from 2010 through the end of 2019 [3], with most of that dedicated to solar (52%) and wind (40%) as shown in Fig. 1.3.

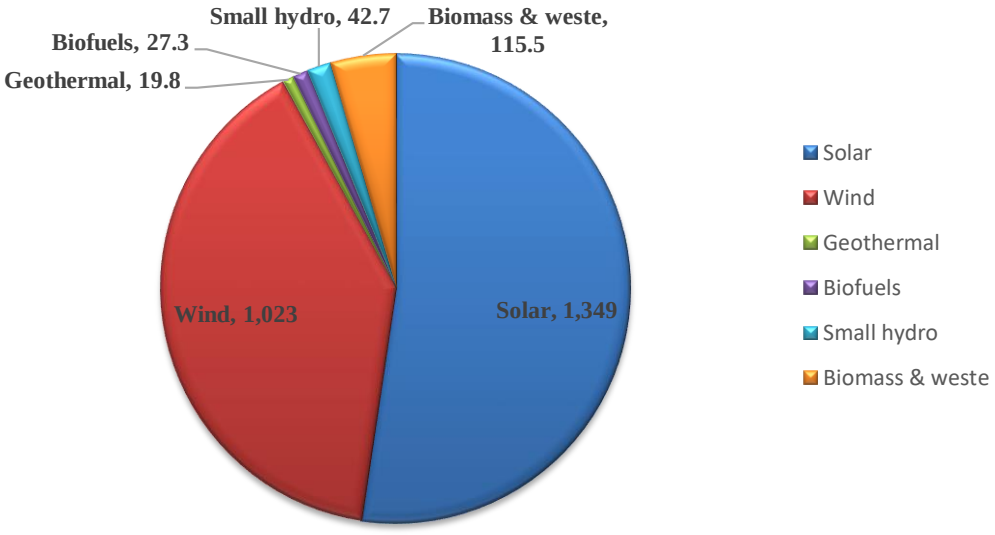

Figure 1.3 Renewable energy capacity investment over the decade, 2010-2019, $bn

Figure 1.4 shows the amount invested in renewable energy capacity in the top 10 markets up to the end of the first half of 2019. China led the way in renewable investment, committing about $758 billion. The U.S. was second to China about $356. Japan was third, investing $202 billion, and Europe, as a whole, invested about $698 billion.

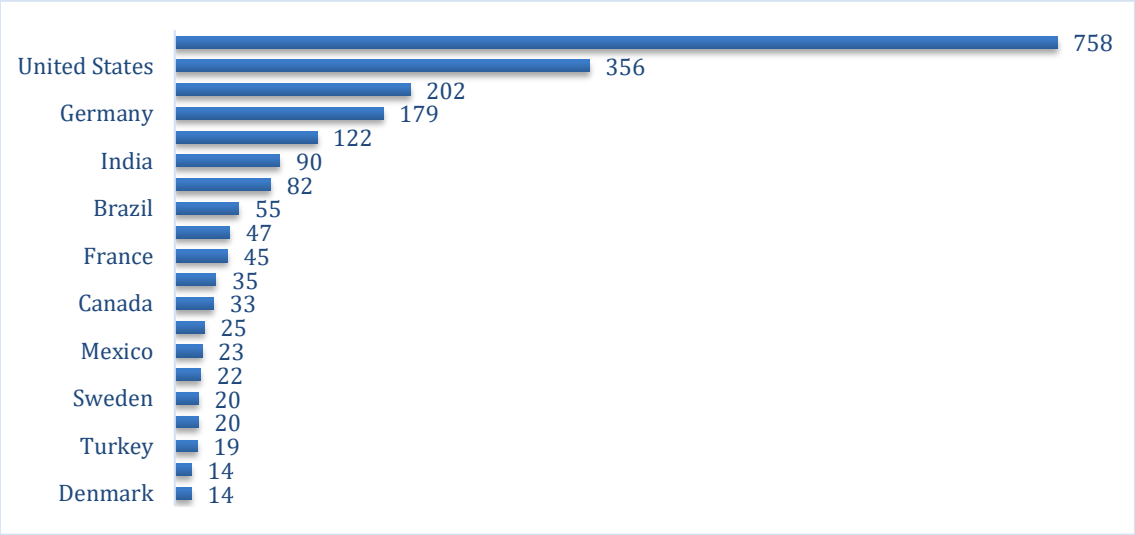

Figure 1.4 Renewable energy capacity investment over the decade, 2010-2019, top 20 countries, $bn

1.3. The Growing importance of wind energy

With increasing fuel prices and environmental concerns, many governments have supported research on renewable energy applications under the consideration of diversifying energy sources. Among the various RESs, wind energy could be one of the most favorable sources to meet the growing global energy demand. Wind energy is one of those energies that is developing around the world, and it is a sector that has been growing very rapidly in recent years. This growth is the strongest of all modes of electrical energy production. Wind power plants use wind energy to generate electricity and can be divided depending on the construction site into onshore and offshore wind power plants [7].

Over the last decade, increasing usage of wind energy has become a global trend. According to the report of the international renewable energy agency (IRENA) of 2021, a total of 111 GW of wind capacity was installed worldwide in 2020, raising the global wind capacity by 17 % to more than 733 GW [8]. According to these stats, 2020 was the best year in history for global wind energy, as it showed a 53% annual growth compared to 2019. Figure 1.5 shows the growth of this shift. This statistic represents the total cumulative wind power capacity in the world from 2010 to 2020. During this period, the investment in wind energy is the total $1.023 trillion, which is 40 % of the total investment in renewable energy [3]. Overall, wind power enjoyed a strong year in 2020.

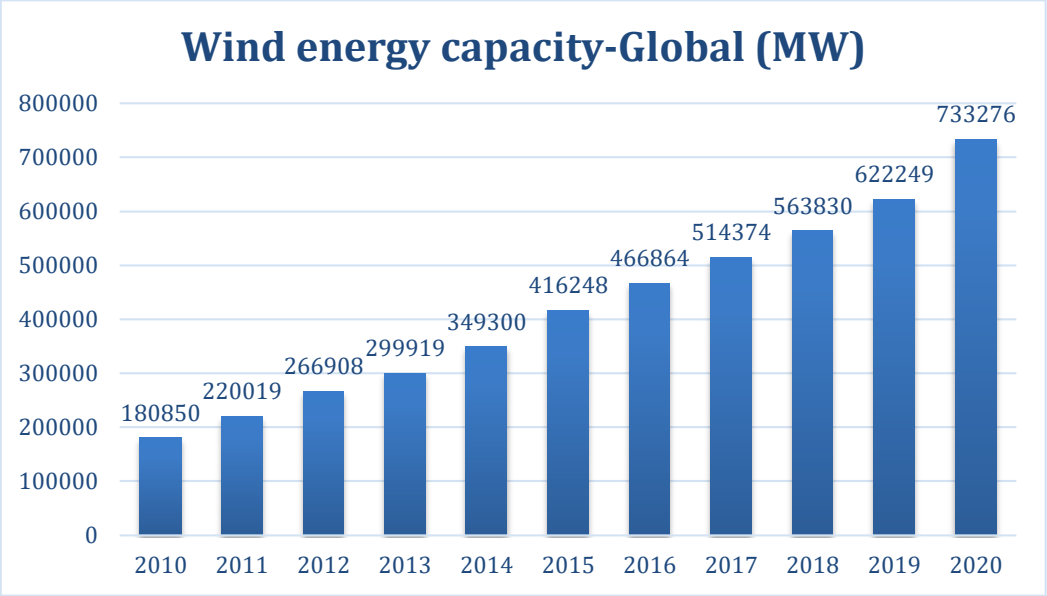

Figure 1.5 Growth of wind energy worldwide, 2010 to 2020

China and the USA are the two largest wind energy generation countries in 2020 with capacities of 281 and 117 gigawatts respectively, contributing 54 % of the total wind energy capacity of 733 GW [8] as shown in Figs. 1.6.

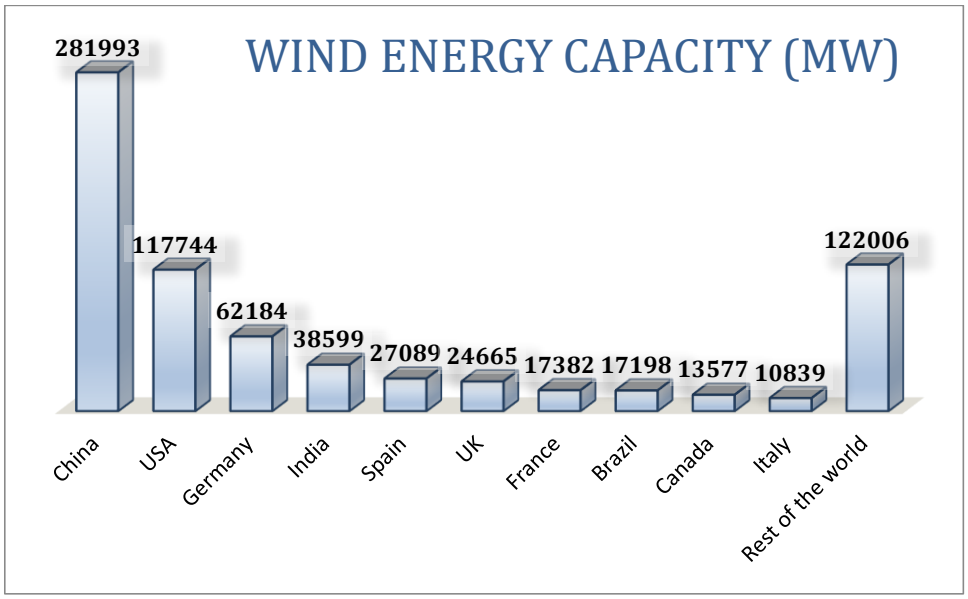

Figure 1.6 Wind energy capacity of Top 10 countries in 2020

According to the global wind energy council, GWEC market intelligence expects that over 469 GW of new wind energy capacity will be added between 2021 and 2025, which is almost 94 GW of new installations annually until 2025 [9]. However, the full effect of the COVID-19 pandemic on wind energy installations is still unknown in light of its possible impacts on the global economy and energy markets.

In recent years, the penetration of offshore wind energy has increased considerably. Offshore wind turbines are referred to the wind turbines that are constructed in the sea or oceans. Higher wind speeds are available offshore compared to onshore, so offshore wind turbines are capable to generate more power electricity. Despite the Covid-19 pandemic, installed offshore wind capacity increased 17.50 % in 2020 (6.1 GW), reaching 34.4 GW at the end of the year, representing about 4.68 % of the global wind power capacity, GWEC estimates. Figure 1.7 shown the growth of offshore wind energy worldwide from 2010 to 2020.

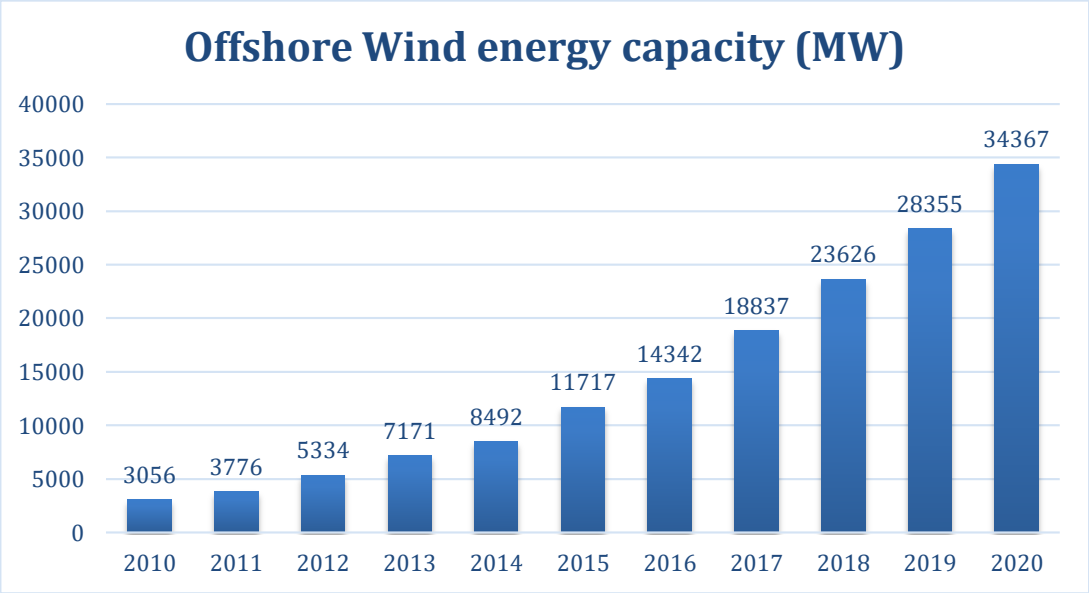

Figure 1.7 Growth of offshore wind energy worldwide from 2010 to 2020

China was the main contributor in 2020, installing half of the world's new offshore wind capacity in a record year. All the largest offshore wind farms are currently in northern European countries, especially in the United Kingdom and Germany, which together account for over two-thirds of the total offshore wind power installed worldwide. The success of offshore wind power in Europe has sparked interest in most other regions such as the USA, which is also a big contributor to offshore wind energy [10]. As of January 2020, the Hornsea One wind farm in the United Kingdom is the largest offshore wind farm in the world at 1,218 MW [11]. Other projects are in the planning stage, including Dogger Bank in the United Kingdom at 3.6 GW [12], and Greater Changhua in Taiwan at 2.4 GW [13]. Another example is the recent development of offshore wind. As the locations are increasingly distant from the shore, for these systems, HVDC is the most techno-economical solution, and several of these projects are currently underway (for example Borwin 1 and 2, Dolwin 1 and 2), and others are planned.

1.4. Wind energy in Algeria

Algeria is located in the Maghreb region of North Africa and is the first country in terms of area in Africa. It consists of four regions, which are the coastal region, the Tel Atlas region, the highlands region, and the Sahara region. Algeria presents a considerable wind potential that can be exploited for the production of electric energy. According to [14] and [15], Algeria ranks fifth among 15 African countries in terms of wind energy potential. Figure 1.8 shows the wind map in Algeria at a 10 m high established by the renewable energy development center (REDC) laboratory. The southwest of the country has high wind speed values which can exceed 5.5 m/s in the region of Tindouf and up to 'at 6.5 m/s in the Adrar region. Several researchers have done theoretical and experimental studies to analyze wind potential in many regions of Algeria, such as in [16]–[19]. These studies have allowed the identification of several sites with very good wind potential, which makes it possible to consider establishing wind farms in the country. The Sahara region (Adrar, Tindouf) and represent the best site for implement large wind farms as shown in the picture below.

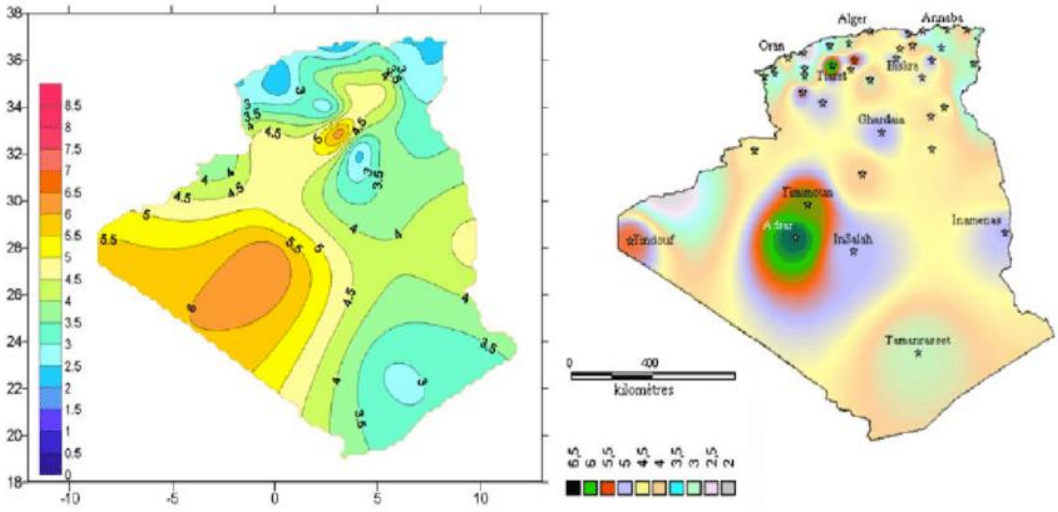

Figure 1.8 Annual maps of wind speed in Algeria at 10 m high

The first attempt to connect wind turbines to the Algeria electrical energy distribution network was in 1957 by the French engineer ANDREAU, with the installation of a 100 kW wind turbine generator at the Grands Vents site (Algiers). Currently, the total wind power installed in Algeria is insignificant. However, the first wind farm of 10MW was installed and commissioned in 2014, in the region of Kabertene in the state of Adrar, southwest of Algeria. This wind farm consists of 12 Gamesa wind turbines of 850 kW power [20]. In addition, the Ministry of Energy and Mines has planned to install additional wind farms with a total capacity of 3000 MW in 2030 as part of its renewable energy program "2011-2030". This strategy should make it possible to reduce the share of fossil fuels (natural gas and oil) which are currently the main resource for the production of electricity in the country.

In our study on integrating wind energy into the Algerian electrical network 114-bus system, the choice of area for the installation of wind turbines in Algeria was made based on the study by Derai *et al.* [18]. According to this study, the two sites "Setif" and "Djelfa" have great wind potential in the Highlands region, whereas sites of "Adrar" and "In Amenas" have great wind potential in the Sahara region. Table 5.2 presents the wind characteristic and the Weibull parameters in these sites. From this table, the scale factor *c* in the site of Adrar is greater than 7 m/s, which means that this site has interesting wind potential compared to other sites.

Table 1.1 Wind characteristic in the four sites studied

Region	Site	Wind speed (m/s)	Power density	Weibull parameters	
				k	c
Highlands region	Setif	3.712	91.7	1.425	4.083
	Djelfa	4.589	112.5	2.008	5.178
Sahara region	Adrar	6.247	246.5	2.350	7.048
	In Amenas	4.515	109.2	1.972	5.094

The annual frequency distributions of wind speeds for the Setif, Djelfa, Adrar, and In Amines sites are depicted in Fig. 5.14.

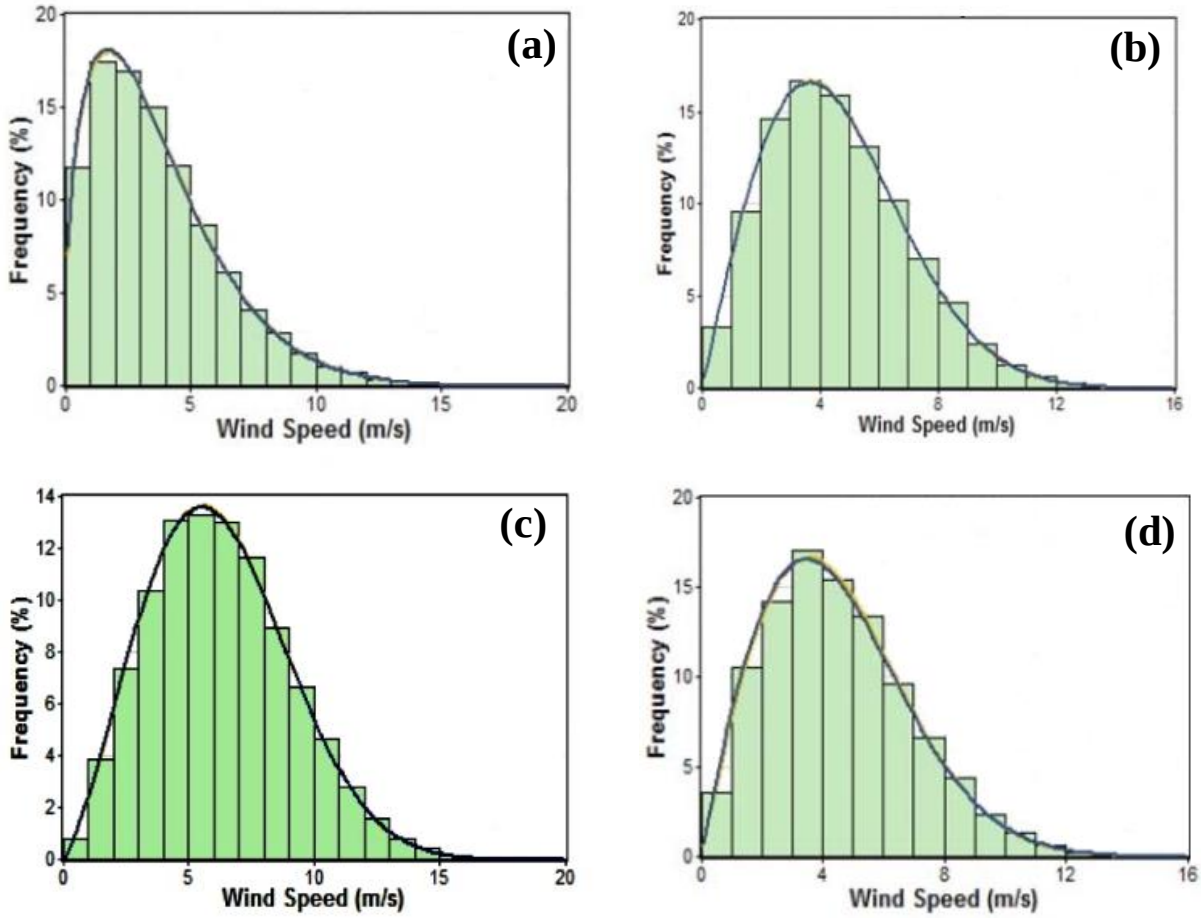

Figure 1.9 Wind speed distribution for **(a)** Setif, **(b)** Djelfa, **(c)** Adrar, **(d)** In Amines [18]

1.5. VSC-FACTS-HVDC technology application in power systems

Recently, the continuous increase in electric energy demand has led to a more complex, stressed, and susceptible power system [21], [22]. As a result, modern transmission systems face new challenges every day to ensure better performance and improve the operating of a transmission system [23]. One of the options that can be employed to accomplish these objectives is the introduction of flexible AC transmission systems (FACTS) devices and the technology of high voltage direct current (HVDC) in the power system.

According to the IEEE, the definition of the flexible alternating current transmission system (FACTS) is as follows: "Alternating current transmission systems incorporating power electronic-based and other static controllers to enhance controllability and increase power transfer capability" [24]. FACTS controllers technologies utilize power semiconductors that offer power grids the ability to efficiently control different electrical quantities (active and reactive powers, voltage profile, phase angle, etc.), which enable faster response than electromechanically switched systems, [24], [25]. In general, FACTS controllers can be divided into four categories depending on the mode of coupling to the network, shunt controllers, series controllers, combined series-series controllers, combined series-shunt controllers.

High voltage direct current (HVDC) technology is playing an increasingly significant role in energy transmission due to its technical and economic superiority over HVAC systems for long-distance transmission. The principle is to convert alternating current to direct current (rectifier) to transport power over long distances, then to convert this power in the opposite direction (inverter). The HVDC is a technology that has been used for long-distance bulk power transfer, connecting different synchronous zones, connecting large renewable energy sources from remotely located. In countries where the development of the economy leads to rapid growth in energy consumption, such as China, India, and Brazil, the HVDC is considered a viable solution for the transport of electricity in bulk on great distances. The rapid evolution of these countries leads the development of the HVDC towards larger systems, both electrically (power and voltage) and as regards the line lengths. Although the HVDC has been in use for over 50 years, its application has been limited. Recent developments of semiconductors for power electronics have led to the development of HVDC technology. Two basic HVDC exist based on categories of converter technologies: The HVDC based on the line commutated converter (LCC-HVDC) and the HVDC based on voltage source converter (VSC-HVDC) which uses insulated-gate bipolar transistor (IGBT).

The voltage source converter-based high voltage direct current (VSC-HVDC) technology was introduced at the end of 1990, thanks to the development of semiconductors for power electronics, such as which uses insulated-gate bipolar transistors (IGBTs), which makes it relatively new compared to CSC technology [26], [27]. The use of VSC-HVDC systems is considered to be a major step in facilitating long-distance power transfer and integrating remotely located renewable energy sources to major consumption centers. Particular attention is paid to VSC-HVDC technology as it has significant advantages over line Commutated converters (LCC) and traditional AC technology. VSC technology can support the AC network by providing fast and independent control of active and reactive power at both extremity terminals contrary to LCC [28].

The FACTS and HVDC equipment uses power semiconductor devices [29] and recent advances in power electronics control technologies that offer the ability to enhance the controllability of the different parameters into the electrical power grids [30]. The latest technological advances of power electronics, control methods, and converter topologies have all been integrated into the FACTS and HVDC fields, giving rise to a new generation of power transmission equipment in both AC or DC with unrivaled operational flexibility [29], [31]. The benefits of FACTS-HVDC devices are increasing the transmission capacities capacity, transporting high-power electricity over long distances, transporting renewable energy, flexibility, and rapidity in power flow control [32]. Table 1.1 lists some of the FACTS and HVDC equipment and the respective areas of power systems application.

Table 1.2 FACTS and HVDC equipment and their power systems applications

Equipment		Active power control	Reactive power control	Voltage control	Wind integrated	AC systems interconnection
Shunt FACTS	SVC		✓	✓		
	STATCOM		✓	✓		
Series FACTS	TSSC	✓				
	TCSC	✓				
	SSSC	✓	✓			
Hybrid FACTS	UPFC	✓	✓			
	IPFC	✓	✓			
VSC-HVDC		✓	✓	✓	✓	✓
CSC-HVDC		✓			✓	✓

SVC: Static var compensator; **STATCOM**: Static compensator; **TSSC**: Thyristor switched series capacitor; **TCSC**: Thyristor-controlled series compensator; **SSSC**: Solid-state series compensator; **UPFC**: Unified power flow controller; **IPFC**: Interphase power flow controller; **CSC-HVDC**: Current source converter high-voltage direct current; **VSC-HVDC**: Voltage source converter high-voltage direct current.

1.6. Wind energy integration using VSC-HVDC technology

In recent years, the power engineering domain is facing major challenges since the increasing interest in renewable energies, among which offshore wind farms present a particular interest. The use of these renewable resources must be carried out in ways that guarantee a healthy, secure, clean and competitive operation [33]. The production of offshore wind energy has rapidly increased worldwide. According to the global offshore wind report by the world forum offshore (WFO) wind, global offshore wind power exceeded 27 GW by the end of 2019 [34]. This is due to the many benefits, notably: wind conditions are more favorable to the sea than on land, thereby producing more energy, and in the absence of obstacles, the wind direction appears to remain more constant [35], [36].

High voltage alternative current (HVAC) transmission provides the simplest and most economic connection method for short distances, but since the distance between the offshore wind farms and the areas of consumption is large (exceeds 300-500 km), which requires transport infrastructure, the transmission with high-voltage direct current (HVDC) technology based on the voltage source converter (VSC) is unavoidable and make a major challenge for power transmission, which has technical and economic advantages over HVAC transmission [37]. In parallel with the growth of the wind energy industry, HVDC technology has also seen major global expansion especially in China, India, and European countries [38]. The VSC technology has been presenting several advantages and is a better fit than LCC technology for transmission offshore, in terms of independent, fast and flexible active and reactive power control and can work without any AC system support, while the line commutated converter (LCC) technology relies on the AC system voltage for operation and demands a large footprint [38]. Those factors exclude LCC-HVDC for transmission offshore wind energy.

The recent development of controllable semiconductor components and VSCs open the door to a higher power range for HVDC which makes an HVDC grid a technical possibility [33]. This HVDC grid can develop into a future offshore grid connecting remotely located large renewable energy sources to the onshore AC grids at various points as shown in Fig. 1.8. This topology has a range of technological and economic advantages to provide a more robust network. In addition, offshore wind power plants have certain distinct technical characteristics, particularly when connected to the MTDC grid (and operating non-synchronously with the main AC grid) [39].

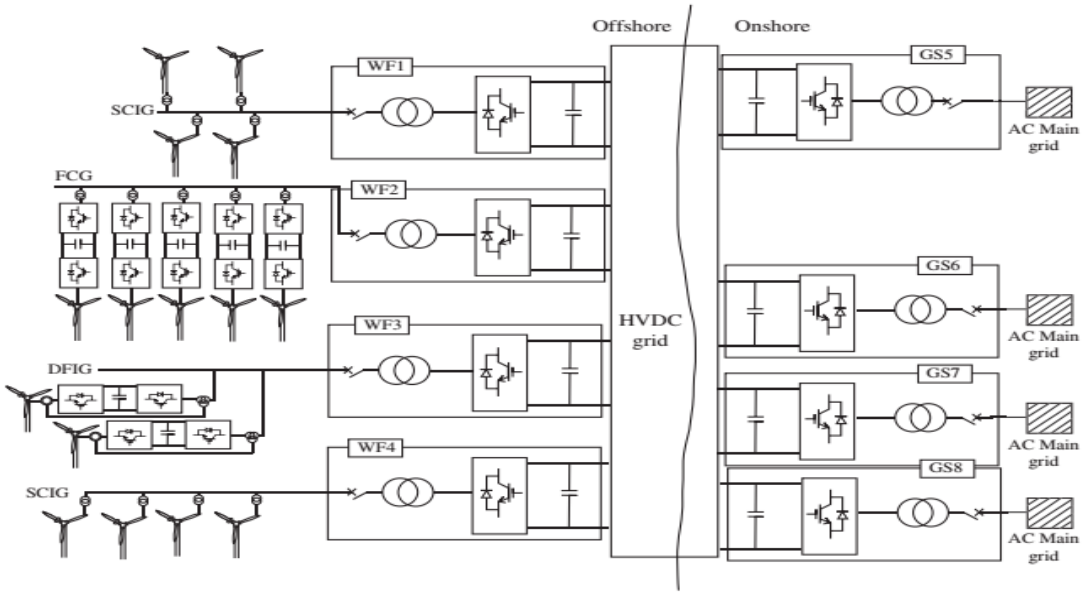

Figure 1.10 HVDC grid for the integration of offshore wind farms [39]

1.7. Problem statement

Nowadays, the current power network faces great challenges to ensure high quality of electricity. Among the main challenges are meeting significant electricity demand and integrate renewable, less expensive, and environmentally friendly energy sources to replace conventional energy sources that cause toxic waste and damage to the environment. Moreover, the high demand for electricity particularly in developing countries has caused many problems in the power system such as a drop in voltage profile, overload on the lines of transmission, and increased power losses.

Incorporating renewable energy sources (RESs) into the electrical grid is one of the main challenges of the modern power system and is a suitable solution to mitigate the increasing energy demand. The variable nature of renewable energy sources such as wind power is a major problem facing their integration into the electrical grid. This is due to its inability to generate energy when the resources that depend on it such as wind speed are not available at all times. In addition, the intermittent nature of renewable energy sources can lead to uncontrollable situations for the power grid operator regarding the balance of production and consumption that must be guaranteed at all times.

In the current power system, the capacity of the RESs plants has increased in recent years, as well as their distance from the consumption areas or the grid-power especially the large offshore wind farms. Thus, there is a need to exploiting the technologies of power transmission for connecting these farms located at a long distance because the AC transmission technology contains a set of limitations and disadvantages such as the problem of timing, dephasing and stability.

1.8. Objectives of the thesis

The main objectives in this thesis can be presented in three main points:

- To solve the optimal power flow (OPF) problems through a artificial intelligence (AI) based on metaheuristic techniques. The slime mould algorithm (SMA) and ant lion optimization (ALO) are proposed in this work to reach a globally optimal solutions to dissimilar objective functions i.e., minimize the fuel cost, reduce the active power transmission losses and improve the voltage deviation. The proposed algorithms for OPF are tested on the IEEE 30-bus, IEEE 57-bus, and the large scale Algerian 114-bus systems.
- To determine optimal location of the static VAR compensator (SVC) and the high voltage direct current system (HVDC) transmission line in the IEEE 30-bus and Algerian 114-bus systems by using the proposed algorithms SMA and ALO. Moreover, to demonstrate the influence of SVC device and HVDC transmission line on the technical parameters of the electrical network (total production cost, voltage profile, active power transit, and active transmission losses).
- To formulate the problem of OPF with wind power integrated into IEEE 30-bus and Algerian 114-bus systems. The formulation considers the stochastic wind power costs, which include the direct cost, the penalty cost due to the underestimation and the reserve cost due to the overestimation of available wind power. The proposed algorithms are proposed to solve the problem with the objective is to minimize the operating cost according to the optimal scheduling of thermal and wind units.

1.9. Organization of the thesis

This thesis is divided into six chapters and it is organized as follows:

Chapter 2 introduces an overview of the optimal power flow (OPF) problem, followed by a brief description of the optimization techniques employed for solving the OPF problem i.e., conventional techniques and recent intelligence techniques. The recent intelligence techniques based on the metaheuristic optimization algorithms are presented in this chapter to solve the OPF problem. Then, it presents a literature review of past research works related to the OPF considering FACTS based on using the metaheuristic optimization techniques. Finally, it presents previous research work to solve the problem of OPF considering stochastic wind power.

Chapter 3 represents a detailed mathematical formulation of the OPF problem. Then, it describes two new flexible and efficient metaheuristic optimization algorithms for solving all of the

optimization problems discussed in this thesis. Both algorithms are called the slime mould algorithm (SMA) and the ant lion optimization (ALO) algorithm. Finally, it presents the implementation of proposed algorithms to solve the OPF problem and demonstrates the validity and efficiency of these algorithms compared with some other optimization techniques in the literature. The simulations are carried out on the IEEE 30-bus, IEEE 57-bus and the large-scale Algerian 114-bus systems, and dissimilar objective functions have been considered.

Chapter 4 presents in the first part, basic concepts on the FACTS-HVDC system, followed by the description and the modeling of static VAR compensator (SVC) and voltage source converters based-HVDC (VSC-HVDC) that used in this work. Then, the formulation of the OPF problem considering FACTS-HVDC systems is briefly described in the second part of this chapter. Finally, the proposed optimization algorithms SMA and ALO are adopted to solve this problem in order to improve the behavior of the electricity grid in contingency conditions. In this context, the proposed algorithms are used to identify the optimal location of the SVC device and HVDC transmission line in the power system. Several simulations are carried out on the IEEE 30-bus and the Algerian 114-bus systems to test the performances of the proposed optimization algorithms.

Chapter 5 presents firstly an overview of the wind power systems followed by a brief description of the wind energy conversion system (WECS) basics when they are integrated with a power system. Then, it introduces the stochastic modeling of output power wind turbines in order to introduce it in the model of the power flow to be optimized. Then, the OPF in a wind integrated either directly to the system or by VSC-MTDC technology is formulated as a stochastic optimization problem in which the objective function is to minimize the total generation cost (TGC) according to the optimal scheduling of thermal and wind units. Finally, the proposed algorithms SMA and ALO are adopted to solve this stochastic optimization problem on the IEEE 30-bus and the Algerian 114-bus systems.

Chapter 6 concludes this study and presents a few research perspectives concerning the general contribution delivered by our work.

1.10. Scientific production

- ***Journal papers:***

  - **R. Kouadri**, L. Slimani, T. Bouktir, I. Musirin, "***Optimal Power Flow Solution for Wind Integrated Power in Presence of VSC-HVDC Using Ant Lion Optimization***", *Indonesian Journal of Electrical Engineering and Computer Science*, vol. 12, pp. 625-633, 2018, **10.11591/ijeecs.v12.i2.pp625-633. Source**

- **R. Kouadri**, I. Musirin, L. Slimani, T. Bouktir, "***OPF for Large Scale Power System Using Ant Lion Optimization: A Case Study of the Algerian Electrical Network***", *IAES International Journal of Artificial Intelligence (IJ-AI)*, vol. 12, pp. 625-633, 2020, **doi:10.11591/ijai.v9.i2.pp252-260**. **Source**
- **R. Kouadri**, I. Musirin, L. Slimani, T. Bouktir, M. M. Othman, "***Optimal Power Flow Control Variables using Slime Mould Algorithm for Generator Fuel Cost and Loss Minimization with Voltage Profile Enhancement Solution***", *International Journal of Emerging Trends in Engineering Research (IJETER)*, vol. 8, pp. 36-44, 2020, **doi.org/10.30534/ijeter/2020/0681.12020. Source**
- **R. Kouadri**, L. Slimani, T. Bouktir, "***Slime mould algorithm for practical optimal power flow solutions incorporating stochastic wind power and static var compensator device***", *Electrical Engineering & Electromechanics*, vol. 6, pp. 45-54, 2020, **doi: 10.20998/2074-272X.2020.6.07. Source**

- ***Conference papers:***
  - **R. Kouadri**, L Slimani and T Bouktir, "***Optimal Power Flow in presence of HVDC lines Using differential Evolution method***", 9th International Conference on Electrical Engineering CEE'16, October 2016, Batna, ALGERIA.
  - **R. Kouadri**, L Slimani and T Bouktir, "***Optimal Placement of SVC and HVDC for Loss Minimization and Improving Voltage Profile using Differential Evolution Algorithm***", 1st national Conference on Modelling, Identification and Control, November 15-17, 2016, Bouira, ALGERIA.
  - **R. Kouadri**, L Slimani and T Bouktir , "***Optimal Power Flow for Combined AC and VSC-MTDC system with large penetration of wind farm***", International Conference on Recent Advances in Electrical Systems (ICRAES'16), Dec. 20-22, 2016, Hammamet, Tunisia.
  - **R. Kouadri**, L. Slimani and T. Bouktir, " ***Optimal Power Flow Control Variables using Slime Mould Algorithm for Generator Fuel Cost and Loss Minimization with Voltage Profile Enhancement Solution***", 2020 International power enginnering, optimization and computing Conference (PEOCO2020), July. 18-19, 2020, Malaysia.

Chapter 02: Literature review

2.1. Introduction

This chapter introduces a literature review of the optimal power flow (OPF) problem. It begins by gives a short overview of the OPF problem followed by the different optimization techniques that are used to solve this problem. Several conventional and advanced intelligence optimization methods have been proposed and developed to find the solution to the OPF problem. Based on the latest research, advanced intelligence optimization methods have advantages over conventional methods to solve the OPF problem. Recent metaheuristic algorithms in the literature are presented in this chapter to solve the OPF problem with different objective functions. Then, it presents the previous research works related to the OPF solutions incorporating FACTS devices. The metaheuristic algorithms have been used to determine the optimal location and sizing of this dispositif. Finally, it presents previous works that used the metaheuristic algorithms to solve OPF problems incorporating stochastic wind power to analyze the planning and operation of modern energy systems.

2.2. Optimal power flow (OPF) overview

Today's power industry needs the development of more complex nonlinear power system models and optimization techniques to solve them, these are called the optimal power flow problem (OPF) techniques. The OPF is a large problem of a nonlinear and non-convex optimization problem with constraints. This problem has been discussed since its introduction by Carpentier in 1962 [40], and it is currently considered one of the most important tools for the operation and planning of power systems. In general, the OPF is a nonlinear problem that involves the procedure of determining the optimal values of the control variables of the system to minimize the desired objective function, subject to certain system constraints [41]. Since the OPF problem was introduced by Carpentier, several research papers have been published and an algorithm has been proposed for this problem.

The OPF has been formulated and successfully applied for several years to various objective functions related to the electrical system, such as minimization of the total costs (fuel cost, renewable energy cost, FACTS installation cost, etc.), reduce the active power transmission losses, voltage deviation improvement, voltage stability index, toxic gas emission, system safety, contingency analysis efficiency, etc.[42]–[44]. The problem of optimization may have a single objective function or multi-objective function.

Typical constraints modeled in the OPF problem can be divided into constraints of equality and inequality. In general, the equality constraint collection consists of equations for both active and reactive power balance at each bus of the electrical system. Whereas the inequality constraints represent several technical limits, e.g., generator power capacity, voltage magnitude limits, regulating transformer adjustments, power flow on transmission lines, etc.

In the OPF problem, optimizing the function objective will minimize considerably the production cost. The optimal value of the objective function that is to be optimized is obtained by an optimal adjusting of the control variables with satisfying the physical and operational constraints such as equality and inequality constraints. The vector of control variables that can be adjusted is composed of active power generating outputs, generators voltage, tap setting of transformers reactive power injected by the shunts compensator, FACTS devices. The OPF has the potential to improve both the quality and economy of the system by optimally adjusting the value of the available active power generation output, especially in the case of increasing demand.

2.3. The optimization techniques employed for the OPF solution

The OPF has gained significant attention over the past half-century due to its significance in the application of power systems [41]. Several different mathematical techniques were developed to solve the OPF problem. These optimization techniques may be classified into two groups; conventional (Classic Methods) methods and recent intelligence methods as shown in Fig. 2.1.

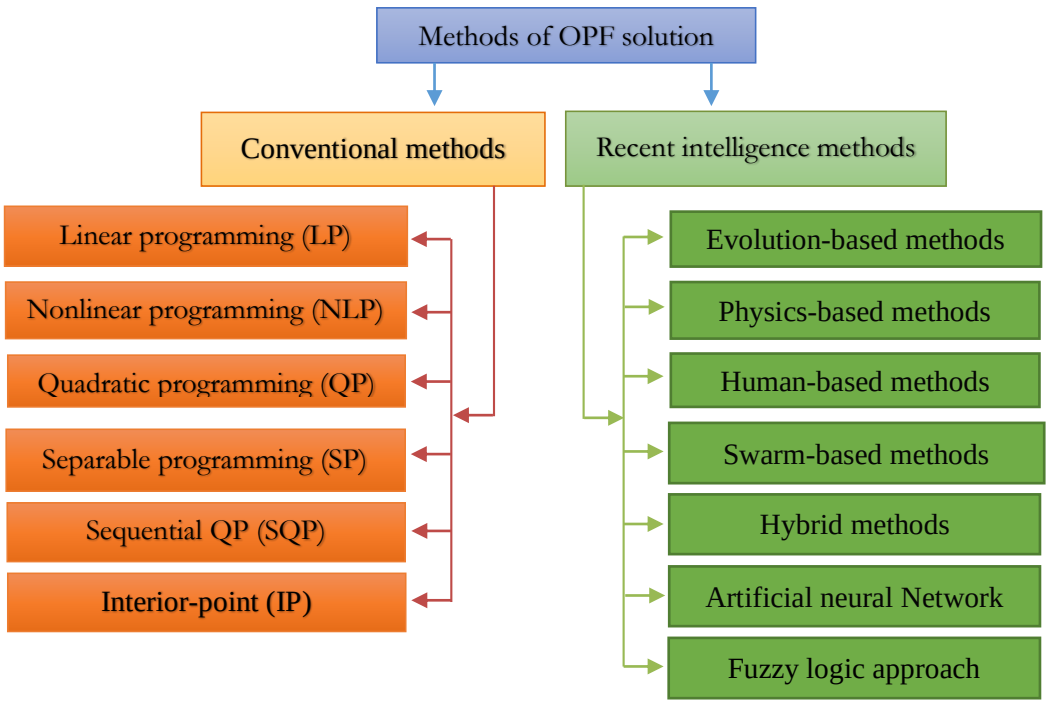

Figure 2.1 Solution methods of an optimal power flow problem

2.3.1. Conventional optimization methods

The majority of traditional optimization methods rely on sensitivity analysis and gradient-based methodologies. In 1968, Dommel and Tinney introduced the first solution approach for the OPF problem [45], since then, many conventional methods have been developed and applied to solve the OPF problem, such as mixed-integer programming (MIP), linear programming (LP), nonlinear programming (NLP), quadratic programming (QP), separable programming (SP), sequential quadratic programming (SQP), interior-point (IP) and the newton method programming [46]. The conventional methods present some disadvantages such as the execution time is very long for convergence, algorithmic complexity, generation of a weak number of nondominated solutions, cannot be applied to real-time operations of power systems and they are unsuitable for large and complex OPF problems which are highly nonlinear and multimodal problems of optimization [41]. Developing optimization methods that can overcome these drawbacks and handle these difficulties becomes essential.

2.3.2. Recent intelligence optimization methods

The recent developments in computer engineering and the growing complexity of the problem of power system optimization have led to a greater need for the implementation of advanced programming techniques for large-scale problems [46]. The recent intelligence methods based on evolutionary or metaheuristic optimization techniques have been proposed to solve the OPF problem in small and large-scale systems, particularly non-linear or non-convex complex optimization problems. Compared to conventional methods, recent intelligence methods converge rapidly into the optimal solution. According to [41], intelligence optimization methods are based on different categories, such as evolutionary methods, metaheuristic methods, artificial neural networks (ANN), fuzzy logic approach (FLA), and combined of these methods.

The metaheuristic term was introduced in 1986 by Glover [47]. The principle of metaheuristic algorithms is to minimize or maximize an objective function to find one or more solutions to difficult and complex optimization problems [48]. The metaheuristic methods mark a great revolution in the field of optimization and are therefore widely used to solve OPF problems. They can be categorized into four main categories based on their nature inspirations that simulate biological or physical phenomena such as; evolution-based methods, physics-based methods, swarm-based methods, and human-based methods [49].

Evolutionary-based methods simulate the natural evolution process where starts from an initial state of variables (population randomly generated) then create new generations of genetically superior individuals to search for optimum value for the decision variables of an optimization problem [50]. Among these methods: Genetic Algorithm (GA), Differential Evolutionary (DE), Evolution Strategy (ES), Memetic Algorithm (MA), Genetic Programming (GP) and Biogeography-Based Optimizer (BBO) and Imperialist Competitive Algorithm (ICA).

Physics-based methods are inspired by physics laws or natural physics phenomena in space [41], [51]. Among these methods: Improved colliding bodies optimization algorithm (ICBO), Gravitational Search Algorithm (GSA), Big-Bang Big-Crunch (BBBC), Electromagnetism Like Mechanism Method (ELM), Black Hole (BH) and Galaxy-based Search Algorithm (GbSA).

Swarm-based algorithms imitate the social behavior of animal groups [50]. Many algorithms have been developed based on the animal group behavior, such as Particle Swarm Optimisation (PSO), Harmony Search algorithm (HS), Artificial Bee Colony algorithm (ABC) and Ant Colony Optimization (ACO).

Human-based algorithms are inspired by human behaviors, especially when it comes to thinking or making decisions [41]. Some of the most popular human-inspired techniques are Biogeography-based optimization (BbO), Group Search Optimizer (GSO), The League Championship Algorithm (LCA), Teaching Learning Based Optimization (TLbO), Firework Algorithm (FA), Symbiotic organisms search algorithm (SOS) and Interior Search Algorithm (ISA).

2.4. The metaheuristic optimization techniques employed for OPF problem

Recently, several metaheuristic algorithms were developed and implemented in the electrical power system for the solution of the OPF problem with different objective functions are considered such as minimize the total fuel cost, reduce the active power transmission loss, voltage profile improvement,..etc. Some of these algorithms are Salp swarm optimizer [52], Moth Swarm Algorithm [53], differential evolution [54], glowworm swarm optimization [55], Differential search algorithm [56], stud krill herd algorithm [57], Artificial bee colony algorithm [58], [59], Symbiotic organisms search algorithm [60], improved colliding bodies optimization algorithm [61], Firefly Algorithm [62], black-hole-based optimization approach [63], [64], adaptive real coded biogeography-based optimization [65], the league championship algorithm [66], chaotic invasive weed optimization algorithms [67], Genetic Algorithm [68], [69], multi-verse optimizer [70], Harmony Search Algorithm [71], Earthworm Optimization Algorithm [72]. moth-flame optimizer (MFO) [73], Sine-Cosine algorithm (SCA) [74], Ant lion optimizer [75], and particle swarm optimization (PSO) [76].

In this present study, two flexible and efficient metaheuristic techniques have been proposed with the aim is solving the OPF problem considering stochastic wind power and FACTS-HVDC technology. These algorithms namely; the slime mould algorithm (SMA) and the ant lion optimization (ALO).

A Slime Mould Algorithm (SMA) is a recent metaheuristic technique nature-inspired proposed by Shimin Li *et. al* in 2020 [77], which is inspired by the swarming behavior and morphology of slime mould in nature. One of the most interesting characteristics of the slime mould is the unique pattern based on the multiple food sources at the same time to form a venous network connecting them. This scheme gives the high capability of escaping from local optima solutions. SMA algorithm is aroused by the diffusion and foraging conduct of slime mould. Slime mould can approach food, depending on the smell in the air. The slime mold morphology varies, with three different forms of contraction [77]. In SMA, the position of the slime mould represents a possible solution to solve optimization problems of constrained engineering. This research work considers the first time solving the OPF problem based on the SMA algorithm to minimize the desired objective functions.

Ant lion optimization (ALO) algorithm is a nature-inspired proposed by Seyedali Mirjalili in 2015 [78]. The ALO is based on the hunting mechanism of Antlions in nature. The exploration and the exploitation by global and local searches in ALO are presented in one algorithm. ALO has a high level of exploration and exploitation which allows it to explore the potential regions of the search space and assist it in rapidly converge to the global optimum due to the use of the roulette wheel selection (RWs) method. In the literature, many researchers are interested in this algorithm to solve the OPF problems. In [79], Júnior *et al*. have been proposed ALO for solving the economic-emission load dispatch (EELD) problem, in which the objective function is to minimize the total fuel cost consumption and carbon emission. In [80]–[82], the authors have been proposed ALO to determine the optimal location and sizing of renewable DG sources with the objective is reduce the active losses in radial distribution systems. In [83], the ALO algorithm has been proposed with used a composite ranking index (CRI) for solving the hydro-thermal-wind scheduling (MOHTWS) problem with the minimization of multiple objectives simultaneously. Also in [84], ALO has been proposed to solve practical wind integration with hydrothermal power generation scheduling (HTPGS) problem. In [85], the ALO algorithm has been modified by incorporating Lévy-flight (LF) for solving the OPF problem when the objective function is to minimize the total fuel cost in the power system. ALO has been proposed for solving the OPF problem considering various mono-objective optimization (Fuel cost, voltage deviation, voltage stability index, active power loss, and reactive power loss) in [86]–[88].

2.5. OPF solutions incorporating FACTS devices

The FACTS technology is a modern technical development of the electrical power system [89]. Using the FACTS device is a more economic solution since it has a lower operational cost and no extra cost will involve the charge in generation and load compared with other corrective control methods i.e. load shedding and generation rescheduling [90], [91]. Since 1970, FACTS technology applications started with the Static Var Compensator (SVC) and were followed by the thyristor controlled series compensator (TCSC) [92]. The optimal power flow (OPF) problem incorporating various FACTS devices in the electrical power system has been proposed by many researchers to solve the stable operation of the system with voltage stability and reduced losses [23], [93]. The optimal location of various FACTS devices is a multimodal, highly constrained, and complex optimization problem [94]. The optimal location of FACTS devices is a key to improve system efficiency and maximizing power system security. In the practical system, the installation of FACTS devices in the optimal locations in power system networks will give different advantages in terms of enhancing voltage stability, minimizing the generation cost and power loss in transmission, and other factors. The optimal locations of the FACTS devices depend on a comprehensive analysis of steady-state stability, line stability [95], voltage stability, small-signal stability, transient stability, and cost of installation [96]–[98]. From the literature, the optimal location and setting of FACTS devices have retained the interest of worldwide researchers in the power system, with different optimization methods and criteria are used in this field.

Among the various FACTS controllers, SVC considered is one of the most used FACTS devices and selected to use in this work. It has absorbed or provides reactive power to the system in order to control specific parameters of an electrical power system, typically bus voltage magnitude. SVC is connected in shunt with the AC system through a step-up transformer and consists of a bank of thyristor-controlled reactors (TCRs) in parallel with a bank of thyristor switched capacitors (TSCs).

In this thesis, SVC is integrated with metaheuristic algorithms based on optimal power flow with the goal is optimize the total generation cost and improve the voltage profile of the system. The optimal location of SVC devices in power systems using proposed metaheuristic algorithms is introduced to improve the performance of the power system. Literature regarding the optimal location and ratings of SVC using optimization techniques especially metaheuristic algorithms are reviewed. Different single objective functions and multi-objective functions were considered for the SVC controller's effect on certain parameters of power system networks such as generation cost, transmission losses, voltage support, etc.

Several metaheuristic optimization techniques have been proposed to find the optimal allocation of SVC devices. In [99], Mohamad *et. al* selected the symbiotic organisms search (SOS) to determine the optimal location and sizing of the SVC device in the IEEE 26-bus Reliability test system with the objective aim to improve voltage security. Kumar *et. al* in [100] and [101] proposed a modified standard bacterial foraging optimization algorithm (MBFOA) to identify the optimal allocation of the SVC device in the IEEE 30-bus test system. The optimal location and size of SVC were identified by minimizing the multi-objective function, whose system security, system overload, and active power losses. In [102], the authors proposed sigma-multi-objective evolutionary PSO (MOEPSO) to finding the optimal placement and power ratings of the SVC device for minimizing the transmission loss and SVC investment costs in the IEEE 30-bus and IEEE 118-bus systems. In [103], PSO is selected for determining the optimal placement of the SVC device to improve the voltage deviation in the island of the Maui grid, Hawaii, USA gird, with high penetration of solar energy. In [104], the gravitational search algorithm (GSA) has been proposed to determine the optimal placement of SVC and TCSC devices for the enhancement of the power system under different loading conditions. In [105], the authors proposed the brainstorm optimization algorithm (BSOA) to find the optimal location and setting of SVC and TCSC devices in the IEEE 57-bus test system underline outage contingencies. Multi-objective functions have been considered in this work to be optimized, such as voltage profile enhancement, loss minimization, and overload mitigation.

2.6. OPF solutions incorporating stochastic wind energy

With the growing penetration of renewable energy sources in the power system, the study of optimal power flow (OPF) becomes necessary to solve power system problems or improve the performance of this system. In general, the problem with wind power is the stochastic nature of wind speed. Thus, it is necessary to confront the stochastic nature of this source for analysis of the planning and operation of modern power systems. Therefore, the model which considers the probability of the available wind power can represent the cost of overestimating and underestimating this power at a certain period. The underestimation situation is due when the actual wind power is higher than the estimated value, while the overestimation situation is due when the actual wind power is less than the estimated value. One purpose of this thesis is to use the metaheuristic optimization algorithms to solve the OPF problem with stochastic wind energy.

The OPF problem incorporating stochastic wind power in power systems has recently been studied by researchers. In this context, different metaheuristic algorithms have been proposed to solve this problem. Panda and Tripathy [106] applied a modified bacteria foraging algorithm (MBFA) to

solve security-constrained OPF problems with wind power, in which a static synchronous compensator (STATCOM) was considered to provide reactive power support against wind uncertainties. In other work of Panda and Tripathy [107], an MBFA has been proposed to solve the OPF problem with the integration of wind power in the IEEE 30-bus test system. Roy and Jadhav applied a Gbest-guided artificial bee colony algorithm (GABC) to solve the OPF problem with stochastic wind power [108]. In attempting the same problem, authors in [109] proposed a modified moth swarm algorithm (MMSA) to solve the OPF problem incorporating stochastic wind power. Three objective functions are considered, which are operating cost minimization, transmission power loss, and voltage profile enhancement. Duman *et. al* in [110] applied a modified hybrid PSOGSA with a chaotic maps approach to solving the OPF problem with stochastic wind power and FACTS devices such as TCSCs and TCPSs. The proposed CPSOGSA method has been applied on the IEEE 30-bus and 57-bus test systems to minimize the total generation cost i.e. minimizes the total fuel cost of thermal and wind generators. Bird swarm algorithm (BSA) has been proposed in [111] to solve the OPF problem in the power system with incorporating stochastic wind and solar power. The simulation carried out on a modified IEEE 30-bus system with the objective function is to minimize the total generation cost. Reference [112] proposes a genetic algorithm (GA) to solve the OPF problem with stochastic wind and solar energy integrated into the power systems, in which the total generation cost minimization is considered as the objective function. Reddy in [113] used a particle swarm optimization (PSO)-based fuzzy satisfaction maximization technique to solve the multi-objective OPF problem with thermal–wind–PV generation units, in which the cost minimization, transmission losses, and voltage stability improvement index are considered as the objective function. Application of hybrid approach combining modified bacteria foraging algorithm (MBFA) and genetic algorithm (GA) for OPF problem considering wind power has been demonstrated on IEEE 30 bus test system [114]. The system includes stochastic wind-solar–small hydropower in conjunction with thermal power generation is optimized and solved by using barnacles mating optimizer (BMO) algorithm [115] and flower pollination algorithm (FPA) [116]. Wind, solar PV, and small hydro generation are considered and modeled with Weibull PDF, lognormal PDF, and Gumbel PDF, respectively. Reference [117], the proposed OPF problem with the consideration of wind and tidal power has been solved by using a moth swarm algorithm (MSA). Reference [118] proposed a particle swarm optimization (PSO) algorithm to solve the OPF problem considering the cost of wind and solar power uncertainty in IEEE New England 39-bus. Solution of multi-objective OPF problem considering wind-solar power with grey wolf optimizer (GWO) algorithm is presented in [119]. In [120], a several multi-objective OPF for stochastic Wind-Thermal power are proposed to minimize by using moth flame optimization (MFO) algorithm. Abdollahi *et al.* in [121] utilized krill herd algorithm (KHA) to

solve OPF problem with wind-thermal generators and two series FACTS device (TCPS and TCSC), which was tested via an modified IEEE-30 bus and IEEE 57-bus systems. In [122], a various recent metaheuristic optimization algorithms are proposed to solve an OPF problem combining stochastic wind and solar power with conventional thermal power generators in modified IEEE 30-bus. The authors in [123] simulated the OPF problem considering stochastic wind power with several single and multiple objective functions , and solved this problem via lévy coyote optimization algorithm (LCOA). In [124], Biswas presented differential evolution (DE) for OPF problem in power system considering stochastic wind and solar power. In [125], Wind power-incorporated OPF problem was solved using cuckoo search algorithm (CSA), firefly algorithm (FFA), and flower pollination algorithm (FPA) in isolated Adrar Algerian power system . The detailed of the mentioned literature paper research that used the recent metaheuristic algorithms to solve the OPF problem incorporating stochastic wind power are presented in the tables of Annex A.

2.7. Conclusion

This chapter introduces in the first the basic concepts related to the optimal power flow (OPF) problem. The OPF problem is a widely studied subject that has been solved through conventional and intelligence optimization methods. In the literature, intelligence techniques based on metaheuristic optimization have been presented to solve the OPF problem. Then, a literature review of metaheuristic techniques employed to determine the optimal location and size of the SVC device has been presented in this chapter. Finally, the previous research work related to solving the OPF problem considering stochastic wind power has been presented by using various metaheuristic optimization techniques. In this context, dissimilar objective functions are considered to optimize such as minimize the total generation cost, reduce the transmission power loss, enhance voltage profile, as well as other factors, were discussed.

Chapter 03: Application of New Metaheuristic Optimization Techniques to solve OPF Problem

3.1. Introduction

The optimal power flow (OPF) is one of the most important tools for efficient planning and controlling the power systems operation. It was first introduced by Carpentier in 1962 [40]. In general, the problem of the OPF can be considered as a large problem of nonlinear and non-convex optimization with constraints. The OPF procedure consists of determining the best suitable values of the control variables in order to reach a globally optimal solution of the objective functions that optimize while satisfying the constraints of equality and inequality of the power system [126]. Different objective functions in the OPF formulation may be optimized such as total generation cost (fuel cost, renewable energy cost, etc.), active or reactive power transmission line losses, cost of FACTS installation, voltage deviation, voltage stability index, toxic gas emission, system safety, etc. [42]–[44]. In this context, several evolutionary or metaheuristic optimization techniques have been proposed and applied to solve the OPF problem. Metaheuristic optimization techniques mark a big revolution through find, generate, or select one or more good solutions to complex optimization problems [48], Hence, it is widely used to solve practical optimization problems in small and large-scale power systems.

This chapter presents in the first part the mathematical formulations of the OPF problem in a detailed way. Three objective functions that we aim to optimize; the quadratic equation of generation fuel cost, the total active power losses, and the voltage profile improvement. In the second part, newly metaheuristic optimization algorithms namely the slime mould algorithm (SMA) and the ant lion optimization (ALO) algorithm have been implemented to solve the OPF problem. The last part of this chapter presents the application of the proposed algorithms to solve the OPF problem on the IEEE-30 bus, IEEE-57, and large scale Algerian 114-bus power systems, and then demonstrate the efficiency of these proposed algorithms by comparing the results to those obtained by the other algorithms in the literature.

3.2. Formulation of Optimal Power Flow (OPF) Problem

3.2.1. Formulation Problem

The optimal power flow problem solution aims to give the optimum value of the objective function by adjusting the settings of control variables. Generally, the mathematical expression of the optimization problem with satisfying various equality and inequality constraints may be represented

as follows:

Min $\mathrm{F}(\mathrm{x},\mathrm{u})$ **(3.1)**

Subjected to $g(x,u)=0$ **(3.2)**

$h(x,\ u)\le 0$ **(3.3)**

where *F(x,u)* represents the objective function that to be optimized, *g(x,u)* is the equality constraints and *h(x,u)* the inequality constraints, x represents the vector of the state variables and u represents the vector of the control variables.

3.2.2. Objective Function

In this study, three objective functions that we aim to optimize are the quadratic equation of generation fuel cost, the total active power losses, and the voltage profile improvement of all load buses (PQ) subject to operating constraints. The formulation of these objective functions are presented in the following sections:

3.2.2.1. Minimization of generation fuel cost

The first objective function used is the sum of the quadratic cost model at each thermal generator unit with satisfying all system constraints (equality and inequality constraints). In this thesis, we distinguish the case of economic dispatching with losses and formulated as follows:

$$F_1(x)=\sum_{i=1}^{NG} a_i+b_iP_{Gi}+c_iP_{Gi}^2 \quad \textbf{(3.4)}$$

where F_1 is the fuel cost of the ith generator, P_{Gi} is the active power generated by the thermal generators, a_i, b_i and c_i are the cost coefficients of ith generator.

3.2.2.2. Minimization of active power transmission losses

In this study, the second objective function investigated for minimizing the active power transmission losses, which is formulated as follows:

$$\boldsymbol{F}_2(\boldsymbol{x})=\sum_{\boldsymbol{i}=1}^{\boldsymbol{N}} P_{loss_i}=\sum_{\boldsymbol{i}=1}^{\boldsymbol{N}} P_{G_i}-\sum_{\boldsymbol{i}=1}^{\boldsymbol{N}} P_{D_i} \quad \textbf{(3.5)}$$

where P_{loss} denotes the active power transmission losses, P_{Gi} is the active power generated by the thermal generators and P_D is the active power demand.

3.2.2.3. Voltage profile improvement

The objective function is to minimize the fuel cost and improve the voltage profile by reducing the total voltage deviation (TVD) of load buses (PQ) from the nominal value of 1.0 p.u. The bus voltage is known as the most important and significant indices of safety and service quality [66]. The expression of the cumulative voltage deviation is presented as follows:

$$TVD = \sum_{i=1}^{N} |V_i - 1.0| \tag{3.6}$$

Thus, the objective function which represents the sum of the total generating fuel cost and the TVD can be given as follows:

$$\boldsymbol{F}_3(x) = \left(\sum_{i=1}^{N} \boldsymbol{a}_i + \boldsymbol{b}_i \boldsymbol{P}_{G_i} + \boldsymbol{c}_i \boldsymbol{P}_{G_i}^2 \right) + \boldsymbol{w}_{VD} * \boldsymbol{TVD} \tag{3.7}$$

where w_{VD} is a suitable weighting factor for balancing target function values and preventing the dominance of an objective over another. In this study, the selected value of w_{VD} is equal to 100.

3.2.3. Control variables

The control variables (independent variables) should be adjusted to satisfy the load flow equations. The set of control variables can be expressed by vector *u* as follows:

$$u = \left[P_{G_2} \ldots P_{G_{NG}}, V_{G_1} \ldots V_{G_{NG}}, Q_{C_1} \ldots Q_{C_{NC}}, T_1 \ldots T_{NT} \right] \tag{3.8}$$

where: P_G is the thermal generator active power, V_G is the generator voltage, Q_C is the reactive power injected by the shunts compensator, T is the tap setting of transformers, NG is the number of generators, NC is the number of shunts compensators units and NT is the number of regulating transformers.

3.2.4. State variables

The set of variables (dependent variables) that characterize any unique state of the optimization problem can be expressed by vector x as follows:

$$x = \left[P_{Gslack}, Q_{G_1} \ldots Q_{G_{NG}}, V_{L_1} \ldots V_{L_{NL}}, S_{l_1} \ldots S_{l_{nl}} \right] \tag{3.9}$$

where P_{Gslack} is the active power generation at the slack bus, Q_G is the reactive power outputs of the generators, V_L is the voltage magnitude at load bus, S_l is the apparent power flow, NG is the number of generators, NL is the number of load buses or PQ buses, and nl is the number of transmission lines.

3.2.5. Constraints OPF

In the problem of optimization, constraints can be classified into equality and inequality constraints as follow:

3.2.5.1. Equality constraints

The equality constraints reflect the physics of the power system which represents the flow equations of the balanced powers. These equality constraints are as follows:

$$P_{G_i} - P_{d_i} = V_i \sum_{j=1}^{N} V_j \left(g_{ij} \cos \delta_{ij} + B_{ij} \sin \delta_{ij} \right) \qquad \forall i \in N \qquad \textbf{(3.10)}$$

$$Q_{G_i} - Q_{d_i} = V_i \sum_{j=1}^{N} V_j \left(g_{ij} \sin \delta_{ij} + B_{ij} \cos \delta_{ij} \right) \qquad \forall i \in N \qquad \textbf{(3.11)}$$

3.2.5.2. Inequality constraints

The inequality constraints reflect the limiting of the power system operation. These inequality constraints can be classified as follows:

- The active and reactive powers of the generators:

$$P_{Gi}^{min} \le P_{Gi} \le P_{Gi}^{max} \qquad \forall \, \mathrm{i} \in \mathrm{NG} \qquad \textbf{(3.12)}$$

$$Q_{Gi}^{min} \le Q_{Gi} \le Q_{Gi}^{max} \qquad \forall \, \mathrm{i} \in \mathrm{NG} \qquad \textbf{(3.13)}$$

- Shunt VAR compensator:

$$Q_{Ci}^{min} \le Q_{Ci} \le Q_{Ci}^{max} \qquad \forall \, \mathrm{i} \in \mathrm{NC} \qquad \textbf{(3.14)}$$

- Generators bus voltages:

$$V_{Gi}^{min} \le V_{Gi} \le V_{Gi}^{max} \qquad \forall \, \mathrm{i} \in \mathrm{NG} \qquad \textbf{(3.15)}$$

- Transformer tap settings:

$$T_{NTi}^{min} \le T_{NTi} \le T_{NTi}^{max} \qquad \forall \, \mathrm{i} \in \mathrm{NT} \qquad \textbf{(3.16)}$$

- Voltage magnitude of load buses

$$V_{Li}^{min} \le V_{Li} \le V_{Li}^{max} \qquad \forall \, \mathrm{i} \in \mathrm{NL} \qquad \textbf{(3.17)}$$

- Apparent power flow in transmission lines:

$$\left| S_{li} \right| \le S_{li}^{max} \qquad \forall \, \mathrm{i} \in nl \qquad \textbf{(3.18)}$$

3.3. Metaheuristic algorithms applied to solve OPF problem

Recently, new flexible and efficient metaheuristic optimization algorithms have been proposed to solve any optimization problem, namely the slime mould algorithm (SMA) and the ant lion optimization (ALO). In this study, SMA and ALO have been presented to solve the optimal power flow (OPF) problem.

3.3.1. Slime Mould Algorithm (SMA)

A slime mould algorithm (SMA) is a new stochastic optimizer technique nature-inspired proposed in 2020 by Shimin Li *et al*. [77]. This technique based on the oscillation mode of slime mould in nature and simulates the swarming behavior and morphology of slime mould in foraging. The SMA algorithm features a special mathematical model that uses the adaptive weight to simulate the combination of positive and negative feedback from the bio-oscillator-based propagation wave that was inspired by slime mould to form the optimal pathway to connect food. Some of the most interesting characters in the slime mould are the unique pattern based on the various food sources to create a venous network connecting them at the same time. This scheme gives the high capability of escaping from local optima solutions. The algorithm is aroused by slime mold diffusion and foraging behavior. In SMA, slime mould can approach food, depending on the smell in the air. The slime mold morphology varies, with three different forms of contraction. In SMA, the position of the slime mould represents a possible solution to solve optimization problems of constrained engineering.

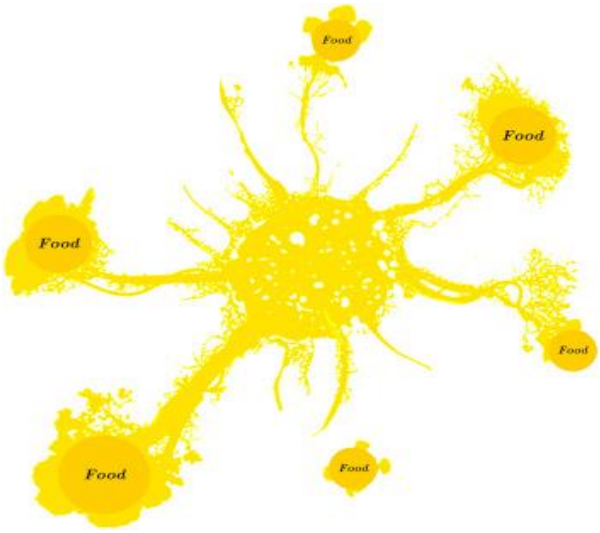

Figure 3.1 Foraging morphology of slime mould [77]

The following section will explain in detail the mathematical model for simulating the behavior of slime mould during foraging [77]:

3.3.1.1. Approach food

The following formulas for imitating the contraction mode is proposed to model the behavior of slime mould to approaching food according to the odor in the air as follows:

$$\overrightarrow{X^*} = \begin{cases} \overrightarrow{X_b(t)} + \overrightarrow{vb} * \left(W * \overrightarrow{X_A(t)} - \overrightarrow{X_B(t)} \right) & r < p \\ \overrightarrow{vc} * \overrightarrow{X(t)} & ir \geq p \end{cases} \quad \textbf{(3.19)}$$

where $\vec{X}$ denotes the slime mould location, $\overrightarrow{X_b}$ is the individual emplacement with the highest odor concentration currently found, $\overrightarrow{X_A}$ and $\overrightarrow{X_B}$ are indicated two randomly selected individuals from the swarm, $\overrightarrow{vb}$ is a parameter distributed in the range of $[-a, a]$, $\overrightarrow{vc}$ decreases linearly from 1 to 0, t shows the current iteration and $\overrightarrow{W}$ represents the slime mould weight and is given by Eq. (3.23). p is the parameter given by Eq.(3.20) as follows:

$$p = \tanh\left| S(i) - DF \right| \quad \textbf{(3.20)}$$

where $S(i)$ represents the fitness of $\vec{X}$, $i \in 1,2,\ldots,n$, , DF is the optimum fitness obtained in all iterations.

The vector of $\overrightarrow{vb}$ is given as follows:

$$\overrightarrow{vb} = [-a, a] \quad \textbf{(3.21)}$$

The parameter of a is given as follows:

$$a = \operatorname{arctanh}\left(-\left(\frac{t}{\max\_t} \right) + 1 \right) \quad \textbf{(3.22)}$$

The expression of $\overrightarrow{W}$ define the location of slime mould and is given as follows:

$$\overrightarrow{W\left(SmellIndex(i)\right)} = \begin{cases} 1 + r * \log\left(\frac{bF - S(i)}{bF - wF} + 1 \right), condition \\ 1 - r * \log\left(\frac{bF - S(i)}{bF - wF} + 1 \right), others \end{cases} \quad \textbf{(3.23)}$$

where $condition$ denotes that $S(i)$ is ranked first half of the population, r represents the random value distributed in the range of $[0,1]$, bF and wF are represented the optimal and worst fitness value obtained in the current iterative process, respectively, $SmellIndex$ represents the sequence of fitness values sorted as follows:

$$SmellIndex = Sort(S) \quad \textbf{(3.24)}$$

3.3.1.2. Wrap food

This portion mathematically simulates the mode of contraction in the slime mould venous tissue structure while searching. In this context, the higher the food concentration reached by the vein, the stronger the bio-oscillator-generated wave, the quicker the cytoplasm flows and the thicker the vein. The following mathematical formula represents updating the emplacement of slime mould:

$$\overrightarrow{X^*} = \begin{cases} rand*(UB-LB)+LB & rand < z \\ \overrightarrow{X_b(t)}+\overrightarrow{vb}*\left(W*\overrightarrow{X_A(t)}-\overrightarrow{X_B(t)}\right) & r < p \\ \overrightarrow{vc}*\overrightarrow{X(t)} & r \geq p \end{cases} \quad \textbf{(3.25)}$$

where Lb and Ub denote, respectively, the lower and upper boundaries of the search range, $rand$ denote the random value distributed in the range of in [0,1].

3.3.1.3. Grabble food

Slime mould depends primarily on the propagation wave to change the cytoplasmic flow in the veins, so that they appear to be in a better food concentration location. Slime mould can approach food more quickly food when the concentration and quality of food are high, while if the food concentration is lower, approach it more slowly, thus increasing the efficiency of slime mould in selecting the optimal source of food.

In the SMA process, the value of $\overrightarrow{vb}$ parameter oscillates randomly in the interval between $[-a, a]$ and progressively approaches zero as the iterations increase. The value of $\overrightarrow{vc}$ oscillates randomly in the interval between [-1,1] and finally tends to be zero.

3.3.2. Implementation of SMA algorithm to OPF problem

The implementation of the SMA algorithm to solve the OPF problem that minimizes the objective function can be summarized in the steps below:

1. Read the system data (bus data, line data, and generator data);
2. Initialize the parameters of search agents, size of the population, the maximum number of iterations, the number and position of the control variables;
3. Initialize the positions of slime mould X_i as the initial population using Eq. (3.19);
4. Maps control variables from ants into the load flow;
5. If the maximum number of iterations is achieved, go to step 6. Otherwise, END of operation;

6. Calculate the fitness of all slime mould using Eq. (3.25);
7. Update the best fitness, X_b;
8. Calculate the W by using Eq. (3.23);
9. Update the parameters of SMA which are: p, vb and vc.
10. Update the best positions of slime mould;
11. The elite comprised the best fitness value was selected. Therefore, the best value of the objective function was determined;

The flowchart of the implementation of the proposed algorithm SMA for solving the OPF problem is shown in Fig. 3.2.

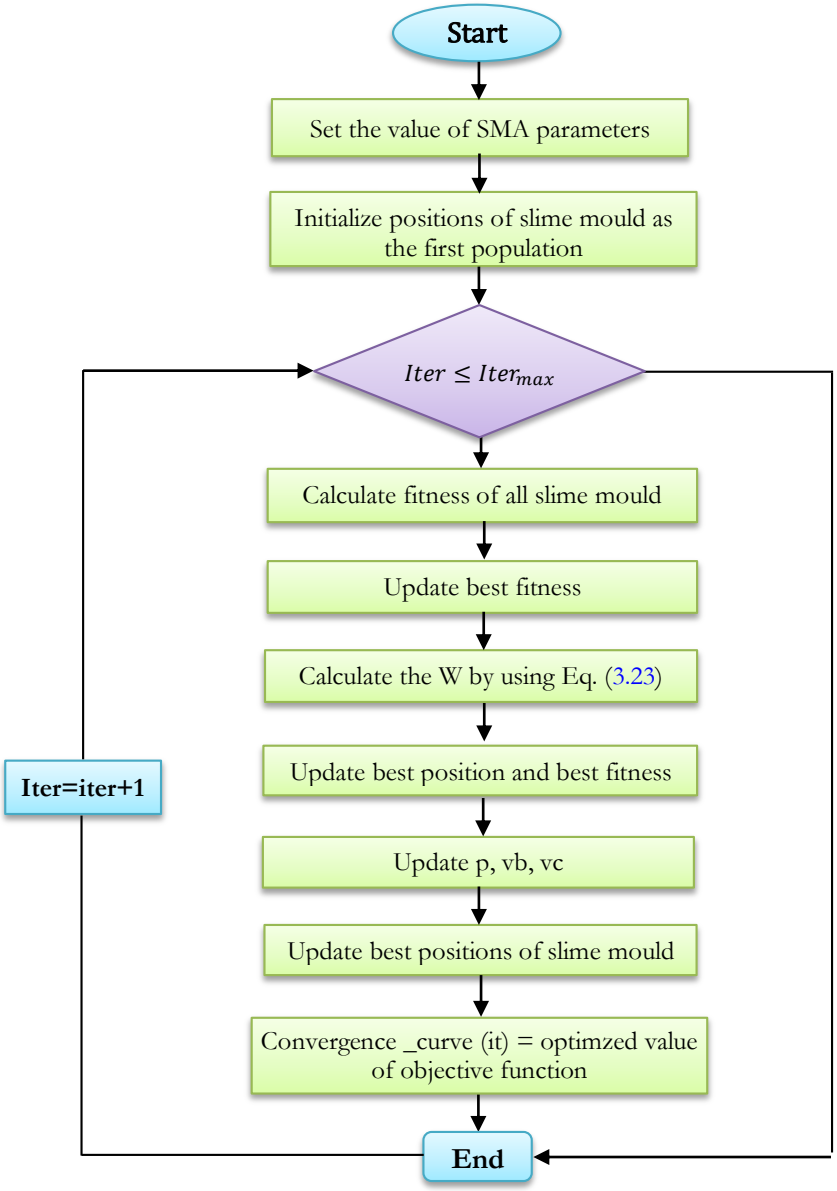

Figure 3.2 Flowchart of the SMA Algorithm based optimal power flow

3.3.3. Ant Lion Optimization Algorithm (ALO)

Ant lion optimization algorithm ALO is a new nature-inspired proposed by Seyedali Mirjalili in 2015 [78], to solve any optimization problems of constrained engineering. The ALO algorithm is modeled based on the hunting mechanism of Antlions in nature. The benefits of the ALO algorithm can find optimal solutions for minimizing the objective function. The ALO algorithm mimics the hunting behavior of ant lions, i.e., the interaction between ant lions and ants. In this context, five main steps of hunting prey as the random walk of ants, trapping in antlions traps, building traps, sliding ants against toward Antlion, Catching prey, and rebuilding traps are implemented. Figure 3.3 shows some of the different steps that describe the relationship between antlions and ants.

a) **b)** **c)**

Figure 3.3 a) Cone-shaped traps **b)** Sliding ants toward Antlion **c)** catching the prey [78]

In this algorithm, ants move stochastically in nature when searching for food. The expression mathematically of being the random walks of ants for detecting the location of food describes in Eq. (3.26):

$$X(t)=\left[0, cumsu\left(2r(t_1)-1\right), cumsu\left(2r(t_2)-1\right), \ldots, cumsu\left(2r(t_n)-1\right)\right] \quad \textbf{(3.26)}$$

where $X(t)$ are the random walks of ants, n is the max-iterations, t is the step of random walk, and $r(t)$ is a function defined as follows:

$$r(t)=\begin{cases}1 & if \quad rand > 0.5\\ 0 & if \quad rand < 0.5\end{cases} \quad \textbf{(3.27)}$$

where *rand* is a randomly generated number uniformly distributed in the range of [0,1].

The Details of different steps of the ALO algorithm describe the relationship between predators (ant lions) and prey (ant) are explained as [78]:

3.3.3.1. Random walk of ants

In every step of optimization, ants update their positions with a random walk, these random

walks are all based on Eq. (3.28), all the positions of ants are inside the boundary of the search space, since every search space has a boundary, the random walks of ants is normalized by using the following equation:

$$X_i^t = \frac{\left(X_i^t - a_i\right) * \left(d_i^t - c_i^t\right)}{\left(b_i - a_i\right)} + c_i^t \quad \textbf{(3.28)}$$

where a_i and b_i are respectively the minimum and maximum of random walk corresponding of i^{th} variable. c_i^t and d_i^t are respectively indicated the minimum and maximum of ith variables at tth iteration.

3.3.3.2. Trapping in antlions traps

The influence of antlions traps on random walks of ants is expressed as follows:

$$c_i^t = Antlion_j^t + c^t \quad \textbf{(3.29)}$$

$$d_i^t = Antlion_j^t + d^t \quad \textbf{(3.30)}$$

3.3.3.3. Building traps

During optimization, The ALO algorithm is required to use a roulette wheel operator for selecting Antlions based on their fitness for giving a high chance for catching ants.

3.3.3.4. Sliding ants against toward antlion

With the mechanisms proposed so far, Antlions are capable to build traps proportional to their fitness, and ants are required to move randomly near the center of the pit. However, once Antlions realize that an ant is in the trap, they shoot sands outwards the center of the pit. This mechanism mathematically is proposed modeled as follow:

$$c^t = \frac{c^{t-1}}{I} \quad \textbf{(3.31)}$$

$$d^t = \frac{d^{t-1}}{I} \quad \textbf{(3.32)}$$

3.3.3.5. Catching preys and rebuilding the traps

The final step of hunting is when an ant reaches into the bottom of the Antlion pit and is caught in the Antlion's jaw. After this step, the predator pulls the ant inside the sand and consumes its body. Then the Antlion is required to update its position to the latest position of the hunted ant to enhance its chance of catching new prey. Catching prey and re-building the pits calculated as given by the following equation:

$$Antlion_i^t = Ant_i^t, \quad if \ f\left(Ant_i^t\right) > f\left(Antlion_j^t\right) \tag{3.33}$$

where $Antlion_i^t, Ant_i^t$ is jth the position of the selected antlion and ant at iteration t.

3.3.3.6. Elitism

Elitism is one of the most important characteristics of all evolutionary algorithms. The elitism of an ant lion is calculated by using the roulette wheel. In this study, the best solution(s) obtained by the ALO algorithm at any iteration is saved as elite. The elitism mechanism is mathematically described as follows:

$$Ant_i^t = \frac{R_A^t + R_E^t}{2} \tag{3.34}$$

where R_A^t is the random walk around the antlion and is selected by using the roulette wheel at *t-th* iteration, R_E^t is the random walk around the elite at *t-th* iteration.

3.3.4. Implementation of ALO algorithm to OPF problem

The implementation of the ALO algorithm to solve the OPF problem that minimizes the objective function can be summarized in the steps below.

1. Read the system data (bus data, line data, and generator data);
2. Initialize the parameters of search agents, size of the population, the maximum number of iterations, the number and position of the control variables;
3. Initialize the random walks of ants and Antlions using Eq. (3.28) as the first population;
4. Maps control variables from ants into the load flow;
5. Find the best Antlions, and consider it as the elite;
6. If the maximum number of iterations is achieved, go to step 7. Otherwise, loop to step 5;
7. Select the antlions based on the roulette wheel and update the *c* and *d* values using Eqs. (3.31) and (3.32);
8. Generate a stochastic walk and use Eqs. (3.26) and (3.28) to normalize it;
9. Update the positions of the ant using Eq. (3.34);
10. If the variables are out of limits, tagging at the limits. Otherwise, go to step 11.
11. Calculate the fitness values of all ants;
12. Replace an antlion with its corresponding ant if it becomes fitter using Eq. (3.33);
13. Update the elite with antlion if an antlion becomes better;
14. The elite comprised the best fitness value was selected. Then, the best value of the objective function was determined;

The flowchart of the implementation of the proposed algorithm ALO for solving the OPF problem is shown in Fig. 3.4.

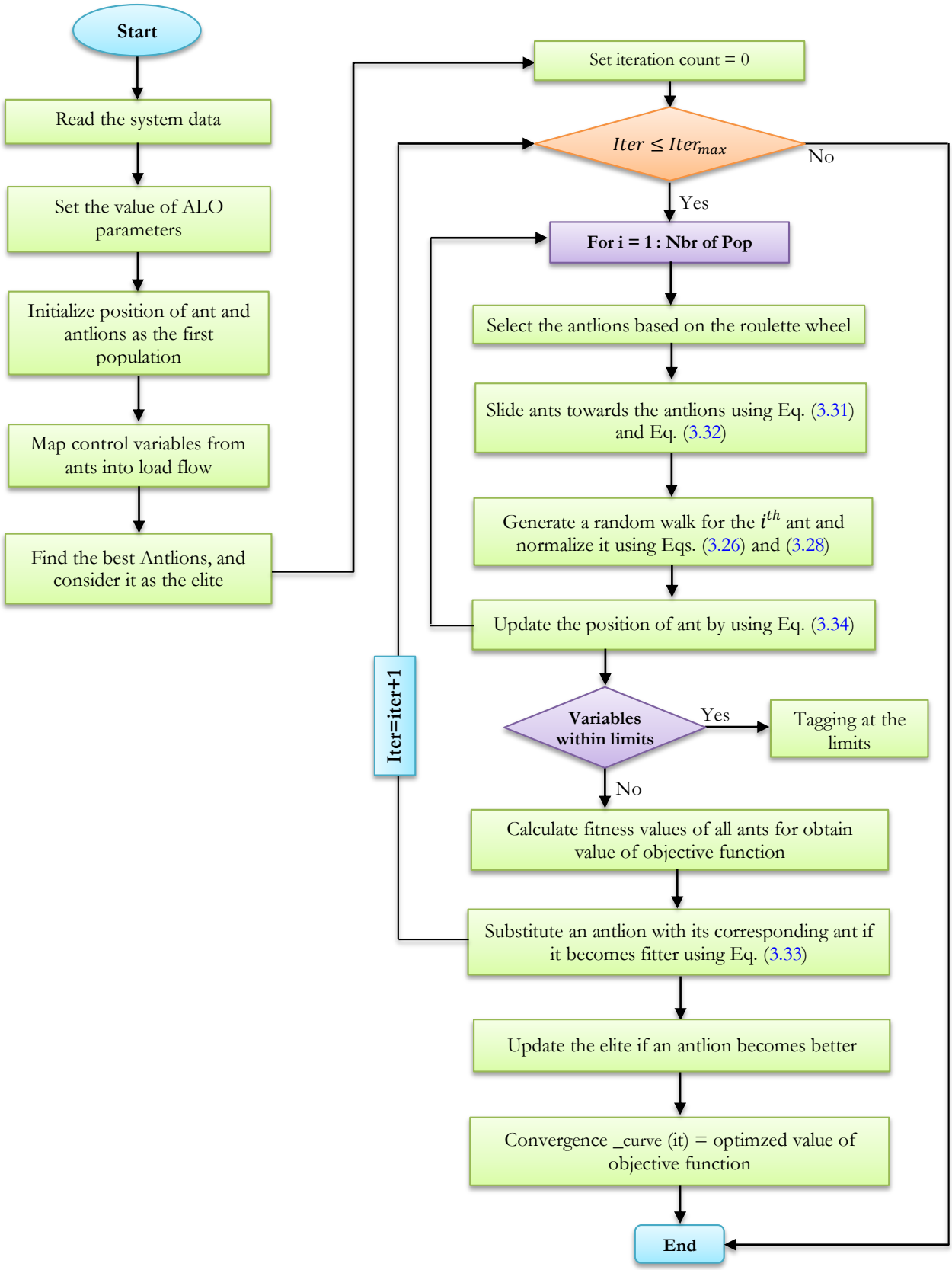

Figure 3.4 Flowchart of the ALO algorithm based optimal power flow

3.4. OPF solution using SMA and ALO algorithms

This section is dedicated to the application of the proposed algorithms SMA and ALO to solve the optimal power flow (OPF) problem on IEEE 30-bus, IEEE 57-bus, and large-scale Algerian 114-bus systems. Dissimilar objective functions have been considered to verify the efficiency and performance of the proposed algorithms according to the optimal adjustment of control variables.

All the simulations are carried out by MATLAB programming language and MATPOWER. MATPOWER is a package of MATLAB M-files for electric power system analysis and simulation. The simulations are performed on a computer with specification Intel® Core™ i5 CPU@1.80 GHz and 8Go RAM. For establishing the superiority of the three proposed algorithms, 30 independent trial runs are performed for all the test cases with a comparative study reported in the following section, the population size (NP = 40) and number of iterations maximal (Max_{iter} = 500).

3.4.1. IEEE 30-bus system

In order to verify the performance and efficiency of the proposed algorithms to solve the OPF problem, we perform simulations in the first test on the standard IEEE 30-bus power system. This system consists of 6 generators, 41 transmission lines of which 4 transformers with off-nominal taps ratio located on lines 6–9, 4–12, 9–12 and 27–28. In addition, nine reactive power sources were installed on buses 10, 12, 15, 17, 20, 21, 23, 24, and 29. This electrical system supplies 20 loads of 283.4 MW and 73.5 MVar. Figure 3.5 shows the IEEE 30-bus power system topology.

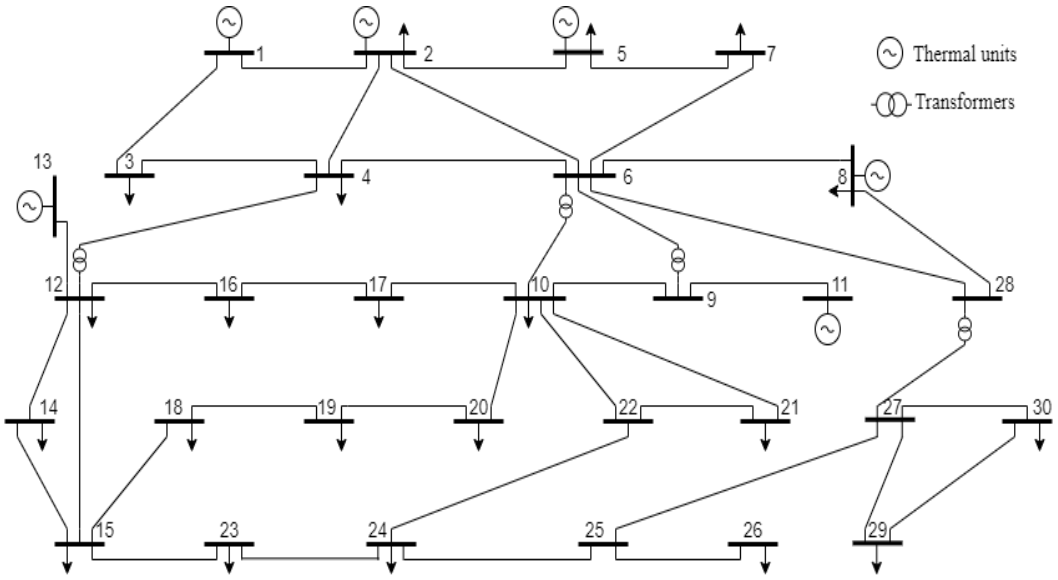

Figure 3.5 Single line diagram of the IEEE 30-bus test system

The parameters of production, consumption and the characteristics of the lines of the IEEE 30-bus test system are indicated in the tables of Annex B. The upper limit and lower limit of the control variables of the IEEE 30 bus system are shown in Table 3.1.

Table 3.1 Limits of various variables for the IEEE 30-bus test system

Variables limits	Lower limits (p.u)	Upper limits (p.u)
Voltages for generator bus	0.9	1.1
Voltages for load bus	0.9	1.1
Tap setting	0.9	1.1
Shunt compensators	0.0	0.05

3.4.1.1. Case 1: Minimization of generation fuel cost

In the first case, the quadratic equation of the generation fuel cost of thermal generators is formulated as the objective function with satisfying all system constraints. This objective function was described by Eq. (3.4). The proposed algorithms are tested to find the optimal fuel cost according to the optimal power distribution of the production units. The best settings of the control variables obtained via the proposed algorithms SMA and ALO are reported in Table 3.2.

Table 3.2 Comparative results of the OPF solution for case 1 via SMA & ALO (IEEE 30-bus system)

Control Variables	Variables limits		SMA	ALO
	Min	Max		
$P_{G1}(MW)$	50	200	177.5784	176.9576
$P_{G2}(MW)$	20	80	48.6770	48.6042
$P_{G5}(MW)$	15	50	21.2668	21.2555
$P_{G8}(MW)$	10	35	21.2316	21.3928
$P_{G11}(MW)$	10	30	12.0890	11.7925
$P_{G13}(MW)$	12	40	12.0000	12.0000
$V_{G1}(p.u)$	0.95	1.1	1.1000	1.1000
$V_{G2}(p.u)$	0.9	1.1	1.0879	1.0881
$V_{G5}(p.u)$	0.9	1.1	1.0618	1.0621
$V_{G8}(p.u)$	0.9	1.1	1.0701	1.0700
$V_{G11}(p.u)$	0.9	1.1	1.1000	1.1000
$V_{G13}(p.u)$	0.9	1.1	1.1000	1.1000
$T_{11}(p.u)$	0.9	1.1	1.0259	1.0337
$T_{12}(p.u)$	0.9	1.1	0.9010	0.9453
$T_{15}(p.u)$	0.9	1.1	0.9803	1.0051
$T_{36}(p.u)$	0.9	1.1	0.9568	0.9823
$Q_{C10}(MVar)$	0	5	4.3806	3.2893
$Q_{C12}(MVar)$	0	5	4.7790	0.0001
$Q_{C15}(MVar)$	0	5	4.8272	1.6464
$Q_{C17}(MVar)$	0	5	4.9942	4.9197
$Q_{C20}(MVar)$	0	5	2.5651	3.8171
$Q_{C21}(MVar)$	0	5	2.8396	4.5247
$Q_{C23}(MVar)$	0	5	3.4609	3.6910
$Q_{C24}(MVar)$	0	5	4.9957	4.4806
$Q_{C29}(MVar)$	0	5	1.1562	3.4357
Fuel cost ($/h)			**798.9709**	**799.0133**
Power losses (MW)			8.5752	8.6026

Table 3.2 summarizes the comparative results of the optimal settings values obtained by SMA and ALO. From this table, it can be seen that all optimal values of control variables are within their acceptable limits. Moreover, the results indicate that the fuel cost and the active power losses applying SMA lead to 798.9709 $/h and 8.5752 MW, respectively, which is less compared to the ALO algorithm. Thus, the SMA is more effective for the OPF solution compared with the ALO. The convergence characteristics of fuel cost minimization for the standard IEEE 30-bus test system via the proposed algorithms over iterations are shown in Fig. 3.6. It can be seen that the SMA algorithm outperforms the ALO algorithm in terms of convergence rate towards the global optimum solution. So, the results achieved showed the SMA was superior and robust compared to the ALO algorithm in order to get the best solution to solve the OPF problem.

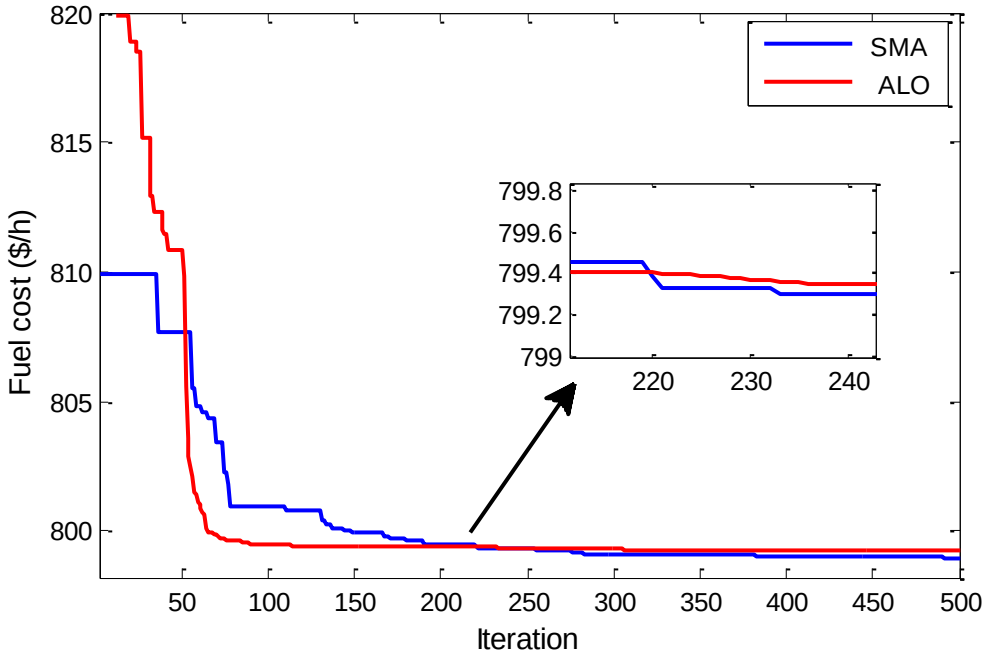

Figure 3.6 Convergence characteristics of SMA and ALO for the IEEE 30-bus system: Case 1

Table 3.3 shows that the results achieved by the SMA and ALO are better compared to some other available algorithms in the literature, which proves the effectiveness of the proposed algorithms to minimize the fuel cost in the IEEE 30-bus system based on optimal adjustment of control variables.

Table 3.3 Comparison of solutions for fuel cost minimization in IEEE 30-bus system: **Case 1**

Method		Fuel cost ($/h)	Method description
SMA		798.9709	Slime mould algorithm
ALO		799.0133	Ant lion optimizer
MFO	[73]	799.072	Moth-Flame Optimizer
GSO	[55]	799.06	Glowworm Swarm Optimization
MSCA	[74]	799.31	Modified Sine-Cosine algorithm
BHBO	[63]	799.921	Black-hole-based optimization
DSA	[56]	800.3887	Differential search algorithm
ABC	[59]	800.6600	Artificial bee colony
MSA	[53]	800.5099	Moth swarm algorithm

3.4.1.2. Case 2: Minimization of active power transmission losses

The second case investigated for minimizing the active power transmission losses. The best values of the control variables obtained by the implemented algorithms SMA and ALO for case 2 are reported in Table 3.4. From this table, the active power losses obtained by the proposed algorithms are 2.8612 MW and 2.8723 MW, which are lowered by 66.63 % (SMA) and 66.61 % (ALO), respectively, compared to case 1 (8.5752 MW and 8.6026 MW). Moreover, the results achieved indicate that the SMA gives better values to minimize the active power losses and fuel cost compared to the ALO algorithm.

Table 3.4 Comparative results of the OPF solution for case 2 via SMA & ALO (IEEE 30-bus system)

Control variables	Variables limits		SMA	ALO
	Min	Max		
$P_{G1}(MW)$	50	200	51.2614	51.2723
$P_{G2}(MW)$	20	80	80.0000	80.0000
$P_{G5}(MW)$	15	50	50.0000	50.0000
$P_{G8}(MW)$	10	35	34.9999	35.0000
$P_{G11}(MW)$	10	30	30.0000	30.0000
$P_{G13}(MW)$	12	40	40.0000	40.0000
$V_{G1}(p.u)$	0.95	1.1	1.1000	1.1000
$V_{G2}(p.u)$	0.9	1.1	1.0979	1.0983
$V_{G5}(p.u)$	0.9	1.1	1.0793	1.0813
$V_{G8}(p.u)$	0.9	1.1	1.0876	1.0884
$V_{G11}(p.u)$	0.9	1.1	1.1000	1.1000
$V_{G13}(p.u)$	0.9	1.1	1.1000	1.1000
$T_{11}(p.u)$	0.9	1.1	1.0331	0.9856
$T_{12}(p.u)$	0.9	1.1	0.9193	1.0171
$T_{15}(p.u)$	0.9	1.1	0.9870	0.9962
$T_{36}(p.u)$	0.9	1.1	0.9834	0.9927
$Q_{C10}(MVar)$	0	5	1.0281	4.9546
$Q_{C12}(MVar)$	0	5	0.2155	5.0000
$Q_{C15}(MVar)$	0	5	4.7108	5.0000
$Q_{C17}(MVar)$	0	5	2.4109	5.0000
$Q_{C20}(MVar)$	0	5	4.9982	5.0000
$Q_{C21}(MVar)$	0	5	4.9042	4.4835
$Q_{C23}(MVar)$	0	5	0.3454	4.5061
$Q_{C24}(MVar)$	0	5	4.9181	3.1373
$Q_{C29}(MVar)$	0	5	2.8276	4.8256
Fuel cost ($/h)			967.0437	967.0702
Power losses (MW)			**2.8612**	**2.8723**
Voltage deviation (p.u.)			1.9139	2.0044

The convergence characteristics of the active power losses with SMA and ALO over iterations are shown in Fig. 3.7. This figure shows that the SMA has a better optimum value of the objective function compared to the ALO algorithm.

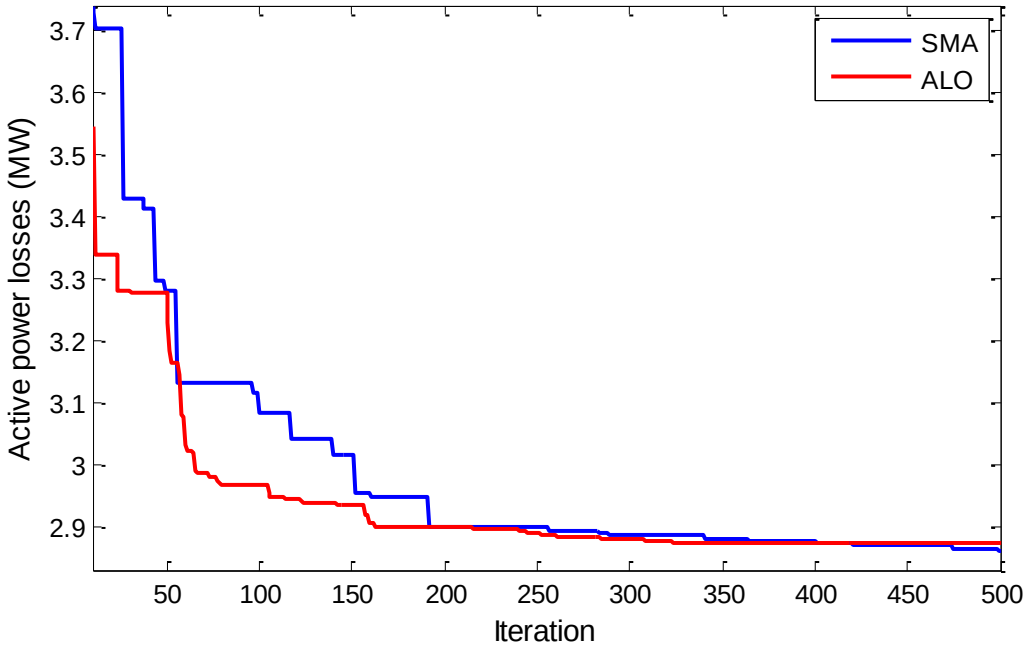

Figure 3.7 Convergence characteristics of SMA and ALO for the IEEE 30-bus system: Case 2

Table 3.5 shows the active power losses achieved via the proposed algorithms compared to several algorithms in the literature, which made sense that the proposed algorithms give the best values compared to those found by MSA, FPA, MSCA, and BHBO.

Table 3.5 Comparison of solutions for active power loss minimization in IEEE 30-bus system: **Case 2**

Method		Real power losses (MW)	Method description
SMA		2.8612	Slime mould algorithm
ALO		2.8723	Ant lion optimizer
MSA	[53]	3.1005	Moth swarm algorithm
FPA	[73]	3.115	Flower Pollination Algorithm
MSCA	[74]	2.9334	Modified moth swarm algorithm
BHBO	[63]	3.503	Black-Hole-Based Optimization

3.4.1.3. Case 3: Voltage profile improvement

This case aimed to improve the voltage profile by minimization of the objective function, which is the sum of the total fuel cost and TVD. Table 3.6 listed the result obtained by the proposed algorithms for this case. From this table, the SMA algorithm leads to a total voltage deviation of 0.1045 p.u, which is lower than the ALO algorithm (0.1122 p.u). Furthermore, the TVD obtained by the proposed algorithms for this case is low compared with case1. The convergence characteristics of the total voltage deviation with SMA and ALO over iterations are shown in Fig. 3.8. It allows us to note, in the first place, that the SMA and ALO algorithms converge to optimal active power loss with a few number iterations.

Table 3.6 Comparative results of the OPF solution for case 3 via SMA & ALO (IEEE 30-bus system)

Control variables	Variables limits		SMA	ALO
	Min	Max		
$P_{G1}(MW)$	50	200	176.6000	165.5240
$P_{G2}(MW)$	20	80	48.7151	46.0460
$P_{G5}(MW)$	15	50	20.6913	20.7869
$P_{G8}(MW)$	10	35	24.0425	27.7180
$P_{G11}(MW)$	10	30	11.1974	17.9640
$P_{G13}(MW)$	12	40	12.0000	14.2826
$V_{G1}(p.u)$	0.95	1.1	1.0386	1.0334
$V_{G2}(p.u)$	0.9	1.1	1.0215	1.0185
$V_{G5}(p.u)$	0.9	1.1	1.0120	1.0043
$V_{G8}(p.u)$	0.9	1.1	1.0012	1.0045
$V_{G11}(p.u)$	0.9	1.1	1.0743	1.0430
$V_{G13}(p.u)$	0.9	1.1	0.9967	0.9983
$T_{11}(p.u)$	0.9	1.1	1.0922	1.0489
$T_{12}(p.u)$	0.9	1.1	0.9000	0.9000
$T_{15}(p.u)$	0.9	1.1	0.9533	0.9570
$T_{36}(p.u)$	0.9	1.1	0.9716	0.9757
$Q_{C10}(MVar)$	0	5	1.1213	4.2708
$Q_{C12}(MVar)$	0	5	0.1221	2.9820
$Q_{C15}(MVar)$	0	5	5.0000	3.5300
$Q_{C17}(MVar)$	0	5	2.8105	2.8405
$Q_{C20}(MVar)$	0	5	5.0000	4.7806
$Q_{C21}(MVar)$	0	5	4.9967	1.8195
$Q_{C23}(MVar)$	0	5	4.9518	4.5700
$Q_{C24}(MVar)$	0	5	4.5074	4.7540
$Q_{C29}(MVar)$	0	5	3.3481	4.7127
Fuel cost ($/h)			803.6474	805.6366
Power losses (MW)			9.8464	8.9216
Voltage deviation (p.u.)			**0.1045**	**0.1122**

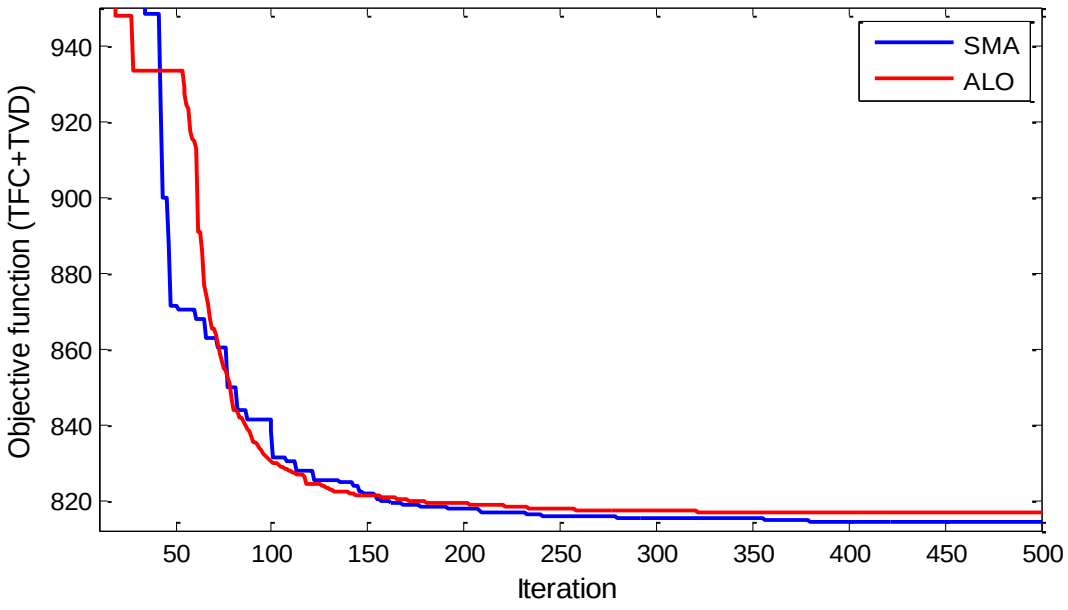

Figure 3.8 Convergence characteristics of SMA and ALO for the IEEE 30-bus system: Case 3

Table 3.7 reveals comparison results of proposed algorithms and other existing algorithms for voltage deviation improvement. This table displays that the results achieved by SMA and ALO are better than PSO, FPA, and BHBO.

Table 3.7 Comparison of solutions for voltage profile improvement in IEEE 30-bus system: **Case 3**

Method		Voltage deviation (p.u)	Method description
SMA		0.1045	Slime mould algorithm
ALO		0.1122	Ant lion optimizer
PSO	[73]	0.1506	Particle Swarm Optimization
FPA	[73]	0.1845	Flower Pollination Algorithm
BHBO	[63]	0.1262	Black-Hole-Based Optimization

3.4.2. IEEE 57-bus system

The second test is carried out on an IEEE-57 bus test system. This system involves the following characteristics, 7 generators at the buses 1, 2, 3, 6, 8, 9 and 13, 80 transmission lines, 15 branches under load tap setting transformer branches and 3 reactive compensators are installed on buses 18, 25 and 53 [127]. The total load demand of this system is 1250.8 MW + j 336.4 MVAR. The parameters of production, consumption and the characteristics of the lines of this test system are indicated in the tables of Annex C. Table 3.8 shows the lower and upper limits of the control variables of the IEEE 57-bus system.

Table 3.8 Limits of various variables for IEEE 57-bus test system

Variables limits	Lower limits (p.u)	Upper limits (p.u)
Voltages for generator bus	0.9	1.1
Voltages for load bus	0.94	1.06
Tap setting	0.9	1.1
Shunt compensators	0.0	0.3

3.4.2.1. Case 4: Minimization of generation fuel cost

In this case, it is aimed to optimize the fuel cost in the IEEE 57-bus test system. The optimal values of control variables obtained by the proposed algorithms are summarized in Table 3.9. From this table, it can be seen that the control variables are all within their acceptable limits. Furthermore, the results obtained indicate that the fuel cost using SMA leads to 41649.0605 $/h, which is less compared to ALO (41685.9465 $/h). The convergence characteristics of fuel cost using SMA and ALO algorithms for the IEEE 57-bus test system are shown in Fig. 3.9. From this figure, we notice that the proposed algorithms converge towards the global optimum solution at iteration 100, which indicates that the SMA and ALO directed quickly towards their optimal solution values.

Table 3.9 Comparative results of the OPF solution for case 4 via SMA & ALO (IEEE 57-bus system)

Control variables	SMA	ALO	Control variables	SMA	ALO
P_{G1}	142.8872	140.6063	T_{24-25}	1.0137	1.0754
P_{G2}	92.4226	91.4841	T_{24-25}	1.0781	1.0247
P_{G3}	44.6670	45.8410	T_{24-26}	1.0470	1.0638
P_{G6}	72.4734	94.8250	T_{7-29}	1.0513	1.0726
P_{G8}	458.4371	445.0079	T_{34-36}	0.9616	1.0282
P_{G9}	97.2759	93.1700	T_{11-41}	0.9000	1.0776
P_{G12}	357.1277	354.8164	T_{15-45}	1.0010	1.0190
V_{G1}	1.0948	1.0964	T_{14-46}	0.9964	1.0116
V_{G2}	1.0940	1.0951	T_{10-51}	1.0132	1.0240
V_{G3}	1.0897	1.0894	T_{13-49}	0.9772	1.0145
V_{G6}	1.0985	1.0991	T_{11-43}	0.9983	1.0137
V_{G8}	1.1000	1.1000	T_{40-56}	0.9263	1.0702
V_{G9}	1.0797	1.0807	T_{39-57}	0.9477	1.0676
V_{G12}	1.0823	1.0866	T_{9-55}	1.0656	1.0814
T_{4-18}	0.9160	1.0853	Q_{C18}	14.6662	23.6474
T_{4-18}	1.0860	1.0959	Q_{C25}	20.1988	21.9625
T_{21-20}	0.9743	1.0831	Q_{C53}	15.5750	15.8937

	SMA	ALO
Fuel cost ($/h)	**41649.0605**	**41685.9465**
Power losses (MW)	14.4910	14.9506
Voltage deviation (p.u)	2.2188	1.8389

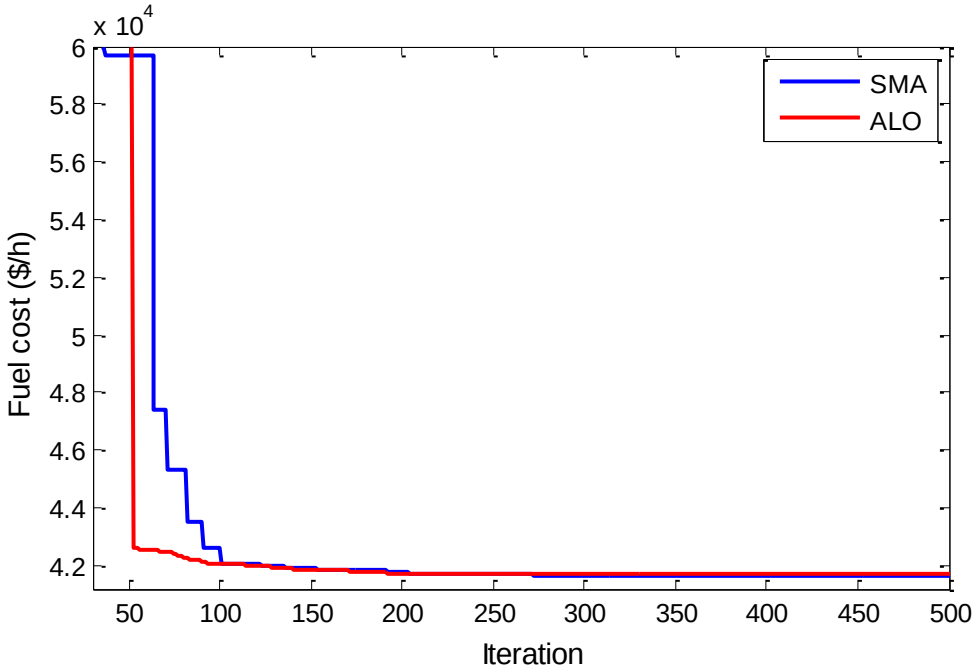

Figure 3.9 Convergence characteristics of SMA and ALO for the IEEE 57-bus system: Case 4

In addition, the best fuel costs obtained by SMA and ALO algorithms are better compared to different algorithms in the literature as shown in Table 3.10. This comparative study shows the ability of the proposed algorithm to reach the global optimum better for the IEEE 57-bus system than the other algorithms previously reported in this table.

Table 3.10 Comparison of solutions for fuel cost minimization in IEEE 57-bus system: **Case 4**

Method		Fuel cost ($/h)	Method description
SMA		41649.0605	Slime mould algorithm
ALO		41685.9465	Ant lion optimizer
IHDE	[128]	41667.9900	Improved Hybrid Differential Evolution
DSA	[56]	41686.8200	Differential search algorithm
MSA	[53]	41673.7231	Moth swarm algorithm
GBICA	[129]	41740.2884	Gaussian bare-bones imperialist competitive algorithm
MGBICA	[129]	41715.7101	Multi- objective GBICA
IEM	[130]	41810.2161	Improved electromagnetism-like mechanism

3.4.2.2. Case 5: Minimization of active power transmission losses

In the present case, the adopted objective function is the active power transmission losses minimization for the IEEE 57-bus system. The optimal control variables of SMA and ALO for case 5 are shown in Table 3.11. From this table, the active power losses obtained by the SMA and ALO are less compared to the base case, which are lowered by 34.40 and 24.82 %, respectively. Furthermore, the results indicate also that the active power losses using SMA lead to 9.5058 MW, which is less compared to the ALO algorithm (11.2398 MW). Thus, The greatest reduction is achieved by SMA.

Table 3.11 Comparative results of the OPF solution for case 5 via SMA & ALO (IEEE 57-bus system)

Control variables	SMA	ALO	Control variables	SMA	ALO
P_{G1}	165.6381	143.8743	T_{24-25}	1.0513	1.0999
P_{G2}	39.9661	49.3870	T_{24-25}	1.0800	1.0510
P_{G3}	132.5205	132.2972	T_{24-26}	1.0233	1.0538
P_{G6}	100.0000	89.4968	T_{7-29}	1.0176	1.0859
P_{G8}	312.1959	341.9428	T_{34-36}	0.9791	1.0652
P_{G9}	99.9851	95.0416	T_{11-41}	0.9872	1.0617
P_{G12}	410.0000	410.0000	T_{15-45}	0.9878	1.0699
V_{G1}	1.0999	1.0999	T_{14-46}	0.9817	1.0663
V_{G2}	1.0971	1.0977	T_{10-51}	0.9962	1.0657
V_{G3}	1.0995	1.0997	T_{13-49}	0.9692	1.0031
V_{G6}	1.0996	1.0980	T_{11-43}	0.9664	1.0886
V_{G8}	1.1000	1.1000	T_{40-56}	1.0293	1.0264
V_{G9}	1.0839	1.0839	T_{39-57}	0.9780	1.0446
V_{G12}	1.0901	1.0905	T_{9-55}	1.0227	1.0508
T_{4-18}	1.0061	1.0749	Q_{C18}	18.8791	25.0555
T_{4-18}	1.0967	1.0738	Q_{C25}	17.3895	25.1494
T_{21-20}	1.0083	1.0538	Q_{C53}	16.5088	25.8328
		SMA			**ALO**
Fuel cost ($/h)		44327.95			44116.89
Power losses (MW)		**9.5058**			**11.2398**
Voltage deviation (p.u)		2.7557			2.0013

The convergence curves of the considered optimizers over iterations are shown in Fig. 3.10. This figure illustrates that the convergence characteristics of the ALO towards the global optimum at iteration 235 whereas the SMA algorithm convergence towards the optimal solution is reached at iteration 240.

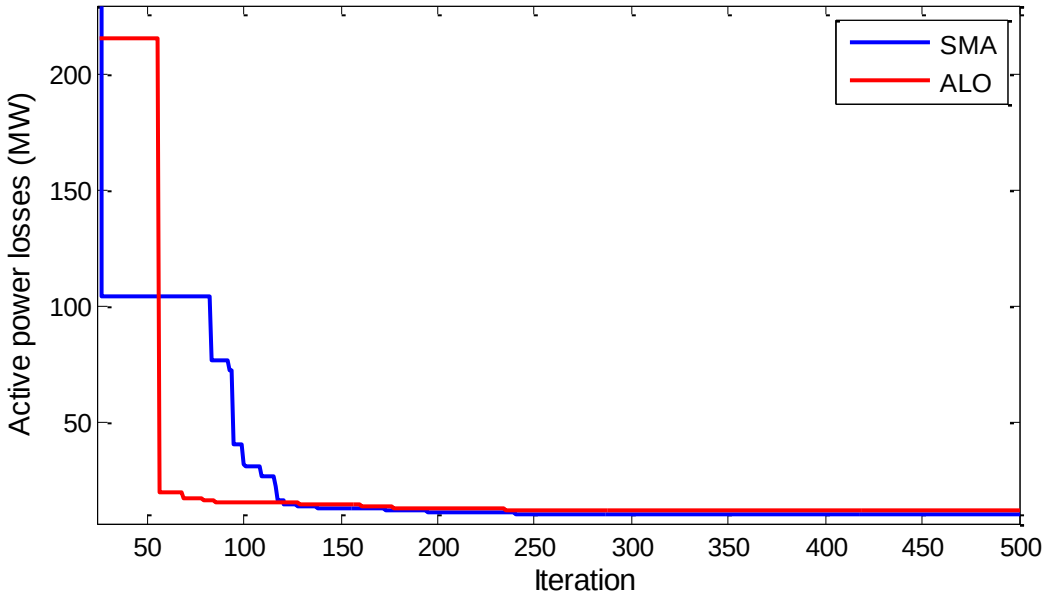

Figure 3.10 Convergence characteristics of SMA and ALO for the IEEE 57-bus system: Case 5

Table 3.12 shows the active power losses obtained by the proposed algorithms and several algorithms in the literature. From this Table, the proposed algorithms can get less active power losses than several algorithms previously reported in this table, which show the ability of the proposed algorithms to reach the global optimum solution.

Table 3.12 Comparison of solutions for active power loss minimization in IEEE 57-bus system: **Case 5**

Method		Active power losses (MW)	Method description
SMA		9.5058	Slime mould algorithm
ALO		11.2398	Ant lion optimizer
AMO	[131]	10.510	Animal migration optimization
ABC	[132]	12.630	Artificial bee colony algorithm
IABC	[132]	11.160	Improved artificial bee colony algorithm
TSA	[133]	12.473	Tree-seed algorithm

3.4.3. Algerian 114-bus system

This scenario aims to test proposed algorithms to solve non-linear problems in larger dimensions. The OPF is performed on the large-scale power system Algerian 114-bus. This test system consists of 15 generators, 175 transmission lines of which 16 transformers with off-nominal taps ratio are located from line 160 to line 175, and 99 load buses [134]. The total load demand for this system is 3,727 MW +j 2070 MVar. Figure 3.11 shows the map of the Algerian electric power system.

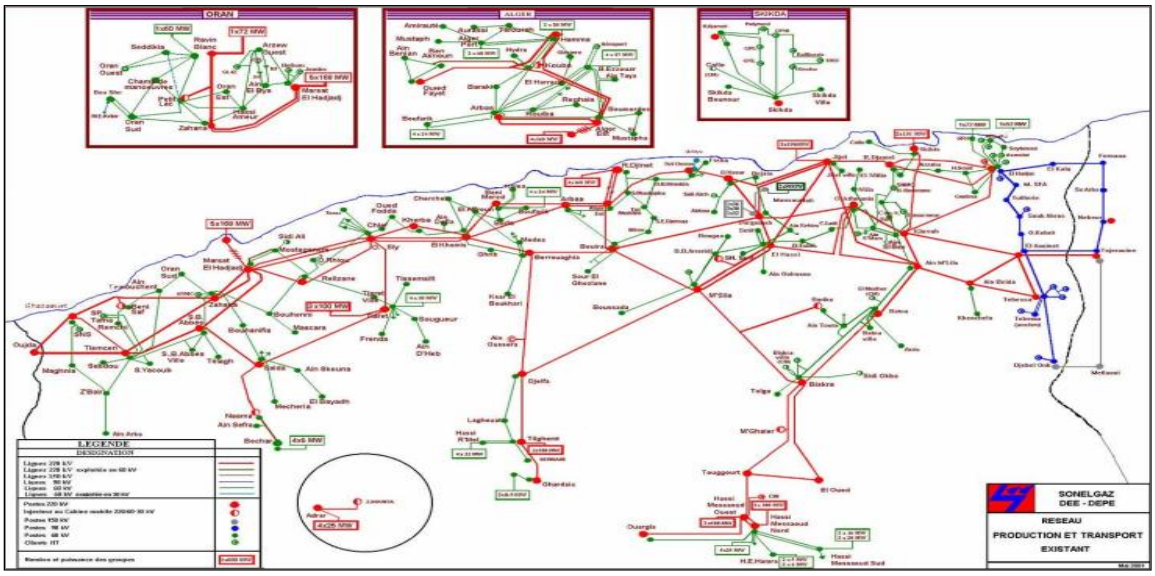

Figure 3.11 Algerian electric power system map

The parameters of production, consumption and characteristics of the lines of this test system are indicated in the tables of Annex D. Table 3.13 displays the technical and economic parameters of fifteen generators of the Algerian electrical network system (ALG 114-bus system). The lower and upper limits of the control variables for the Algerian 114-bus system are represented in Table 3.14.

Table 3.13 Technical admissible parameters of generators and the fuel cost coefficients

JB N°	P_i^{max}	P_i^{min}	A_i ($/h$)	B_i($/MW*h$)	C_i($/MW^2*h$)
4	135,00	1350,00	0	1,500	0,0085
5	135,00	1350,00	0	1,500	0,0085
11	10,000	100,000	0	2,500	0,0170
15	30,000	300,000	0	2,500	0,0170
17	135,00	1350,00	0	1,500	0,0085
19	34,500	345,000	0	2,500	0,0170
22	34,500	345,000	0	2,500	0,0170
52	34,500	345,000	0	2,500	0,0170
80	34,500	345,000	0	2,500	0,0170
83	30,000	300,000	0	2,500	0,0170
98	30,000	300,000	0	2,500	0,0170
100	60,000	600,000	0	2,000	0,0030
101	20,000	200,000	0	2,000	0,0030
109	10,000	100,000	0	2,500	0,0170
111	10,000	100,000	0	2,500	0,0170

Table 3.14 Limits of various variables for the ALG 114-bus test system

Variables limits	Lower limits (p.u)	Upper limits (p.u)
Voltages for generator bus	0.9	1.1
Voltages for load bus	0.9	1.1
Tap setting	0.9	1.1
Shunt compensators	0.0	0.25

3.4.3.1. Case 6: Minimization of generation fuel cost

In the last case, the proposed algorithms are applied for the total fuel cost minimization in the ALG 114-bus system. The optimal values of control variables achieved for this case using SMA and ALO algorithms over 30 independent runs are summarized in Table 3.15. From this table, all control variables are within the specified limits. In addition, the total fuel cost, as well as active power losses obtained by the SMA algorithm, are 18868.9917 $/h and 52.8438 MW respectively, which are less compared to the optimal solutions obtained by the ALO algorithm (18930.7826 $/h and 58.4519 MW). As a result, obtained results confirm that the SMA can define the optimal solution in a large-scale power system.

Table 3.15 Comparative results of the OPF solution for case 6 via SMA & ALO (ALG 114-bus system)

Control variables	SMA	ALO	Control variables	SMA	ALO
P_{G4}	454.0793	439.4925	V_{G101}	1.0998	1.1000
P_{G5}	450.7834	452.3345	V_{G109}	1.1000	1.0836
P_{G11}	100.0000	99.3464	V_{G111}	1.0743	1.0923
P_{G15}	190.3169	191.9859	T_{160}	0.9035	1.0669
P_{G17}	446.1000	448.7036	T_{161}	0.9553	0.9776
P_{G19}	191.0548	202.2739	T_{162}	0.9695	0.9917
P_{G22}	192.0894	177.1619	T_{163}	0.9892	1.0868
P_{G52}	188.6942	205.2245	T_{164}	0.9490	1.0686
P_{G80}	187.6992	188.8209	T_{165}	0.9687	1.0642
P_{G83}	188.1846	183.0188	T_{166}	0.9874	1.0871
P_{G98}	190.8419	197.0890	T_{167}	0.9613	1.0566
P_{G100}	600.0000	600.0000	T_{168}	0.9689	1.0610
P_{G101}	199.9999	200.0000	T_{169}	0.9753	1.0490
P_{G109}	100.0000	100.0000	T_{170}	0.9889	1.0964
P_{G111}	100.0000	100.0000	T_{171}	0.9746	1.0581
V_{G4}	1.0923	1.1000	T_{172}	1.0026	1.0751
V_{G5}	1.0900	1.0998	T_{173}	0.9905	1.0496
V_{G11}	1.0785	1.0960	T_{174}	1.0067	1.0776
V_{G15}	1.0909	1.1000	T_{175}	0.9803	1.0558
V_{G17}	1.0975	1.1000	Q_{C41}	20.3717	18.8666
V_{G19}	1.0965	1.0403	Q_{C50}	8.9973	17.7671
V_{G22}	1.1000	1.0657	Q_{C55}	14.1005	9.6416
V_{G52}	1.1000	1.0505	Q_{C66}	24.3168	20.5759
V_{G80}	1.0990	1.1000	Q_{C67}	10.8673	22.8733
V_{G83}	1.0999	1.1000	Q_{C77}	3.3790	22.6442
V_{G98}	1.0996	1.1000	Q_{C93}	18.0328	12.4224
V_{G100}	1.1000	1.1000			

	SMA	ALO
Fuel cost ($/h)	18868.9917	18930.7826
Power losses (MW)	52.8438	58.4519
Voltage deviation (p.u)	6.5130	4.7255

The convergence curves of SMA and ALO algorithms are depicted in Fig. 3.12. From this figure, the proposed algorithms converge to high-quality solutions after the first quarter of iterations.

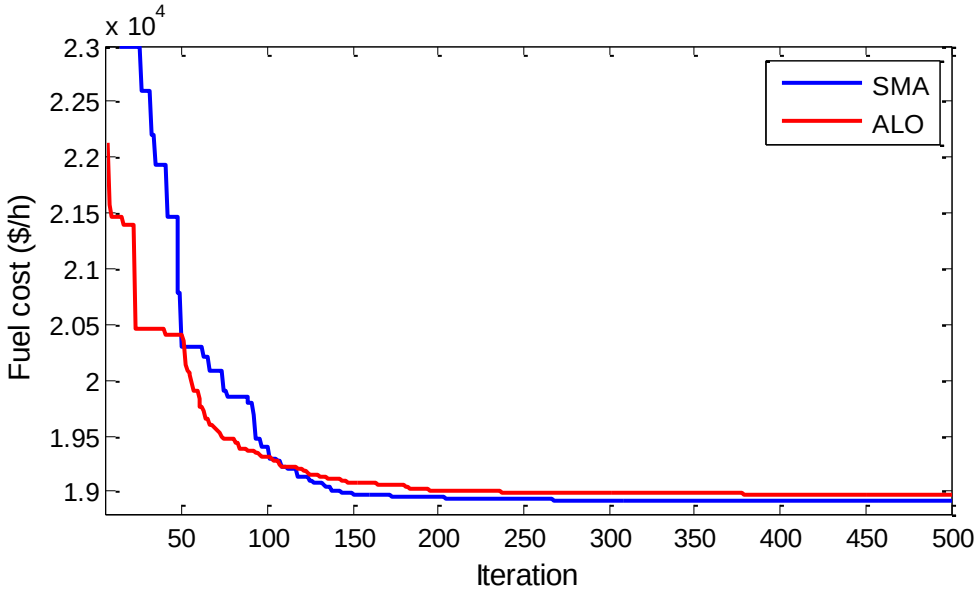

Figure 3.12 Convergence characteristics of SMA and ALO for the ALG 114-bus system: Case 6

To illustrate the performance of the proposed algorithms to solve the OPF problem in larger dimensions, the results achieved by the proposed algorithms are compared to some algorithms in the literature as presented in Table 3.16. SMA and ALO stand competitively regarding total fuel cost minimization compared to these reported algorithms. These results achieved by the proposed algorithms show the ability of SMA to find a better solution for large-scale power systems.

Table 3.16 Comparison of solutions for fuel cost minimization in IEEE ALG 114-bus system: **Case 6**

Method		Fuel cost ($/h)	Method description
SMA		18868.9917	Slime mould algorithm
ALO		18930.7826	Ant lion optimizer
PSO	[134]	19235	Particle Swarm Optimization
DE	[134]	19203.340	Differential evolution
GWO	[135]	19171.9582	Grey wolf optimizer
GA-ED-PS	[136]	19199.444	Hybrid GA-DE-PS
MOALO	[137]	19355.859	Multiobjective ant lion algorithm

3.5. Comparing the proposed algorithms based on solution quality

In the optimization field, comparing optimization algorithms is a difficult task that necessitates many delicate considerations in order to obtain a fair and unbiased evaluation. It can be very useful when done correctly. On the other hand, comparing algorithms can reveal an algorithm's strengths and defects, and thus evaluate its performance to help users for selecting the best algorithm for working with a real-world problem. The performance measures are divided into three categories:

efficiency, reliability, and quality of the solution [138]. In this study, the performance of proposed algorithms is tested based on the quality of the solution i.e., better final solution value. To evaluate the proposed algorithms which are most suitable in solving the OPF problem, each algorithm is run 30 times for better validation of the result. Table 3.17 presents the comparison of minimum, maximum, and mean values of the fuel cost obtained using the proposed algorithms. From this table, it can be seen that SMA outperformed the ALO algorithm for the three power systems.

Table 3.17 Statistical results of the proposed algorithms for fuel cost minimization

Bus system	Algorithms	Min ($/h)	Max ($/h)	Mean ($/h)
IEEE 30-bus system	SMA	798.9709	799.1454	799.05828
	ALO	799.0133	799.6989	799.34497
IEEE 57-bus system	SMA	41649.0605	41699.6105	41662.0686
	ALO	41685.9465	41776.1275	41722.1452
ALG 114-bus system	SMA	18868.9917	18916.3897	18893.5906
	ALO	18930.7826	19361.4635	19143.9013

The boxplot of obtained fuel cost using SMA and ALO for 30 times run for the three power system are shown in the Fig 3.13. From this figure, SMA obtained the least cost for best, worst, and average scenarios compared to the ALO algorithm which gave the worst cost. Thus, SMA has better and robust performance compared to the ALO algorithm in solving the OPF problem.

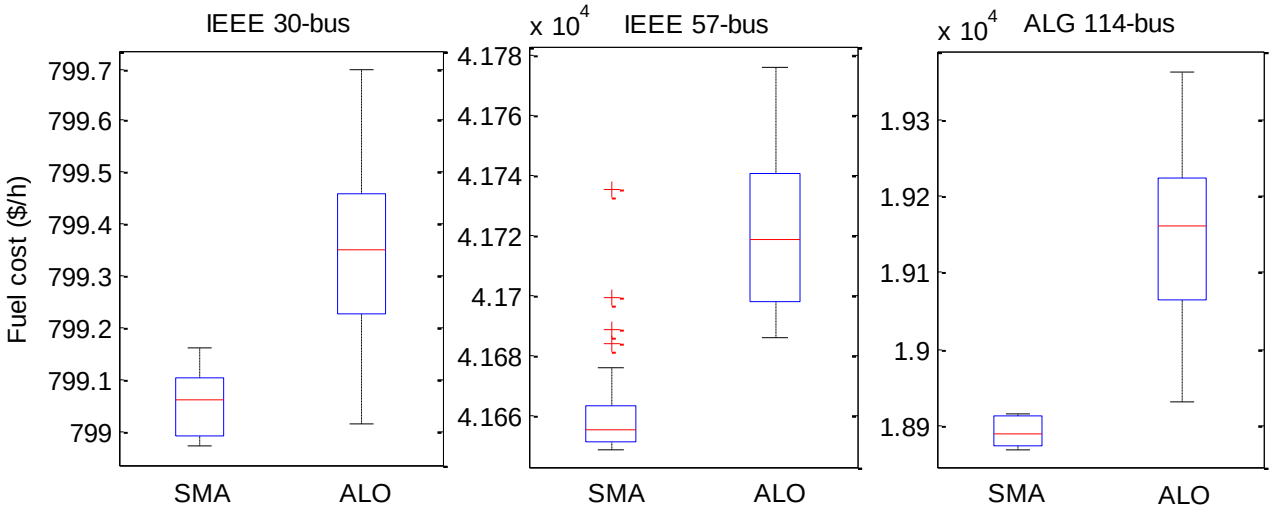

Figure 3.13 Boxplot of fuel cost obtained using the proposed algorithms for 30 times run

3.6. Conclusion

In this chapter, the formulation of the OPF problem has been discussed in a detailed way. Three objective functions have been presented to be optimized i.e., minimization of total fuel cost, minimization of active power loss as well as voltage profile improvement. Two recent metaheuristic techniques namely slime mould algorithm (SMA) and ant lion optimization (ALO) have been

employed to solve the OPF problem. The simulations have been carried out on the IEEE 14-bus, IEEE 57-bus and Algerian 114-bus systems to examine the effectiveness of the proposed algorithms. The result of simulations proves the capability and efficiency of the proposed algorithms to find a better solution compared to several algorithms previously reported in this chapter. The comparative analysis of the proposed algorithms was performed and shows that the SMA optimized the values of control variables in a technically and economically better way than ALO, and thus SMA produces very competitive performance in solving the OPF problem.

Chapter 04: Optimal Power Flow Solution Incorporating FACTS-HVDC technology

4.1. Introduction

The increase of the demand for energy in electric power grids has led to the introduction of flexible AC transmission systems (FACTS) devices and the technology of high voltage direct current (HVDC), which opens new perspectives to ensure better performance and operation of networks like increasing the transmission capacities, enhance the controllability of the power systems, transporting high-power electricity over long distances, avoid line overloading, improve voltage stability, reduce power losses as well as transporting remote renewable energy, ..Etc. The FACTS devices and HVDC technology use recent advances in power electronics technologies based on new and powerful semiconductor devices. As a result, FACTS-HVDC systems have very high reliability and virtually unlimited flexibility. Optimizing the size and optimal placement of FACTS-HVDC systems has become an important requirement for the best benefit of these devices to achieve several desired objective functions in the power system.

This chapter presents in the first part, a general introduction on the FACTS-HVDC system, following by the description and the modeling of static VAR compensator (SVC) and voltage source converters based HVDC (VSC-HVDC). Then, the formulation of the OPF problem incorporating SVC devices and HVDC transmission lines is presented. Finally, the proposed algorithms SMA and ALO have been used to solve this problem in order to improve the behavior of the electricity grid in contingency conditions. Moreover, the proposed algorithms have been used to identify the optimal location of the SVC device and HVDC transmission line in the power system based on determining the lowest voltage busses and overloading lines, respectively.

4.2. Flexible AC Transmission System (FACTS) technology

The term of the flexible alternating current transmission system (FACTS) was first introduced by Hingorani in 1988 [139], and is defined by the institute of electrical and electronics engineers (IEEE) as follows: “Alternating current transmission systems incorporating power electronic-based and other static controllers to enhance controllability and increase power transfer capability” [24]. The FACTS technology use power semiconductors that offer the ability to enhance the controllability of the different parameters into the electrical power networks such as, active and reactive powers, bus voltage, phase angle, …etc [30]. These modern technologies enable faster response than electromechanically switched systems, [24], [25].

4.2.1. Advantages of the FACTS devices

The FACTS systems are extremely reliable and offer virtually unlimited flexibility. The advantages of FACTS devices in a power system are as follows [140]–[142]:

- Maintaining the bus voltage profiles at their desired level;
- Improve the stability of a power system;
- Reduce reactive power flow allow to increase the active power capacity of lines and reduce power losses;
- Control the power flow in transmission lines to ensure optimal power distribution under normal and contingency states operation;
- Improve the power system security;
- Enhance power system performance;
- Reducing the heavily loaded lines flow and limits the short circuit currents level;
- Improve the performance of the HVDC converter terminal and wind power integration system;

4.2.2. Classification of FACTS devices

The network connection mode is an essential characteristic that largely determines the controller's mode of action. In general FACTS controllers can be classified into four categories depending on the mode of coupling to the network:

- Shunt controllers
- Series controllers
- Combined series-series controllers
- Combined series-shunt controllers

4.2.2.1. Shunt controllers

These controllers are connected in parallel to the transmission lines and could be variable impedance, variable source, or a combination of these. All shunt controllers inject current into the system at the connection point. This current injection modifies the active and reactive powers transmitted in the line. The benefits of shunt controllers are to control bus voltage profiles and increase the transmittable power. The most commonly used shunt controllers in power grids are:

- Static Var Compensator (SVC)
- Static synchronous compensator (STATCOM)

4.2.2.2. Series controllers

Series controllers are connected in series with the transmission line and could be variable impedance (inductive or capacitive) or a power electronics-based variable source of main frequency, sub-synchronous, and harmonic frequencies. All series controllers are meant to inject voltage in series with the transmission line. The series controller only supplies or absorbs variable reactive power as long as the voltage is in phase quadrature with the line current. The most used series controllers are:

- ❖ Thyristor Controlled Series Capacitor (TCSC)
- ❖ Thyristor Switched Series Capacitor (TSSC)

4.2.2.3. Combined Series-Series Controllers

This category could be a combination of individual series controllers which are controlled in a coordinated manner in a multiline transmission system to perform a predefined control. Further, it could be also a unified controller in which separate series controllers provide in each transmission line the series reactive power compensation and also facilitate real power transfer between the lines via the power link. Examples of these combined controllers are:

- Interline Power Flow Controller (IPFC)
- Thyristor-Controlled Voltage Limiter (TCVL)

4.2.2.4. Combined Series-Shunt Controllers

This category could be a combination of separate series and shunt controllers which are controlled in a coordinated manner, or a unified power flow controller with series and shunt elements. These combined controllers inject current into the system using the shunt part of the controller and series voltage in the transmission line using the series part of the controller. Moreover, there can be real power exchange between the shunt and series controllers via the power link if both controllers are unified. Examples of combined series-shunt controllers are:

- Unified power flow controller (UPFC)
- Thyristor Controlled Phase Angle Regulator (TCPAR)

This part of the chapter deals with one of the most important, powerful, and widely used types of FACTS devices, known as the static Var compensator (SVC) device.

4.3. Static Var Compensator (SVC) device

4.3.1. Definition of SVC device

Static Var compensator (SVC) is a shunt device of the FACTS family which is used to provide or absorbs reactive power at the bus to which it is connected in order to control specific parameters in the power system, such as primarily the voltage and reactive power. It consists of a parallel combination of a thyristor switched capacitor (TSC), thyristor controlled reactor (TCR), and harmonic filters. This combination is connected to the network through a shunt transformer as shown in Fig. 4.1.

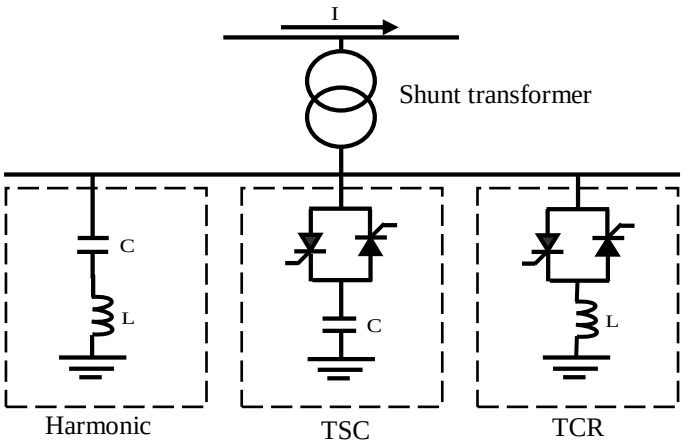

Figure 4.1 Simplified single-line diagram of an SVC connected to power system

A TCR circuit is composed of a fixed reactor connected in series with a bidirectional thyristor valve. A TSC circuit is composed of a capacitor connected in series with a bidirectional thyristor valve.

The voltage-current (V-I) static characteristic of SVC is represented in Fig. 4.2. From this figure, three zones are considered in terms of the curve V-I of an SVC as follow:

- For $V_{min} \leq V_{ref} \leq V_{max}$: is an adjustment zone where the reactive energy is regulated by combining TSC and TCR control;
- For $V_{ref} > V_{\max}$: this is the zone where the TCR absorbs its maximum reactive energy to decrease the voltage of the network, the capacitors are disconnected;
- For $V_{ref} < V_{\min}$: this is a zone where only the capacitors are connected to the network, the TSC provides reactive power to increase the voltage;

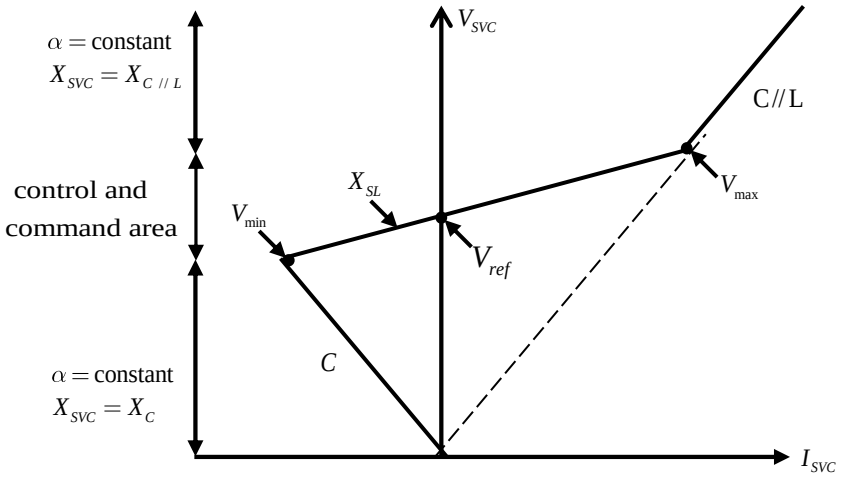

Figure 4.2 The static characteristic of SVC

4.3.2. Modeling of SVC device

The SVC device is modeled by shunt variable admittance as shown in Fig. 4.3. This model uses the priming angle of the thyristors to control the current in the reactance while the reactive power control by this method is fast and continuous.

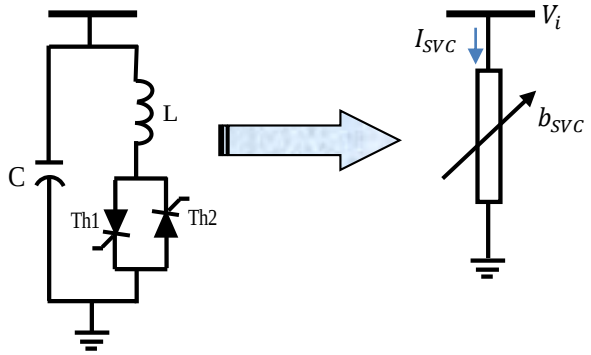

Figure 4.3 SVC equivalent circuit

In the power flow formulation, the SVC device is considered in the power system as a generator PV bus (or absorber) of reactive power where the voltage is controlled and equal to the unit with the real power generation equal to 0 MW. A negative value indicates that the SVC generates reactive power and injects it into the network (capacitive state) and a positive value indicates that the SVC absorbs the reactive power of the network (inductive state) [143]. The susceptance b_{SVC} can be capacitive or inductive to respectively provide or absorb the reactive power Q_{SVC}.

Since the power loss of the SVC device is assumed negligible, so the admittance is assumed purely imaginary as follow:

$$\bar{y}_{SVC} = jb_{SVC} \qquad \textbf{(4.1)}$$

The reactive power Q_{SVC} absorbed or injected by the SVC device into node *i* is expressed as follows [23]:

$$Q_{SVC} = -V_i^2 . b_{SVC} \quad \textbf{(4.2)}$$

with $Q_{SVC}^{min} \le Q_{SVC} \le Q_{SVC}^{max}$ **(4.3)**

where V_i is the nominal voltage at node *i*, Q_{SVC}^{min} and Q_{SVC}^{max} respectively denote the minimum and maximum limits of the reactive power of SVC Q_{SVC}.

The current value consumed by the SVC device is given by Eq. (4.4) and the limits of the susceptance B_{SVC} is given by Eq. (4.5):

$$\bar{I}_{SVC} = jB_{SVC}V_i \quad \textbf{(4.4)}$$

with $B_{SVC}^{min} \le B_{SVC} \le B_{SVC}^{max}$ **(4.5)**

where B_{SVC}^{min} and B_{SVC}^{max} respectively denote the minimum and maximum limits of the susceptance B_{SVC}

In general, two locations of the SVC device are considered, at the near end bus and the midpoint of the transmission line. When the SVC device is located at the near end bus, only the element Y_{ii} of nodal admittance matrix is changed, and the admittance of the SVC being added to it as follow:

$$\bar{Y}_{ii}^{'} = \bar{Y}_{ii} + \bar{y}_{SVC} \quad \textbf{(4.6)}$$

Figure 4.4 illustrates the case of an SVC located at the near-end bus.

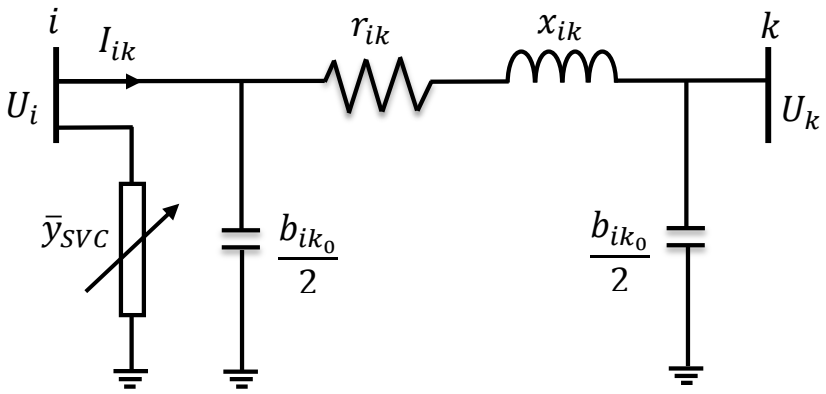

Figure 4.4 SVC placed at the near end bus

In this case, the admittance matrix is modified as follows:

$$\bar{Y} = \begin{pmatrix} \bar{y}_{ik} + \frac{\bar{y}_{ik0}}{2} + y_{SVC} & -\bar{y}_{ik} \\ -\bar{y}_{ik} & \frac{\bar{y}_{ik0}}{2} + y_{ik} \end{pmatrix} \quad \textbf{(4.7)}$$

When the SVC is placed in the midpoint of the transmission line, this later is divided into two identical sections as shown in Fig. 4.5.

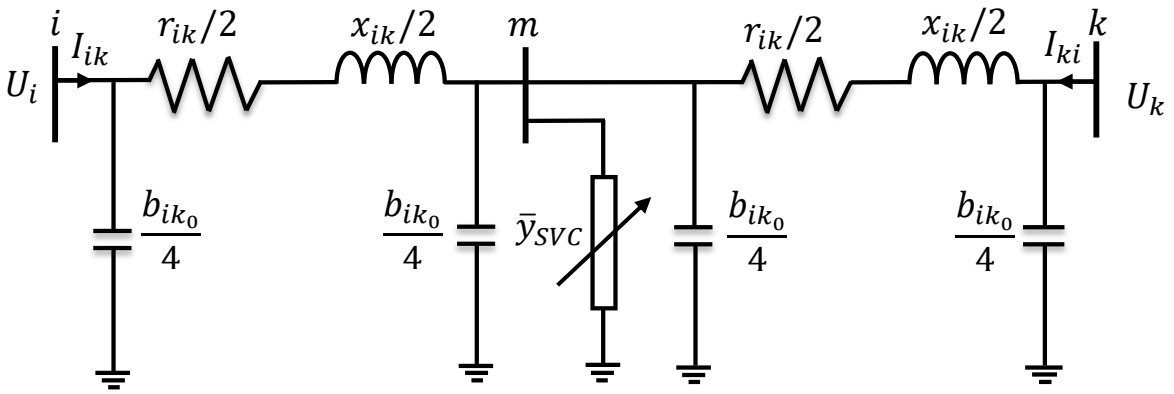

Figure 4.5 SVC placed in the midpoint of the transmission line

In the case when the SVC placed in the midpoint, all the elements of the admittance matrix of a line are modified as follow:

$$\bar{Y}_{mod} = \begin{pmatrix} \bar{y}_{ik} + \frac{\bar{y}_{ik0}}{2} & -\bar{y}_{ik} \\ -\bar{y}_{ik} & \bar{y}_{ik} + \frac{\bar{y}_{ik}}{2} \end{pmatrix} \quad \textbf{(4.8)}$$

4.4. High Voltage Direct Current (HVDC) transmission system

High voltage direct current (HVDC) transmission system is one of the most important components of network systems which offer more attractive solutions for long-distance energy transmission, connecting different synchronous zones and large-scale renewable energy sources (RESs) integration due to its technical and economic superiority over high voltage alternating current (HVAC) system. Recently, the transmission of electric power by HVDC system technology developed during the introduction on the market of power electronics components. In general, there are two types of HVDC transmission system exist based on categories of converter technologies. The first type is line commutated converter (LCC) which uses thyristors, also named current source converters (CSCs), and the second type is voltage source converter (VSC) which uses insulated-gate bipolar transistor (IGBT) [144], [145].

4.4.1. Comparison of AC and DC transmission systems

Various factors should be compared to justify the choice between the uses of AC or DC transmission systems, which are as follows:

- **Asynchronous AC interconnections**; DC transmission system permits to interconnect between two asynchronous AC networks that operate at the different frequency [26], which that is not possible with AC transmission system.
- **Long-distance transmission**; DC transmission system allows transferring of bulk power over long distances than AC transmission system. DC technology avoids problems caused by limited cable capacity while the capacity of AC cable is limited by its characteristic or surge impedance [146]. HVDC technology enables the enhancement of renewable energy sources integration (e.g. offshore wind farms) that are placed at locations far from the load centers.
- **Controllability and stability**; DC technology increases system stability under diverse conditions by very fast and precise power controlling from the control station at each extremity of the link. The direction of the power flow can be changed very fast (Bidirectional power flow).
- **Environmental impact**; DC transmission system provides environmental benefits over AC technology, which means that for the same transmitted power, DC transmission links require smaller right of way (RoW) and simpler towers [147], whereas in AC technology, the higher the voltage is, requires more space to build larger towers [145]. In addition, a DC system has less noise intensity unlike the noise levels on AC electric lines, which means that the environmental effects on people are less for the DC transmission system [148].
- **Transmission costs**; DC technology is less expensive compared to AC technology for power transmission over long distances which is the main advantage of DC interconnection. DC line needs only two wires of transmission while AC line needs 3 conductors in 3-phase AC systems. As a result, for a given power level, a DC line needs cheaper towers, as well as lower conductor and insulator costs [147]. It is financially interesting to transfer power in DC. Figure 4.6 shows that the DC tends to be more economical than AC for distances greater than 500 km in overhead lines, but is more expensive for short distances.

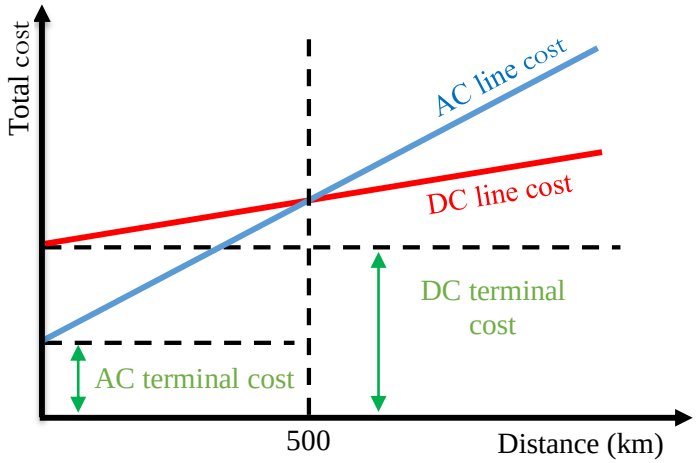

Figure 4.6 Comparison of the transmission costs in an AC and DC lines

4.4.2. Configurations of HVDC transmission system

HVDC transmission systems can be classified into several configurations, depending on the earthing, converter connections, asymmetric or symmetric connections [145], as shown in Fig. 4.7. The main configurations of HVDC transmission systems are described below:

- **Monopolar link**: In this connection, a single cable or line at a positive or a negative high DC voltage is required to connect two converters stations. The path of return current either with the ground, metallic return, a mid-point ground, and sea electrodes in the submarine cable crossings [145],[149], [150].
- **Bipolar configuration**: The bipolar link consists of two combined monopolar HVDC systems, one at a positive voltage (positive polarity) and the other at a negative voltage (negative polarity), using either earth electrodes or metallic return as the return path [4], [149], [150]. The advantage of the bipolar link is that it is possible to use 50% of the system power capacity when any single transmission line/cable on the bipolar link has a fault [4].
- **back-to-back configuration**: In the back-to-back configurations, the two converters stations are located close to each other and no transmission line or cable is required [145]. This system is the common configuration for connecting two asynchronous alternating current systems [151].
- **Multi-terminal configuration**: In the multi-terminal configuration, there are three or more terminals connected to a DC network. The multi-terminal DC (MTDC) systems are usually divided into two systems, series and parallel systems [151], [152]. MTDC can be more attractive in many cases, to exploit all the economic and technical advantages of the HVDC system [152].

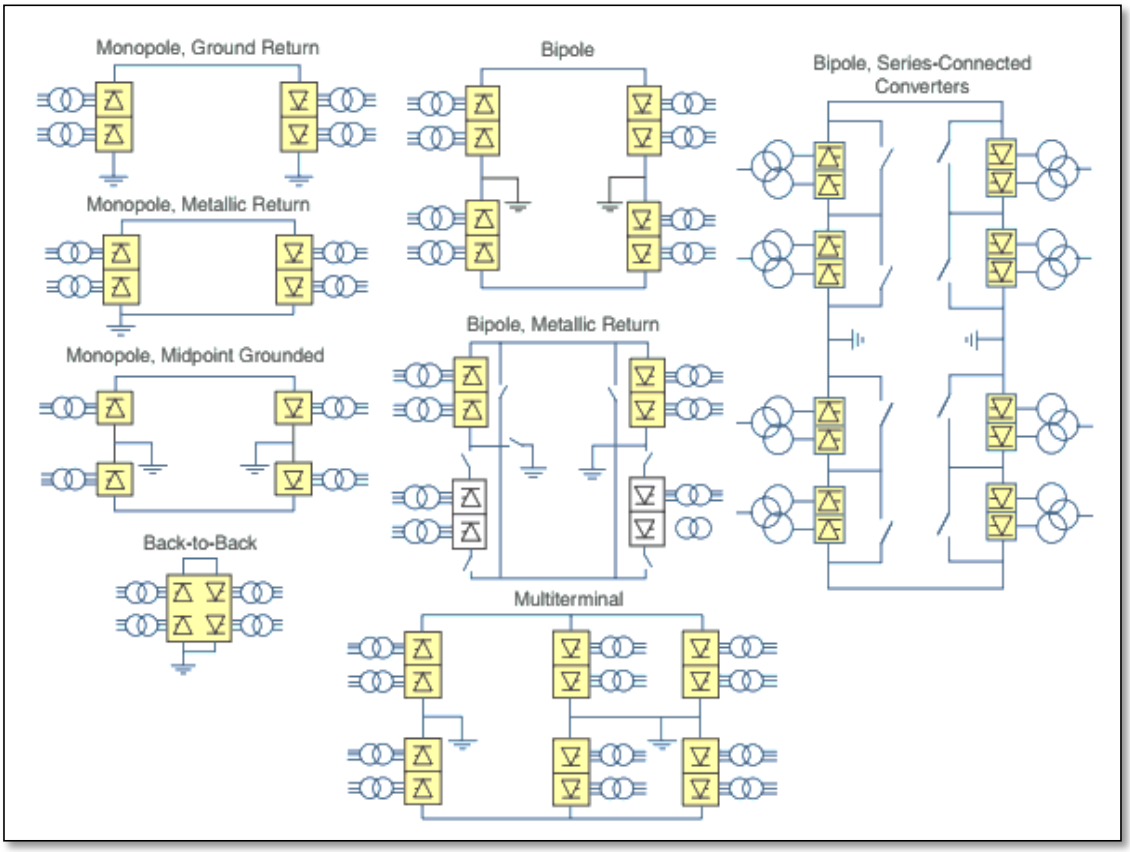

Figure 4.7 Different configurations of the HVDC system [149]

4.5. VSC-based HVDC technology

Voltage source converter (VSC) based HVDC utilize a power electronic valve based on insulated gate bipolar transistor (IGBT) technology, which can be switched on and off freely via a well-developed control signal. The converters use pulse width modulation (PWM) for working [153]. The first commercial of VSC-HVDC transmission was installed on the island of Gotland in Sweden in 1999, with ratings of ±80 kV and 50 MW underground cable [154]. Since then, VSC technology has improved significantly thanks to the new development of semiconductors for power electronics. Recently, VSC-HVDC technology has proven itself as a key market competitor and has become a new trend for the integration of remote RESs to the power system [144], especially in Europe and China. VSC-HVDC is also referred to as HVDC Light (ABB), HVDC Plus (Siemens), or MonSin (GE/Alstom) [153].

4.5.1. Advantages of VSC-HVDC over LCC-HVDC

Particular attention is paid to VSC-HVDC technology as it has significant advantages over LCC-HVDC technology. The main advantages of VSC-HVDC over LCC-HVDC technology are given below:

- VSC technology uses recent switching techniques like the use of PWM to create the desired voltage waveform, any phase angle and magnitude of the fundamental frequency component, allowing for significant reductions in harmonic filter sizing and reactive equipment compared to LCC technology [4].
- VSC HVDC technology has great controllability due to the use of PWM which allows fast and independent control of active and reactive power at both converter stations [26], [28]. Contrary to LCC-HVDC, which can control active power only [150].
- VSC HVDC can be used to feed islands and passive AC networks because the VSC converter can create its own AC voltage. This feature makes VSC technology suited for supply industrial installations or connecting offshore wind farms [26], whereas LCC-HVDC link, the offshore converter requires an external voltage to commutate against [155]. Thus, connecting remote RESs (e.g. offshore wind farms) to the power system would only be realistic with VSC technology [28].
- VSC-based HVDC technology can support the AC network by providing a variety of ancillary services, such as reactive power support for voltage control [26], attenuation of energy quality disturbances, flicker attenuation and unbalanced voltage compensation, reduced risk of commutation failure [155], black start capabilities [26].

4.5.2. Components of VSC-HVDC

A VSC-based HVDC transmission system is a power electronics equipment consisting of the IGBT (or GTO)-based converters, transformers, phase reactors, DC cables, DC capacitors, the grounding electrodes, as shown in Fig. 4.8. The major components are discussed in the following sections:

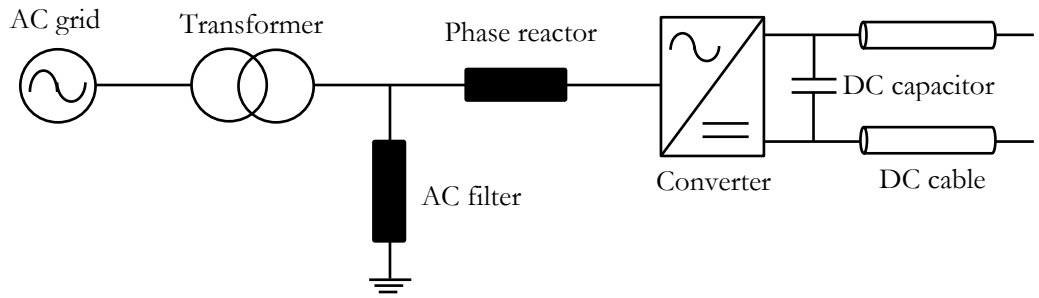

Figure 4.8 Main components of the VSC-HVDC transmission system

4.5.2.1. Converter

The VSC-HVDC consists of several converter valves, each converter valve consisting of a

series connection of IGBTs/diodes switches as shown in Fig. 4.9. All the switches are activated and deactivated simultaneously, depending on the command generated by the PWM. The VSC converter performs the conversion from AC to DC (rectifier) and vice versa (inverter).

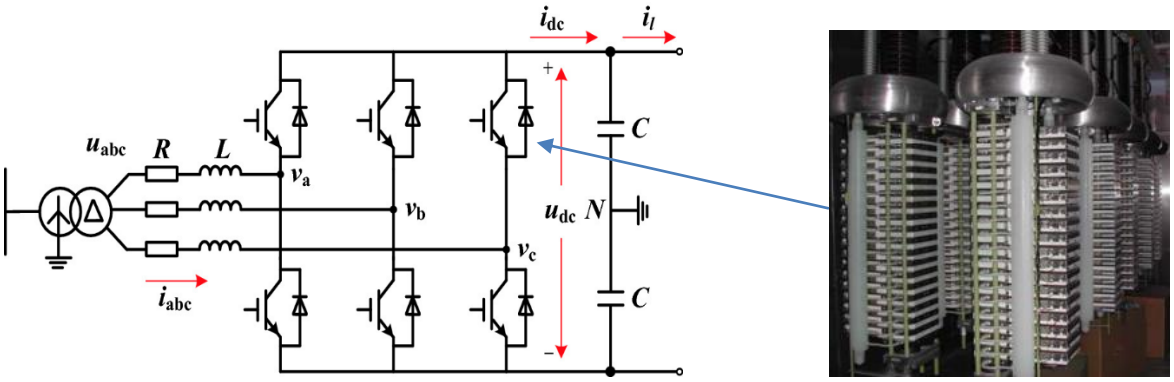

a) Two-level voltage source converter b) IGBT valves

Figure 4.9 IGBT valve arrangement for VSC

4.5.2.2. Transformers

In a VSC-HVDC system, both VSC converters are connected to AC systems via transformers. These transformers consist of several coils with a magnetic circuit that is used to elevate or lower the voltage level of an electrical energy source. The most important function of the transformers is to transform the AC system voltage to the suitable level input voltage required of the converters for the proper operation of the converter, as well as adjust the AC voltage level to the line DC voltage level. Transformers are equipped with socket changers. Their design is generally simple and conventional, due to the lower harmonic content of the current in the VSC-HVDC scheme.

4.5.2.3. DC cable

The DC cable used in the VSC-HVDC technology is a newly developed and are typically XLPE (Cross-Linked Poly-Ethylene) polymer extruded cables [151], where their insulation is improved, lower power losses, more flexibility and low weight [155], [144], and it used to several applications, as offshore power transmission or overhead links [144].

4.5.2.4. Phase reactors

Phase reactors are installed in the AC side between the converter and transformer and are widely used for controlling the active and reactive power flow [155]. Moreover, Phase reactors are also used to reduce the inrush currents upon energization and for smoothing the current [156].

4.5.2.5. AC filter

The AC currents and voltage output contain high-order harmonics, caused by the power electronics elements (IGBT switching). Therefore, must be limited these high-order harmonics emitted to prevent them from causing malfunction of all AC system equipment [144], [155], [156]. For this purpose, high-pass filters are installed in the transmission system to attenuate these high-order harmonics, providing the AC system with almost sinusoidal currents and voltages [144]. With VSC converter technology, there is no necessity to compensate for the reactive power and the current harmonics are directly related to the PWM frequency [155].

4.5.2.6. DC filter

DC filters are installed to reduce harmonics created by HVDC converters for all modes of operation. These harmonics can create disturbances in telecommunications systems. DC filters are generally much smaller and less expensive than AC filters. They are made up of passive components (capacitors, inductors, resistors) and also power electronics devices that inject into the current line or harmonic tensions of the same amplitude as the converters but in phase opposition.

4.5.2.7. DC side capacitor

At the end of the DC transmission side, there are two capacitor stacks of the same size, each DC capacitor is connected to a pole to the ground [144], [155], [156]. The size of these DC capacitors depends on the required DC voltage. The objective of these DC capacitors is to maintain a stable DC voltage at the desired level and keep the power balance during transients [151], [155], [156].

4.5.3. Modeling of the VSC-HVDC system

In order to perform the theoretical analysis, VSC converters can be modeled on the AC side by a controllable voltage source connected to the common coupling point (PCC) through a complex impedance Z_c as shown in Fig. 4.10. This complex impedance $Z_c = R_c + jX_c$ includes both the converter reactance and the transformer. On the DC side, VSC is assumed to be an ideal current source connected to the DC bus in parallel with a DC capacitor, where the magnitude of the current is such that the power in the AC side and the DC side of the converter are equal. Applying Kirchhoff's law to the AC side of the VSC, the basic equation of this circuit is derived for each phase *i*, and given as follow:

$$u_{c,i} - u_{s,i} = L_c \frac{di_{c,i}}{dt} + R_c i_{c,i} \quad \textbf{(4.9)}$$

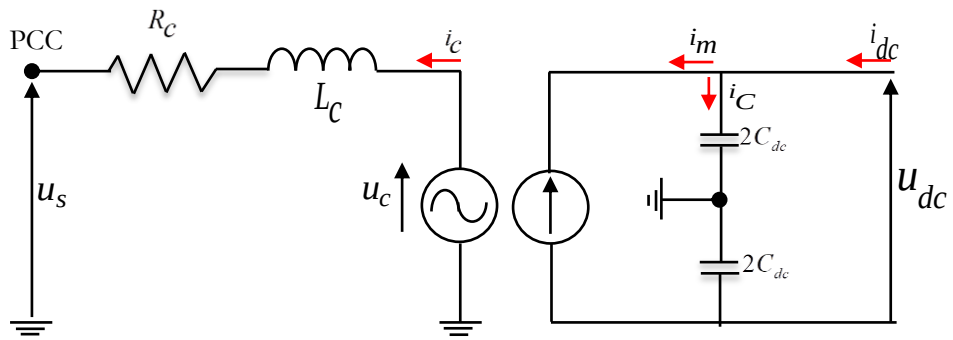

Figure 4.10 A single-phase diagram of the SVC without filter

The three-phase equations are transforming to the rotating plane dq_0 and the voltage converters are assumed ideal and assuming that the voltage of the u_s grid is fully oriented in the direction q, the converter equations become:

$$R_c i_{cq} + L_c \frac{di_{cq}}{dt} = u_{cq} - w_g L_c i_{cd} - u_{sq} \tag{4.10}$$

$$R_c i_{cd} + L_c \frac{di_{cd}}{dt} = u_{cd} - w_g L_c i_{cq} \tag{4.11}$$

where w_g is the AC grid angular frequency.

Figure 4.11 shows the DC transmission line which is modeled by a π-equivalent scheme.

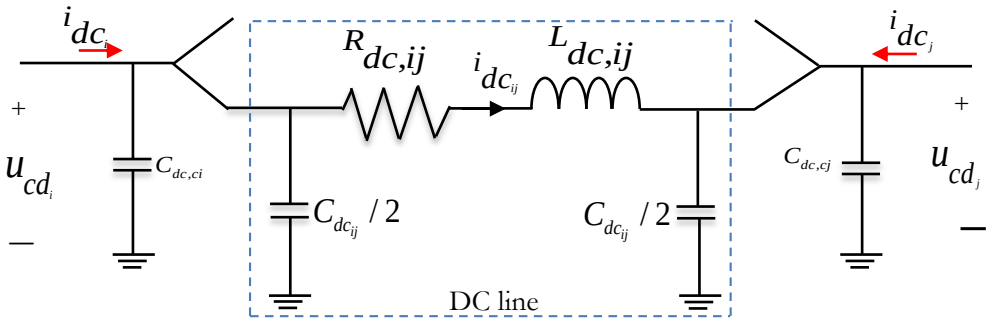

Figure 4.11 Lumped section model of a DC line

The DC voltage dynamics at node i are determined by:

$$C_{dc_i} \frac{du_{dci}}{dt} = i_{dci} + \sum_{j=1}^{i-1} i_{dc_{ij}} - \sum_{j=i+1}^{N} i_{dc_{ij}} \tag{4.12}$$

With $C_{dc_i} = C_{dc,ci} + \sum_{j=1}^{N} \frac{C_{dc_{ij}}}{2}$ **(4.13)**

with u_{dci} and i_{dci} respectively the voltage and current in DC side at node i. $C_{dc,ci}$ denote the DC capacity of the converter, $i_{dc_{ij}}$ is the current in the branch between nodes i and j and $C_{dc_{ij}}$ represented the capacity of the branch between nodes i and j.

4.5.4. VSC-HVDC power flow modeling

4.5.4.1. Converter power flow modeling

In the AC side, the VSC converter can be represented by a controllable voltage source $\bar{U}_c$, and connected to the common coupling point (PCC) through the phase reactor. The phase reactor represented by a complex impedance $\bar{Z}_c = R_c + jX$. The low pass filter is represented as a B_f susceptance. The filter bus is connected to the AC network via a transformer, this transformer is represented by a complex impedance $\bar{Z}_{tf} = R_{tf} + jX_{tf}$. Figure 4.12 shows the equivalent single-phase power flow model of a converter station connected to the AC grid.

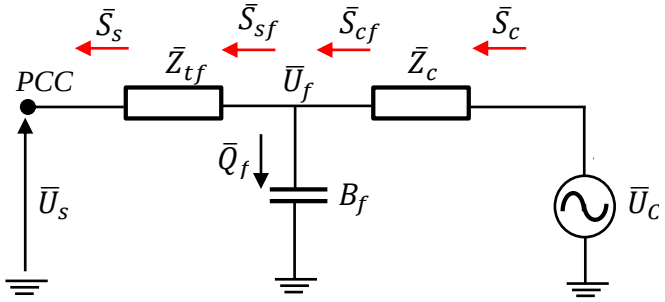

Figure 4.12 Single-phase power flow model of a converter station

The detail of power flow in the converter station connected to the AC grid is as follows:

The active and reactive powers transmitted to the AC network are given as follow:

$$P_S = -\bar{U}_S^2 G_{tf} + \bar{U}_s \bar{U}_f \left[G_{tf} \cos\left(\delta_s - \delta_f\right) + B_{tf} \sin\left(\delta_s - \delta_f\right) \right] \quad \textbf{(4.14)}$$

$$Q_s = \bar{U}_s^2 B_{tf} + B_s B_f \left[G_{tf} \sin\left(\delta_s - \delta_f\right) - B_{tf} \cos\left(\delta_s - \delta_f\right) \right] \quad \textbf{(4.15)}$$

with $\bar{U}_s = U_s \angle \delta_s$ et $\bar{U}_f = U_f \angle \delta_f$ respectively the voltages of complex grid AC side and filter bus.

The active and reactive powers at the converter side can be written in the following equations:

$$P_c = \bar{U}_c^2 G_c - \bar{U}_f \bar{U}_c \left[G_c \cos\left(\delta_f - \delta_c\right) - B_c \sin\left(\delta_f - \delta_c\right) \right] \quad \textbf{(4.16)}$$

$$Q_c = -\bar{U}_c^2 B_c + \bar{U}_f \bar{U}_c \left[G_c \sin\left(\delta_f - \delta_c\right) + B_c \cos\left(\delta_f - \delta_c\right) \right] \quad \textbf{(4.17)}$$

The filter's reactive power is given by Eq. (4.18) as follow:

$$Q_f = -\bar{U}_f^2 B_f \quad \textbf{(4.18)}$$

The equations for the power flowing of the filter side complex through the transformer are written by equations (4.19) and (4.20) as:

$$P_{sf} = \bar{U}_f^2 G_{tf} - \bar{U}_f \bar{U}_s \left[G_{tf} \cos\left(\delta_s - \delta_f\right) - B_{tf} \sin\left(\delta_s - \delta_f\right) \right] \quad \textbf{(4.19)}$$

$$Q_{sf} = -\overline{U}_f^2 B_{tf} + \overline{U}_f \overline{U}_s \left[G_{tf} \sin\left(\delta_s - \delta_f\right) + B_{tf} \cos\left(\delta_s - \delta_f\right) \right] \quad \textbf{(4.20)}$$

while the expressions for the power flowing through the phase reactor side are:

$$P_{cf} = -\overline{U}_f^2 G_c + \overline{U}_f \overline{U}_c \left[G_c \cos\left(\delta_f - \delta_c\right) + B_c \sin\left(\delta_f - \delta_c\right) \right] \quad \textbf{(4.21)}$$

$$Q_{cf} = \overline{U}_f^2 B_c + \overline{U}_f \overline{U}_c \left[G_c \sin\left(\delta_f - \delta_c\right) - B_c \cos\left(\delta_f - \delta_c\right) \right] \quad \textbf{(4.22)}$$

The losses of the converter station are also included in this model, which is based on a generalized loss formula, with the losses of the converter quadratically dependent on the current of the converter:

$$P_{loss} = a + b * I_c + c * I_c^2 \quad \textbf{(4.23)}$$

where a, b and c are the loss coefficients of the converters.

The direct current I_c is given by the following expression:

$$I_c = \frac{\sqrt{P_c^2 + Q_c^2}}{\sqrt{3} U_c} \quad \textbf{(4.24)}$$

4.5.4.2. DC grid power flow modeling

The DC grid can be represented by a resistive grid with current injections and DC voltages at the different nodes [28]. The current injected into the DC node i can be written as the current flowing to the other (n-1) node of the grid and written as:

$$I_{dci} = \sum_{\substack{j=1 \\ j \neq i}}^{n} Y_{dc,ij} \left(U_{dci} - U_{dcj} \right) \quad \textbf{(4.25)}$$

with $Y_{dc,ij} = {}^{1}/_{R_{dc,ij}}$

Combining all currents injected in an n bus DC network results in

$$\overline{I}_{dc} = \overline{Y}_{dc} \overline{U}_{dc} \quad \textbf{(4.26)}$$

where I_{dc} is the direct current vector given as $I_{DC} = \left[I_{DC_1}, I_{DC_2}, .. I_{DC_k}, 0 \ldots 0 \right]^T$, U_{dc} is the vector of DC voltages and given by $U_{DC} = \left[U_{DC_1}, U_{DC_2}, .. U_{DC_k}, 0 \ldots 0 \right]^T$, and Y_{dc} is the matrix of admittance DC bus.

The active power injected into node i for a monopolar DC grid can be written as follows:

$$P_{dci} = \rho I_{dci} U_{dci} \quad \textbf{(4.27)}$$

Thus, the active power injections can be written by combining the Eq. (4.25) and Eq. (4.27) as follows:

$$P_{dci} = \rho U_{dci} \sum_{\substack{j=1 \\ j \neq i}}^{n} Y_{dcij} \left(U_{dci} - U_{dcj} \right) \tag{4.28}$$

where $\rho = 1$ for a monopolar system or $\rho = 2$ for a monopolar symmetrically grounded or bipolar system.

4.6. Sequential formulation of AC/DC power flow

This system of non-linear equations can be solved with an iterative method. Several methods for calculating power flow in AC/DC networks are presented in the literature. They can be classified into two categories: simultaneous and sequential methods. In this study, the sequential method has been used based on its simplicity. The calculation of the power flow by the sequential method is based on the resolution of the AC and DC system equations separately and sequentially. Figure 4.13 shows the AC/DC power flow algorithm flowchart.

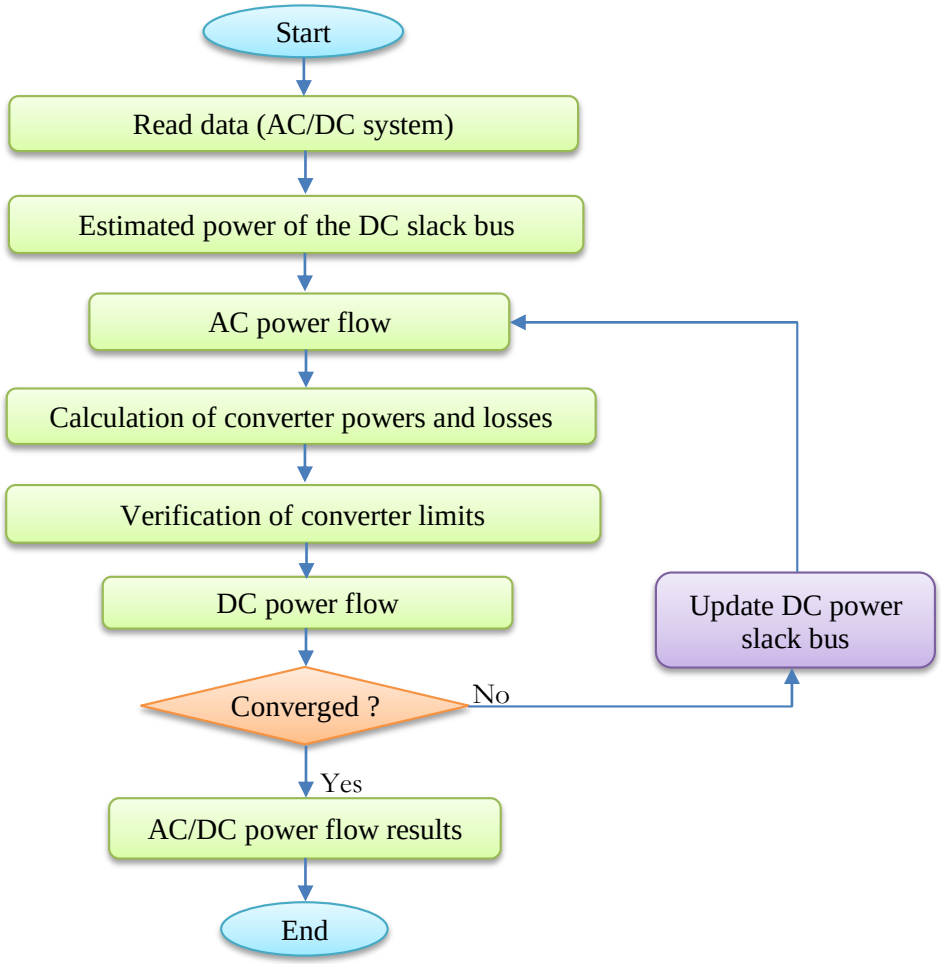

Figure 4.13 Flowchart of the sequential AC/DC power flow method

4.6.1. AC power flow

The power injections at bus i in the AC grid can be written as follow:

$$P_i(U,\delta) = U_i \sum_{j=1}^{p} U_j \left[G_{ij} \cos\left(\delta_i - \delta_j\right) + B_{ij} \sin\left(\delta_i - \delta_j\right) \right] \quad \textbf{(4.29)}$$

$$Q_i(U,\delta) = U_i \sum_{j=1}^{p} U_j \left[G_{ij} \sin\left(\delta_i - \delta_j\right) + B_{ij} \cos\left(\delta_i - \delta_j\right) \right] \quad \textbf{(4.30)}$$

The set of nonlinear power flow equations can be solved using the Newton-Raphson method. In general, we can write the vectors of power mismatch which include the active and reactive powers injections *Ps* and *Qs* of the converter in the following form:

$$\Delta P_i^{(j)} = P_i^{gen} - \left(P_i^{dem} - P_{s_i}\right) - P_i\left(U^{(j)}, \delta^{(j)}\right) \quad \textbf{(4.31)}$$

$$\Delta Q_i^{(j)} = Q_i^{gen} - \left(Q_i^{dem} - Q_{s_i}\right) - Q_i\left(U^{(j)}, \delta^{(j)}\right) \quad \textbf{(4.32)}$$

After calculating the power flow in the AC side, the power injected into the DC grid becomes:

$$P_{dc_i} = -P_{c_i} - P_{loss} \quad \textbf{(4.33)}$$

where P_c is the active power injected into the DC grid, P_{loss} is the active power loss of the converter.

4.6.2. DC power flow

The active power injected at bus i in the DC grid is represented in Eq. (4.28). The non-linear DC grid equations can be solved by always using the Newton-Raphson method as:

$$\left(U_{dc} \frac{\partial P_{dc}}{\partial U_{dc}} \right)^j . \frac{\Delta U_{dc}^j}{U_{dc}} = \Delta P_{dc}^j \quad \textbf{(4.34)}$$

In this system, the vector of the power mismatch is given by:

$$\Delta P_{dci}^j + \begin{cases} P_{dci}^k - P_{dci}\left(U_{dc}^j\right) & \nabla\, i \le k \\ -P_{dci}\left(U_{dc}^j\right) & \nabla\, k \le i \le nbus \end{cases} \quad \textbf{(4.35)}$$

where the superscripts j and k denote the inner NR iteration and the outer AC/DC power flow iteration, respectively. The terms of the Jacobian are:

$$\left(U_{dc_j} \frac{\partial P_{dc}}{\partial U_{dc}} \right)^j = -2U_{dc,i}^j Y_{dc,ij} U_{dc_j}^j \quad \textbf{(4.36)}$$

$$\left(U_{dc,i} \frac{\partial P_{dc}}{\partial U_{dc}} \right)^j = P_{dc,i}^j + 2U_{dc,i}^{j^2} \sum_{\substack{j\neq 1 \\ j\neq i}}^{n} Y_{dc,ij} \quad \textbf{(4.37)}$$

4.7. OPF formulation considering FACTS-HVDC systems

The OPF problem solution in this part of the study aims to give the optimum value of the objective function considering the presence of the SVC device and HVDC transmission line by adjusting the settings of control variables. In this section, two single objective functions are to be optimized using the proposed algorithms. The first objective is to minimize the generation fuel cost and the second objective function is to reduce the active power losses.

- ***Minimization of generation fuel cost***

$$F_1(x) = \sum_{i=1}^{NG} a_i + b_i P_{Gi} + c_i P_{Gi}^2 \quad \textbf{(4.38)}$$

- ***Minimization of active power transmission losses***

$$\boldsymbol{F}_2(\boldsymbol{x}) = \sum_{\boldsymbol{i}=1}^{\boldsymbol{N}} P_{loss_i} = \sum_{\boldsymbol{i}=1}^{\boldsymbol{N}} P_{G_i} - \sum_{\boldsymbol{i}=1}^{\boldsymbol{N}} P_{D_i} \quad \textbf{(4.39)}$$

Subject to:

- **Equality constraints:**

The equality constraints in this section represent the balance of active and reactive power systems and can be written as:

$$P_{g_i} - P_{d_i} = V_i \sum_{j=1}^{N} V_j \left(g_{ij} \cos\delta_{ij} + z_{ij} \sin\delta_{ij} \right) \quad \textbf{(4.40)}$$

$$Q_{g_i} - Q_{d_i} = V_i \sum_{j=1}^{N} V_j \left(g_{ij} \sin\delta_{ij} + z_{ij} \cos\delta_{ij} \right) \quad \textbf{(4.41)}$$

- **Inequality constraints:**

The inequality constraints represent the limiting of the power system operation considering the presence of SVC device and HVDC transmission line as follow:

$$\begin{cases} P_{Gi}^{min} \le P_{Gi} \le P_{Gi}^{max} \\ Q_{Gi}^{min} \le Q_{Gi} \le Q_{Gi}^{max} \\ V_{Gi}^{min} \le V_{Gi} \le V_{Gi}^{max} \\ T_{NTi}^{min} \le T_{NTi} \le T_{NTi}^{max} \\ Q_{Ci}^{min} \le Q_{Ci} \le Q_{Ci}^{max} \\ Q_{SVCi}^{min} \le Q_{SVCi} \le Q_{SVCi}^{max} \\ SVC_i^{min} \le SVC_i \le SVC_i^{max} \\ HVDC_i^{min} \le HVDC_i \le HVDC_i^{max} \\ |S_{Li}| \le S_{Li}^{max} \end{cases} \quad \textbf{(4.42)}$$

- **Control variables**

The set of control variables can be represented by the vector u_1 for OPF problem considering SVC devices and by vector u_2 for OPF problem considering the HVDC transmission line as follows:

$$u_1 = \left[P_{G2} \ldots P_{GNG}, V_{G1} \ldots V_{GNG}, Q_{C1} \ldots Q_{CNC}, T_1 \ldots T_{NT}, Q_{SVC1} \ldots Q_{SVCNS}, SVC_1 \ldots SVC_{NSVC}\right] \quad \textbf{(4.43)}$$

$$u_2 = \left[P_{G2} \ldots P_{GNG}, V_{G1} \ldots V_{GNG}, Q_{C1} \ldots Q_{CNC}, T_1 \ldots T_{NT}, HVDC_1 \ldots HVDC_{NHVDC}\right] \quad \textbf{(4.44)}$$

where P_G is the generator active power, V_G is the generator voltage, Q_C is the reactive power injected by the shunts compensator, T is the tap setting of transformers, Q_{SVC} is the reactive power injected by the shunts compensator, SVC is the static VAR compensator device, HVDC is high voltage direct current line, NG is the number of generators, NC is the number of shunts compensators units and NT is the number of regulating transformers, *NSVC* is the number of SVC devices, *NHVDC* is the number of HVDC lines installed on the power grid.

- **State variables**

The vector of the state variables x which characterize any unique state of the optimization problem in the case to solve OPF problem considering SVC device and HVDC transmission lines is represented in Eq. (4.45) as follow:

$$x = \left[P_{Gslack}, Q_{G_1} \ldots Q_{G_{NG}}, V_{L_1} \ldots V_{L_{NL}}, S_{l_1} \ldots S_{l_{nl}}\right] \quad \textbf{(4.45)}$$

where P_{Gslack} is the active power generation at the slack bus, Q_G is the reactive power outputs of the generators, V_L is the voltage magnitude at load bus and S_l is the apparent power flow, *NG* is the total number of generator buses, *NL* is the total number of load buses or PQ buses, and nl is the total number of transmission lines.

4.8. OPF solution considering FACTS-HVDC systems

In this section, we analyze the operation of the electrical grid in the presence of the FACTS-HVDC systems, in particular, the static VAR compensator (SVC) and voltage source converter-based high voltage direct current (VSC-HVDC) transmission line. This optimization is based, first, on the application of the proposed algorithms to determine the optimal location and size of each technology, then demonstrate the influence of each of them on the technical parameters of the electrical network such as the total production cost, voltage profile, active power transmission losses as well as power lines.

4.8.1. OPF solution considering SVC devices

This part aims to solve the OPF problem considering SVC devices with the objective function is to minimize the total fuel cost. The proposed algorithms SMA and ALO have been implemented to find the optimal allocation of the SVC based on the determination of the lowest voltage in the load buses (PQ). In the power system, SVC is modeled by shunt variable admittance (provide or absorb reactive energy). In this case, IEEE 30-bus and Algerian 114-bus systems power systems are considered to test the performance and robustness of the proposed algorithms, and to study the impact of SVC on both power systems under the contingency state (load variation and line outage) for minimizing total generation cost as well as improve the voltage profile.

4.8.1.1. Application on the IEEE 30-bus system

To test the performance and robustness of the proposed algorithm and to study the effect of SVC on the IEEE 30-bus system, the ALO algorithm was adapted to solve the OPF problem considering SVC under contingency conditions. The contingency state is to uniformly increase the load variation index to 1.45 % from the base case as well as loss of the transmission line 6-28. In this context, the active and reactive powers consumed by the loads are multiplied by the same indices. The goal to install the SVC device in the IEEE 30-bus system is to test the influence of this device on the power system under the contingency state (load variation and line outage) to improve the voltage profile, minimize total generation cost as well as reduce the active power loss. The vector of control variables, in this section, contains the active powers generated, the generator voltage as well as the reactive power injected by the SVC devices as mentioned in Eq. (4.44).

The optimal allocation of SVC in the IEEE 30-bus system was determined by the proposed algorithm. Thus, to install one SVC, the proposed algorithm selected load bus N°30 as an optimal allocation, and to install two SVCs, the optimal allocations selected are load busses N°26 and N°30 respectively. The SVC's capacity in this work is ±25 MVar, which means that the SVC can absorb or inject the value of 25 MVar into the system. Three different cases are considered in this test based on the optimal location of SVC devices as follow:

- **Case 1**: OPF solutions without considering SVC;
- **Case 2**: OPF solutions considering one SVC installed at bus N° 30;
- **Case 3**: OPF solutions considering two SVCs installed at buses N°26 and N°30;

The obtained results by the proposed algorithm ALO for OPF considering SVC devices in all cases are tabulated in Table 4.1.

Table 4.1 Comparison of results obtained by ALO for IEEE 30-bus system considering SVC

Control variables	Limits		Active power loading 410.93 MW		
	Min	Max	Case 1	Case 2	Case 3
P_{G1}	50	200	200.0000	200.000	200.0000
P_{G2}	20	80	80.0000	79.9996	80.0000
P_{G5}	15	50	40.2930	40.2450	40.0971
P_{G8}	10	35	35.0000	35.0000	34.9992
P_{G11}	10	30	29.9951	30.0000	30.0000
P_{G13}	12	40	39.9942	39.9198	39.9999
V_{G1}	0.95	1.1	1.1000	1.1000	1.1000
V_{G2}	0.9	1.1	1.0856	1.0854	1.0848
V_{G5}	0.9	1.1	1.0601	1.0577	1.0579
V_{G8}	0.9	1.1	1.0737	1.0723	1.0695
V_{G11}	0.9	1.1	1.0890	1.1000	1.1000
V_{G13}	0.9	1.1	1.0980	1.0664	1.0999
T_{11}	0.9	1.1	1.0998	1.0999	1.0937
T_{12}	0.9	1.1	0.9998	1.0291	1.0499
T_{15}	0.9	1.1	1.0614	1.0979	1.1000
T_{36}	0.9	1.1	1.0895	1.0363	1.0494
Q_{C10}	0	5	3.1504	3.4762	4.3282
Q_{C12}	0	5	4.4374	79.9996	4.7278
Q_{C15}	0	5	4.5345	40.2450	80.0000
Q_{C17}	0	5	4.2268	35.0000	40.0971
Q_{C20}	0	5	3.8170	30.0000	34.9992
Q_{C21}	0	5	4.0411	39.9198	30.0000
Q_{C23}	0	5	4.0729	1.1000	39.9999
Q_{C24}	0	5	4.5764	1.0854	1.1000
Q_{C29}	0	5	4.6269	1.0577	1.0848
Q_{SVC_26}	-25	+25	-	9.3320	5.7594
Q_{SVC_30}	-25	+25	-	-	7.3043
V_{min} (p.u)			0.9176	0.9621	0.9786
Total generation cost ($/h)			1340.1299	1339.4886	1338.9976
Power losses (MW)			14.3522	14.2344	14.1663
Voltage deviation (p.u)			0.8320	0.5566	0.5467

Table 4.1 presents the simulation results obtained by the proposed algorithm ALO with and without the presence of SVC. From this table, the optimal installation of the SVC in cases 2 and 3 improved considerably the fuel cost, reduced the active power loss as well as improved the voltage profiles compared to case 1 (without SVC). In addition, it can be noted that the values of the fuel cost, the active power losses, as well as voltage deviation in case 3 when two SVCs are placed, are 1338.9976 $/h, 14.1663 MW and 0.5467 p.u, respectively, which are less compared to the values obtained in case 2 when only one SVC is placed at bus N°30. Moreover, the performance of the proposed algorithm SMA is high to converge towards the global solution based on the optimal values of control variables.

The convergence curve of fuel cost obtained by the ALO algorithm for the different case studies is shown in Fig. 4.14. From this figure, it can be noted that the proposed algorithm converges towards the global optimum at a few iterations for all cases studied, which indicates that the proposed algorithm is robust to solve the OPF problem considering SVC under contingency state.

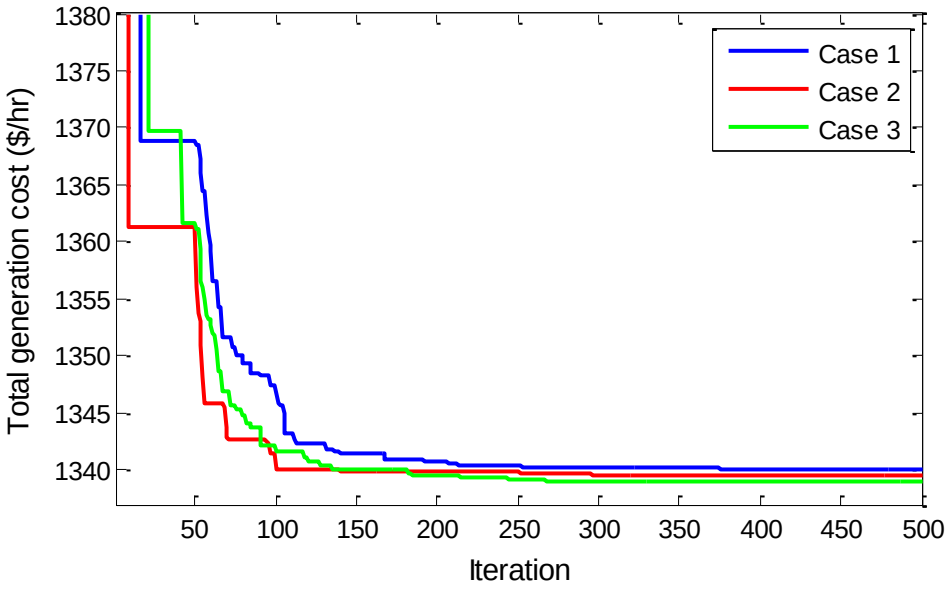

Figure 4.14 Convergence characteristics of ALO for the IEEE 30-bus system considering SVC device

Figure 4.15 shows the voltage profiles in the IEEE-30 bus system for the three case studies. In the case without the SVC, it can be noted that the load busses which are relatively far from the production units have lower voltages like busses N° 26, 29 and 30. These lower voltages are due to the long distance between these busses and the production units. Thus, the installation of the SVC devices in the optimal locations has improved considerably the voltage profile at the various load busses within acceptable limits.

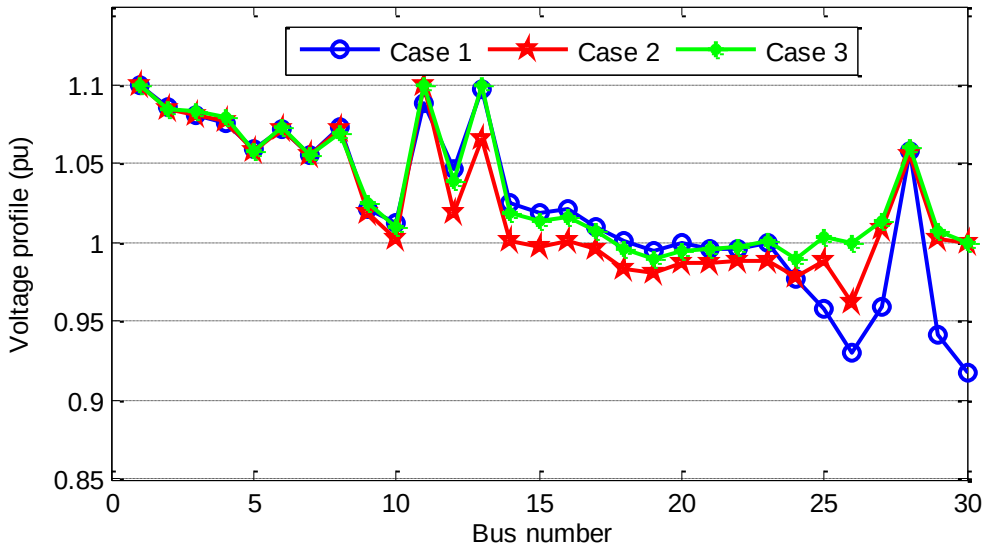

Figure 4.15 The effect of SVC installation on voltage profile in IEEE 30-bus system

4.8.1.2. Application on the Algerian 114-bus system

To illustrate the effectiveness of the proposed algorithm SMA in presence of SVC devices on the large-scale power system under the contingency state, the Algerian electrical network system ALG 114-bus is considered with loss of line 87-100. The objective function used in this case is similar to the previous section. The vector of control variables contains the active powers generated, the generator voltage as well as the reactive power injected by the SVC devices. The proposed algorithm is selected the bus N°89 (Souk Ahras) as an optimal location in the ALG 114 bus power system to install one SVC, to install two SVCs, the optimal locations selected are bus N°89 and bus N°92 (Djebel Onk - Bir El Ater), and for three SVCs, the optimal locations selected are bus 68 (Sedjerara), bus N°89 and bus N°92. To verify the effectiveness of the proposed algorithm SMA, three different cases are considered based on the optimal location of SVC devices as follow:

- **Case 1**: OPF solutions without considering SVC;
- **Case 2**: OPF solutions considering one SVC installed at bus N°89;
- **Case 3**: OPF solutions considering two SVCs installed at buses N°89 and N°92 ;
- **Case 4**: OPF solutions considering three SVCs installed at buses N°68, N°89 and N°92;

The simulation results obtained by the SMA algorithm for the three different study cases under the contingency state are tabulated in Table 4.2. From this table, total generation cost (TGC) and the active power losses obtained by using the proposed algorithm in the case without SVC are 18624.9978 $/h and 57.8726 MW, respectively, these both values are reduced to 18904.8603 $/h and 56.8991 MW with one SVC connected at bus 86, and to 18899.4372 $/h and 56.2617 MW with two SVCs connected simultaneously at buses 68 and 86, and to 18899.4372 $/h and 56.2617 MW with three SVCs connected simultaneously at buses 68, 89 and 92. As well as the voltage deviation was also improved from 5.1342 p.u (without SVC) to 4.6913 p.u, 4.6068 p.u, and 4.3313 p.u for case 2, case 3, and case 4, respectively. Moreover, it can be observed that the connection of SVC devices simultaneously at buses 68, 89 and 92 improved considerably the total generation cost, the active power loss as well as the voltage deviation compared to all other cases.

The convergence curve of the proposed algorithm is shown in Figure 4.16. From this figure, we notice that the algorithm ALO converges towards the global optimum at iteration 180 for all cases studied, which indicates the effectiveness of the proposed algorithm to solve the OPF problem considering SVC devices in the large-scale power system under contingency state.

Table 4.2 Comparison of results obtained by SMA for ALG 114-bus system considering SVC

Control variables	Limits		Case 1	Case 2	Case 3	Case 4
	Min	Max				
P_{G4}	135	1350	452.8530	453.2336	452.7252	451.7440
P_{G5}	135	1350	452.5042	451.6624	451.1290	450.4921
P_{G11}	10	100	100.0000	100.0000	99.9999	99.9980
P_{G15}	30	300	193.8506	192.5448	193.9547	191.9765
P_{G17}	135	1350	446.1043	446.7541	448.3210	450.8239
P_{G19}	34,5	345	196.6415	195.7762	195.1458	194.1114
P_{G22}	34,5	345	192.1810	192.4438	190.9080	191.9021
P_{G52}	34,5	345	190.9253	190.4791	191.4374	190.8379
P_{G80}	34,5	345	192.7280	193.0400	192.0309	192.2265
P_{G83}	30	300	190.4878	190.4750	190.6741	189.7601
P_{G98}	30	300	188.4344	188.7790	188.4296	190.3091
P_{G100}	60	600	600.0000	599.9996	600.0000	600.0000
P_{G101}	20	200	199.9990	200.0000	200.0000	200.0000
P_{G109}	10	100	100.0000	100.0000	100.0000	100.0000
P_{G111}	10	100	100.0000	99.9998	100.0000	100.0000
V_{G4}	0.9	1.1	1.1000	1.1000	1.1000	1.1000
V_{G5}	0.9	1.1	1.1000	1.1000	1.0999	1.0998
V_{G11}	0.9	1.1	1.0962	1.0959	1.0957	1.0967
V_{G15}	0.9	1.1	1.0997	1.0997	1.0999	1.1000
V_{G17}	0.9	1.1	1.1000	1.1000	1.1000	1.1000
V_{G19}	0.9	1.1	1.0647	1.0632	1.0603	1.0568
V_{G22}	0.9	1.1	1.0743	1.0725	1.0715	1.0663
V_{G52}	0.9	1.1	1.0723	1.0694	1.0689	1.0667
V_{G80}	0.9	1.1	1.1000	1.1000	1.1000	1.1000
V_{G83}	0.9	1.1	1.1000	1.1000	1.1000	1.0997
V_{G98}	0.9	1.1	1.1000	1.1000	1.1000	1.0999
V_{G100}	0.9	1.1	1.1000	1.1000	1.1000	1.1000
V_{G101}	0.9	1.1	1.1000	1.1000	1.1000	1.1000
V_{G109}	0.9	1.1	1.0997	1.1000	1.0997	1.1000
V_{G111}	0.9	1.1	1.0999	1.0591	1.0684	1.0582
Q_{SVC_68}	-45	45	-	-	22.6000	22.500
Q_{SVC_89}	-45	45	-	39.900	36.100	36.200
Q_{SVC_92}	-45	45	-	-	14.700	14.800
V_{min} (p.u)			0.8825	0.9162	0.9234	0.9466
Fuel cost ($/h)			19066.0147	19007.2159	19003.2572	18997.8522
Power losses (MW)			69.7092	68.1875	67.7557	67.1816
Voltage deviation (p.u)			5.1342	4.6913	4.6068	4.3313

On the other hand, SVC devices have managed to improve the voltage profiles as shown in Fig. 4.17. From this figure, it can be noted that the case without the presence of SVC, the two circles in this figure determine the two areas that have minimum load bus voltage values in the Algeria 114-bus power system. Also, it can be seen that bus 88 and bus 92 have exceeded the lower acceptable limits (0.9 p.u). Thus, when the SVCs devices were installed at different optimal locations, the voltage profiles obtained via the proposed algorithm are improved especially in the load buses from 88 to 93. Furthermore, the installation of SVCs simultaneously at buses 68, 89, and 92 improved considerably the voltage profiles at all critical load buses.

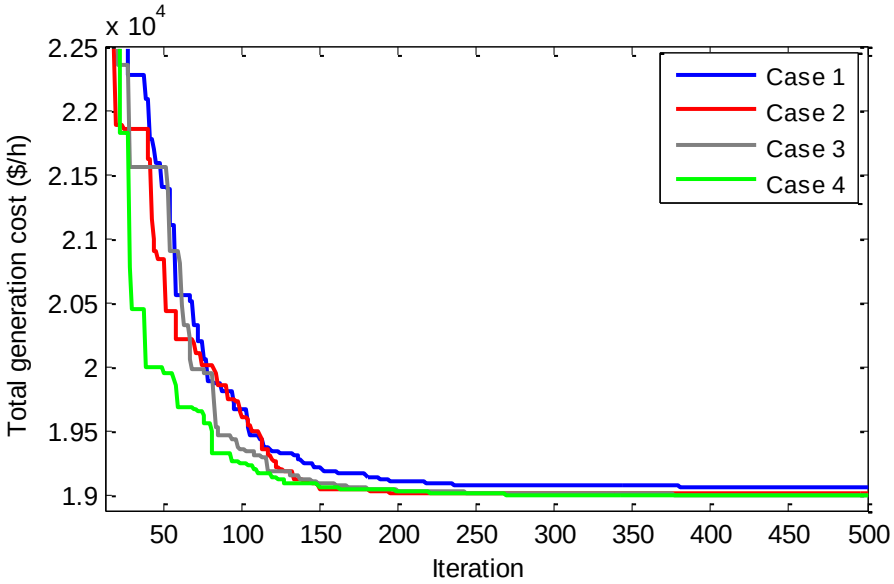

Figure 4.16 Convergence characteristics of SMA for the ALG 114-bus system considering SVC device

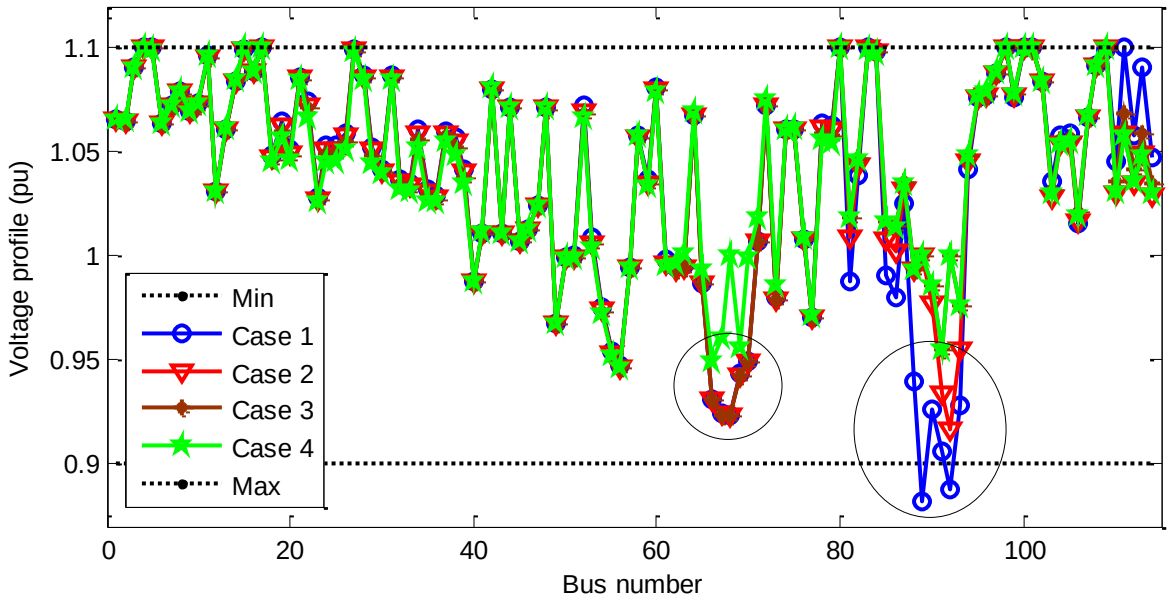

Figure 4.17 The effect of SVC installation on voltage profile in Algerian 114-bus system

4.8.2. OPF solution considering HVDC transmission line

This part will be devoted to the optimization of the power flow with consideration of a VSC-HVDC transmission line. Two objective functions are defined for the OPF problem based on total fuel cost and active power loss. The OPF is based first on the application of the proposed algorithms to determine the optimal location of the HVDC transmission line, then demonstrate the effect of HVDC transmission line on the technical parameters of the electrical network, especially, fuel cost, active power loss, active power transit as well as voltage profile. In this study, the results obtained with HVDC are compared with the results obtained without HVDC for the same power system to demonstrate the effect of the HVDC transmission line on the technical parameters of the electrical

network. The optimal location of the HVDC transmission line is based on the overload index of a transmission line in an electrical grid.

4.8.2.1. Application on the IEEE 30-bus system

To illustrate the effectiveness of the proposed algorithms in the AC/DC system, IEEE 30-bus was modifying by connected a VSC-HVDC link between busses N°2 and N°5 (this link is considered an optimal location of VSC-HVDC in the IEEE 30-bus system). The topology of this system is shown in Fig. 4.18. In this section, the first converter VSC1 is connected to bus 2 and works as a rectifier, the second converter VSC2 is connected to bus 5 and works as an inverter. The DC system voltage is +/- 200 kV. The data of converter stations are shown in Table 4.3.

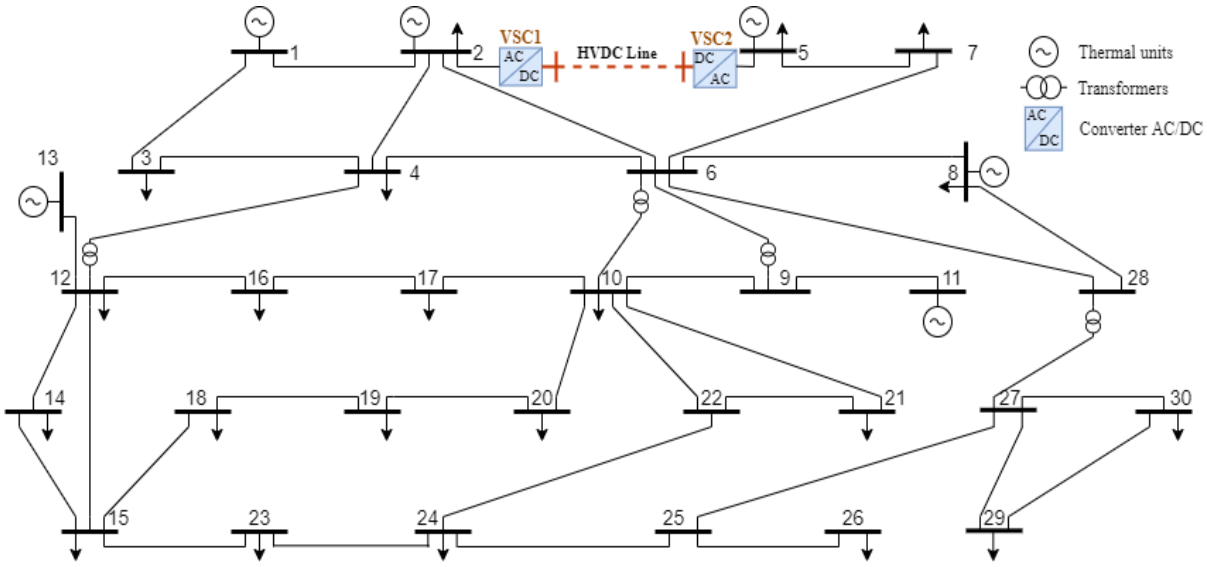

Figure 4.18 Modified IEEE-30 bus system with VSC-HVDC line

Table 4.3 The parameters of the converters stations

Converter parameters		**Voltage & Converter loss data 1 and 2**	
$\boldsymbol{X_{tr}(p.u)}$	0.1121	$\pm V_{dc}$	400
$\boldsymbol{R_{tr}}$ $\boldsymbol{(p.u)}$	0.0015	a	1.103
$\boldsymbol{B_f}$ $\boldsymbol{(p.u)}$	0.0887	b	0.887
$\boldsymbol{X_c}$ $\boldsymbol{(p.u)}$	0.1642	c_{rec}	2.885
$\boldsymbol{R_c}$ $\boldsymbol{(p.u)}$	0.0001	c_{inv}	4.371

In this part, the proposed algorithms are applied to solve AC/DC OPF problem under the contingency state, which is increased loading at 45%. Thus, the active power loading is 410.93 MW. In this section, two objective functions have been considered to verify the efficiency and performance of the proposed algorithms to solve the AC/DC OPF problem:

- **Case 1**: Minimization of fuel cost considering HVDC line
- **Case 2**: Minimization of active power transmission loss considering HVDC line

The DC bus data of the HVDC transmission line are presented in Table 4.4, and the simulation results obtained by using the proposed algorithms for two different objective functions are presented in Table 4.5.

Table 4.4 DC bus data in the IEEE 30-bus for two cases

	Voltage limites (p.u)		Voltage (p.u)	Active power (MW)
	Min	Max		
Rectifier	0.9	1.1	1.021	-89.886
Inverter	0.9	1.1	1.000	88.056

Table 4.5 Comparison of results obtained by SMA and ALO for IEEE 30-bus system considering HVDC line

Control variables	Limits		Active power loading 410.90 MW				
			Without HVDC	With HVDC: Case 1		With HVDC: Case 2	
	Min	Max		SMA	ALO	SMA	ALO
P_{G1}	50	200	199.9977	199.8913	199.9252	186.8361	186.9352
P_{G2}	20	80	78.8218	80.0000	79.9964	80.0000	80.0000
P_{G5}	15	50	42.4211	38.3108	40.0413	49.9985	50.0000
P_{G8}	10	35	34.9915	35.0000	34.9856	34.9935	35.0000
P_{G11}	10	30	29.9997	30.0000	29.9696	30.0000	30.0000
P_{G13}	12	40	38.2946	40.0000	38.4263	39.9704	40.0000
V_{G1}	0.9	1.1	1.1000	1.1000	1.1000	1.0999	1.1000
V_{G2}	0.9	1.1	1.0843	1.0743	1.0839	1.0848	1.0852
V_{G5}	0.9	1.1	1.0286	1.0429	1.0773	1.0512	1.0591
V_{G8}	0.9	1.1	1.0616	1.0588	1.0791	1.0618	1.0665
V_{G11}	0.9	1.1	1.1000	1.0974	1.1000	1.0925	1.0992
V_{G13}	0.9	1.1	1.1000	1.0061	1.0997	1.0535	0.9933
T_{11}	0.9	1.1	1.0189	1.0757	1.0540	0.9758	1.0628
T_{12}	0.9	1.1	1.0211	1.0910	1.0484	1.0715	1.0911
T_{15}	0.9	1.1	1.0511	1.0977	1.0025	1.0483	1.0998
T_{36}	0.9	1.1	0.9609	0.9876	1.0618	0.9922	1.0242
Q_{C10}	0	5	4.8813	4.0199	2.9404	4.5349	0.5538
Q_{C12}	0	5	1.9164	2.9859	1.9888	0.0156	2.8975
Q_{C15}	0	5	3.1109	4.9612	4.9968	4.8729	1.7648
Q_{C17}	0	5	4.9727	4.3501	4.1204	1.2838	4.8973
Q_{C20}	0	5	1.3915	2.8958	4.1967	2.5071	5.0000
Q_{C21}	0	5	4.9937	4.9989	4.9266	2.2143	1.6644
Q_{C23}	0	5	2.9808	4.6071	79.9964	4.9958	3.6108
Q_{C24}	0	5	4.6307	4.9977	40.0413	4.8841	2.7319
Q_{C29}	0	5	1.1981	2.8892	34.9856	3.7469	3.3808
Optimal location of HVDC			-	Line 5	Line 5	Line 5	Line 5
Total generation cost ($/h)			1339.4776	**1328.0798**	**1330.3884**	1359.10	1359.60
Power losses (MW)			13.5964	12.2720	12.4143	**10.8684**	**11.0052**
Voltage deviation (p.u)			0.7413	1.4189	1.5566	1.5518	1.3304

Table 4.5 shows the effect of the HVDC transmission line to minimize the total fuel cost and reduce the active power losses for both cases. Based on the results obtained, the proposed algorithms gave a better result for the case of connected the HVDC line between busses 2 and 5 for both different objective functions compared to results obtained in the case without the presence of the HVDC line. For case 1, the fuel cost is reduced from 1339.4776 $/h (without HVDC) to 1328.0798 $/h and 1330.3884 $/h by using SMA and ALO, respectively. For case 2, the active power loss is reduced from

13.5964 MW (without HVDC) to 10.8684 MW and 11.0052 MW by using SMA and ALO, respectively. Thus, a VSC-based HVDC transmission line gives a greater benefit on the total generation cost and total active power losses compared to either a high voltage AC (HVAC) system.

The convergence curve of fuel cost obtained via the SMA and ALO algorithms for case 1 is shown in Fig. 4.19. In this case, the total fuel cost and active power loss provide by the SMA algorithm are 1328.0798 $/h and 12.2720 MW, respectively, which are minimum than obtained by the ALO algorithm (1330.3884 $/h and 12.4143 MW).

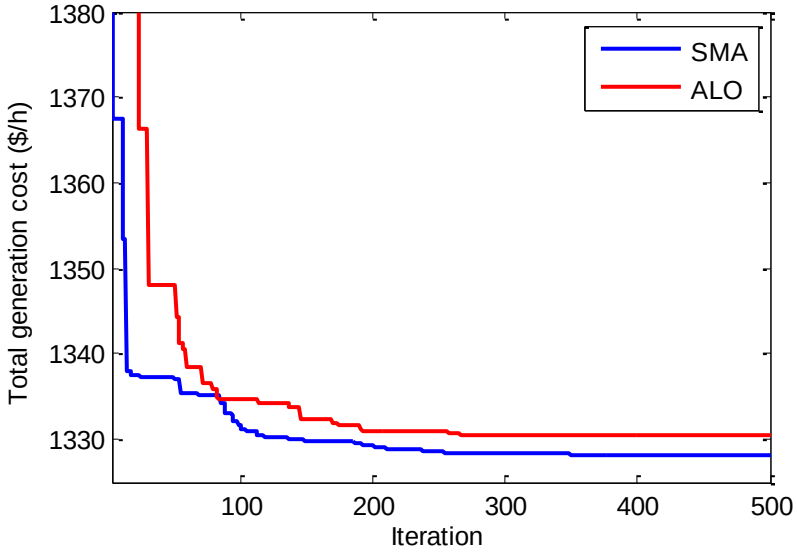

Figure 4.19 Convergence characteristics of SMA&ALO for IEEE 30-bus system considering HVDC: **Case1**

The convergence curve of active power loss obtained via the SMA and ALO algorithms for case 2 is shown in Fig. 4.20. In this case, the SMA algorithm provides 10.8684 MW and 1359.10 $/h, respectively, for the active power loss total fuel cost, these values are better compared to results achieved by the ALO algorithm (11.0052 MW and 1359.60 $/h).

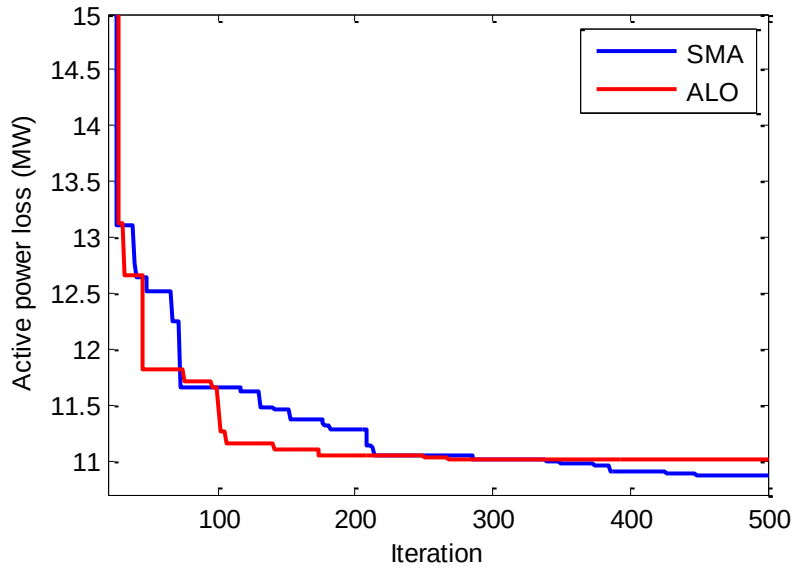

Figure 4.20 Convergence characteristics of SMA&ALO for IEEE 30-bus system considering HVDC: **Case2**

Figure 4.21 shows the active power transmitted for different cases studied. In the case without an HVDC transmission line, the power transmitted between busses 2 and 5 is 82.7915 MW, this value has exceeded the maximum limit of this line evaluated at 80.00 MW. Also, the power transmitted between busses 1 and 2 is near the maximum limit value. With a connected HVDC transmission line in the optimal location between busses 2 and 5, the active power transmission in all lines has improved especially in case 2. Thus, the effect of the HVDC transmission line is clear to solve the problem of overloading power lines based on its large capacity for transport power.

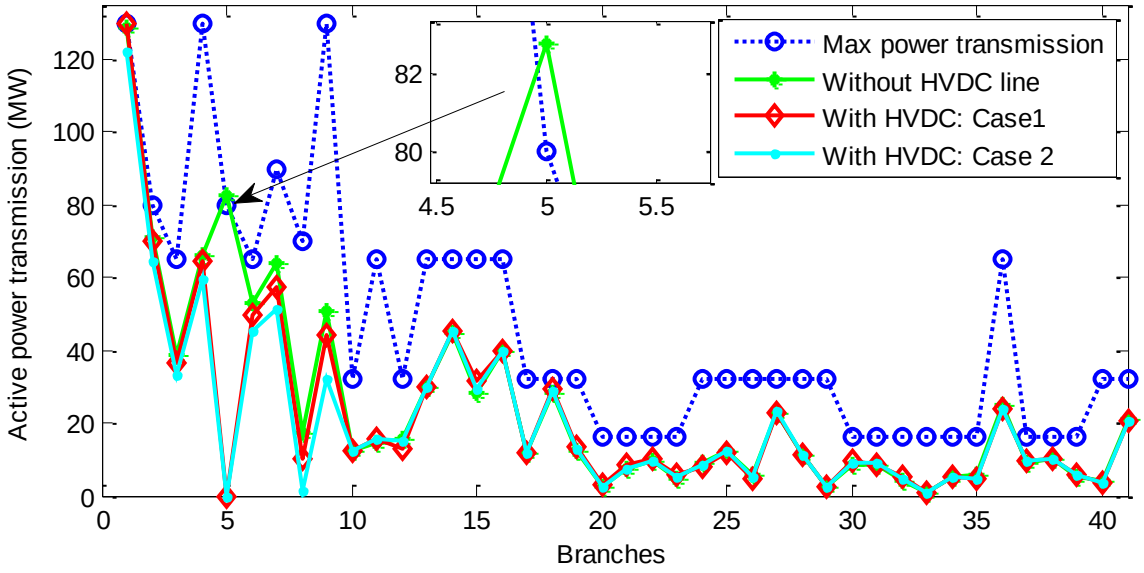

Figure 4.21 The effect of HVDC installation on line power transmission in IEEE 30-bus system

4.9. Conclusion

In this chapter, we have presented in the first part an overview of FACTS devices and HVDC technology and their classification and advantages in enhancing power systems. The static VAR compensator (SVC) device and the voltage source converters-based HVDC technology (VSC-HVDC) have been detailed and modeled which will be used in this study. Finally, we have explored and tested the application of the proposed metaheuristic algorithms SMA and ALO on the IEEE 30-bus and Algerian power system 114-bus system to solve the optimal power flow (OPF) problem considering the SVC device and VSC-HVDC system under contingency conditions. The choice of optimal locations of SVC device and HVDC transmission line was determined by the proposed algorithms to satisfy the main objectives such as improve voltage profile, minimize fuel cost, reduce active power loss, and avoid line overloading. The simulation results obtained showed the feasibility of the proposed algorithms to solve the OPF problem considering the SVC device and VSC-HVDC, as well as demonstrated the effectiveness of the SVC device and HVDC transmission line to ensure the efficient operation and control of the power grids, especially with growing power demand.

Chapter 05:Optimal Power Flow Solution Incorporating Stochastic Wind energy

5.1. Introduction

Electrical energy is an essential factor for the development and evolution of human societies, whether in terms of improving living conditions or in the development of industrial activities. In recent years, the energy demand has steadily increased which has caused a decrease in the natural resources and also the appearance of environmental problems as generates high pollution that causes an irreversible climate change, and to remedy this, we have turned more and more towards renewable energies. After several decades of continuous research and development efforts in renewable energy sources (RESs), the annual capacity growth of these RESs plants is higher than the total investment capacity added in the combined coal, natural gas, and oil power plants. Among the many types of RESs, wind energy is one of the most popular renewable energy sources which are available in abundance both on land (onshore) and at sea (offshore). This present work focuses on the incorporation of wind energy which keeps developing thanks to the technological advances made in the field of the wind generators.

This chapter presents in the first part an overview of the wind power systems followed by a brief description of the wind energy conversion system (WECS) basics. Then, it introduces the stochastic modeling of output power wind turbines in order to introduce it in the model of the power flow to be optimized. In this chapter, the formulation of the OPF problem incorporating wind power that needs to be solved is presented. Finally, the proposed algorithms have been implemented to solve the OPF problem considering stochastic wind power with the presence of an SVC device and VSC-MTDC technology.

5.2. Renewable energy

Renewable energy can be known as green energy or clean energy, is the energy that comes from natural resources or processes that are constantly replenished [1], even if their availability depends on weather and weather conditions, and whose exploitation causes the least possible ecological damage, does not cause toxic waste and does not cause damage to the environment. However, there are many types of renewable energy sources such as solar, wind, tidal, wave, organic

decomposition of the biomass of matter, hydropower, and geothermal that is earth heat, etc. The main renewable energy sources and their uses are presented in Table 5.1.

Table 5.1 Renewable energy sources and their use [157], [158]

Renewable energy sources	Usage options
Wind	Power generation, wind generators, windmills, water pump
Solar	Solar home systems, solar dryers, solar cookers
Hydraulic	Power generation
Geothermal	Urban heating, power generation, hydrothermal, hot dry rock
biomass	Heat and power generation, pyrolysis, gasification, digestion
Wave and tide	Numerous design, barrage, tidal stream

5.2.1. Wind energy

Wind energy is a very simple process. Kinetic energy is captured from air mass displacements using an air generator, this kinetic energy can be exploited to produce mechanical power by a technology known as a wind turbine, that can be used to convert mechanical power into electricity [158]. The turbines need the wind to operate, which is just natural moving air, and the air is everywhere. Wind means free, abundant and sustainable energy that will not depreciate if we take advantage of it. The wind speed of a site may be obtained by direct measurement on-site or from wind resource maps [159]. In this work, we focus on this type of renewable energy.

5.2.2. Solar energy

Solar-derived energy is known as solar energy, the most abundant renewable resource for most countries. Solar energy is transformed into electricity by solar technologies known as photovoltaic technology (PV) or concentrated solar power (CSP). PV technology is a method of producing electrical energy by transforming solar radiation into direct current electricity using semiconductor materials [1]. The second technology CSP is an indirect technology because it first uses mirrors and lenses to concentrate naturally available solar energy to heat the water to steam that is used in the steam turbine to produce electricity [160], the conversion efficiency of this CSP technology is varied from 20% to 24% [159]. Solar energy, therefore, has the advantage of being inexhaustible and usable at any point in a territory. In recent years, the deployment of photovoltaic has broken records year after year. After almost a period of stagnation, it has become one of the leading technologies in terms of installed capacity [161].

5.2.3. Hydropower

Among other renewable energy sources, hydroelectric energy is one of the most natural ways of producing high-power renewable electricity [159]. Hydroelectric power plants use the kinetic energy of the waterfall (rivers, dams, waves and tidal) to run hydro turbines coupled with electric generators. Also, hydroelectricity is a RES storage technology since electricity can be produced on demand [159]. Hydropower is by far the most widespread renewable energy as it is also used in centralized production. Hydroelectric power generation is the most efficient process and one of the least polluting [161].

5.2.4. Geothermal energy

Geothermal energy is present in the earth's interior in the form of a heat energy source [157], is about 250°C a few kilometers from the earth's surface and about 600°C near the center below the surface [159], and stored in rocks, in the form of hot water or steam tanks. In general, geothermal resources provide power in the form of electricity and the form of heating/direct cooling [161]. Geothermal power plants use the heat from the earth's interior, this hot water is pumped to the surface to pass through exchangers and the steam produced is turbinated in a conventional thermal plant.

5.2.5. Bioenergy

Bioenergy is a renewable energy source obtained from biomass, It is an important source that can be used for many applications such as electricity generation, biodiesel, heating, cooking, etc [157]. There are three main forms of fundamental bioenergy energy as mechanical energy, heat energy and electricity, all of these forms can be obtained from biomass sources [161]. Bioenergy is derived from organic materials such as wood, agricultural crops, animal and plant waste, etc. these resources or industrial and domestic waste are used as a primary source of fuels in some thermal power plants. Biomass can be used to produce electricity, when biomass is burned, the chemical energy is released as heat and can produce electricity with a steam turbine [159]. Since animal and plant waste is produced naturally, biomass is a renewable energy resource.

5.2.6. Ocean energy

Ocean or marine energy is extracted from the ocean waves, tidal energy (resulting from the movement of water created by tides), tidal currents, ocean currents, thermal energy from the seas (produced by exploiting the difference in temperature between the surface water and the deep water of the oceans), and salinity gradients [161]. Like other renewable sources, it is non-polluting during

production. It is also noted that the potential energy available is enormous and that this technology has a bright future.

5.3. Wind turbine system

Wind power was used to provide mechanical work. This energy is generated by variations in temperature due to solar energy and air pressure around the earth's surface. The existence of wind energy has been alive for at least three thousand years, initially, it was a design of pumping water, grinding grains, and other agricultural reasons. During the middle ages, windmills were in great use across the Mediterranean area, by the end of the 18th cycle around 10,000 wind turbines (WTG) were in service only in the Netherlands. The wind turbine used for the generation of electricity was invented in 1888 in Cleveland, Ohio by Charles F. Brush, and it generated about 12 kilowatts (kW) of power. The technological improvement of wind turbines since the 1990s has made it possible to build wind turbines of more than 5 MW and the development of 12 MW wind turbines is underway. The largest turbine in the world is GE's Haliade-X, the industry's first 12 MW turbine. The first prototype was installed at the Port of Rotterdam in 2019 for testing. Its commercialization is expected in 2021 [162]. In the offshore wind farm, the average size of offshore turbines installed in 2019 was 7.8 MW, up from 6.8 MW in 2018 according to trade body WindEurope [162]. Recently, government subsidies have enabled their development in a large number of countries. Wind turbines are now used to produce alternating current for electricity grids, in the same way as a thermal power plant. There has been a major global shift in electricity generation in recent decades.

5.3.1. Types of wind turbine

Indeed, there is a great diversity of wind turbines (WT) and tend to distinguish by their size (their speed or nominal power) and the shape of the orientation of the axis (the geometric arrangement of the shaft on which the propeller is mounted) [163]. There are two basics of wind turbine technologies available depending on the turbine's axis of rotation, namely [159]:

- Horizontal axis wind turbines (HAWTs)
- Vertical axis wind turbines (VAWTs)

5.3.1.1. Horizontal axis wind turbine

The horizontal axis wind turbines are currently the most used and have been studied and developed to a large extent in the past centuries [164]. Recently, modern wind turbines use horizontal axis wind turbines model and operate either downwind or upwind configuration [165]. The propeller has two or three rotor blades that are directed towards the wind and turn aerodynamically, therefore,

the rotor has tail blades attached to continuously steer the blades in the wind direction [159]. Two-blade wind turbines and three-blade wind turbines operate on the same principle. The efficiency of horizontal axis wind turbines is higher than that of vertical axis wind turbines [159], [166].

Figure 5.1 Horizontal axis wind turbine

5.3.1.2. Vertical axis wind turbine

The vertical axis wind turbine type operates independently of the wind direction and does not need to be oriented towards the wind. The blades of the vertical axis wind turbine rotate around a vertically positioned shaft, as its name suggests. It can capture weaker winds, allowing it to be exploited more frequently. in recent years, the performance of VAWTs has been improved with advancements in research and rotor technology and integrated with other beneficial features such as wider operational range and better performance within more complex urban terrains [164]. The two main structures of VAWT are derived from either the Darrieus or the Savonius rotors [163], which are detailed in the following sections.

a. Darrieus Rotor Wind Generators

This type of wind generator uses long airfoil-shaped blades (i.e. tapered such as aircraft wings) to extract the energy that the wind hits the blades perpendicular [163]. Wind turbines of type Darrieus with vertical, parabolic, or helical blades use the wind lift forces, like conventional wind turbines. Darrieus wind turbines tend to be less efficient than HAWT wind turbines in an ideal environment with low turbulence. But in conditions of high turbulence and directional wind fluctuations in urban areas, Darrieus machines can operate more smoothly and produce more energy than HAWTs [167]. The efficiency of Darrieus wind turbines is lower than that of HAWTs [163].

Figure 5.2 Darrieus type vertical axis wind turbine

b. Savonius rotor wind turbines

This type of wind turbine consists of half-cylinders connected to a vertical axis. Looking down from the top, a Savonius rotor turbine would look like two spoons oriented in opposite directions and connected to the center of the rotor axis as shown in Fig. 5.4 [163]. They are based on the principle of differential drag which stipulates that an engine torque can be obtained by a different pressure exerted by the wind on the concave and convex parts of the structure. The efficiency of Savonius wind turbines is lower than that of wind turbines that use the lift, but this type of machine allows for lower wind speeds and is ideal for urban integration because of their small size and quieter than other wind turbines.

Figure 5.3 Sovonius type vertical axis wind turbine

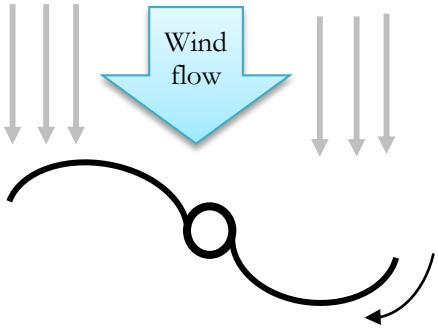

Figure 5.4 Diagram of a Sovonius rotor from above

5.3.2. Operation and main components of a wind turbine

The different main components of a wind turbine are illustrated in Fig. 5.5, and the detail of these components are represented below:

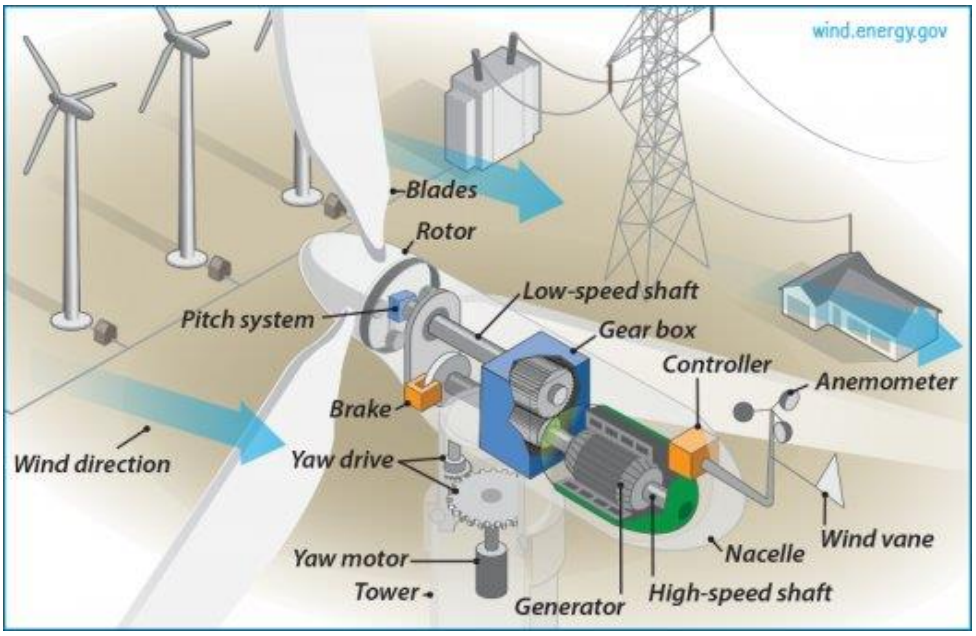

Figure 5.5 Wind turbine constitution

- **The Foundation**: For onshore wind turbines, the foundation is a concrete foundation on which the entire structure must be able to withstand storms and extreme winds. For offshore wind turbines (known as offshore), the foundation, a structure of high size exceeding the surface of the sea. This structure can be essentially concrete or made of concrete and huge steel tubes, which allows maintaining the overall structure.
- **Nacelle**: The nacelle is located atop the tower and contains the gearbox, low- and high-speed shafts, generator, controller, and brake. All this machinery allows transforms the slow rotation of the blades into electricity and that which allows the best orientation of the machines.

- **Blades**: These are the kinetic energy sensors that transmit energy to the rotor, and lifts and rotates when the wind is blown over them, causing the rotor to spin. They can be made of wood, aluminum alloy or composite materials.
- **The electric generator**: It ensures electric production, it is usually an off-the-shelf induction generator and its power can reach up to 5 MW. It can be a dynamo (DC product) or an alternator (AC product). The alternator is used most for reasons of cost and efficiency.
- **Tower**: it's consisting of the mast, the electrical control system and the transformer, generally of conical shape. The mast's a steel pipe and supports the nacelle, it measures between 50 and 130 m high. Its height is important: the higher it increases, the more the wind speed increases but at the same time the cost of the structure increases. The electrical control system manages the overall operation of the wind turbine and its steering mechanism.
- **The hub**: It is equipped with a system that allows the orientation of the blades to regulate the rotation speed. It is usually a piece of cast steel.

5.4. Wind energy conversion system (WECS)

The wind energy conversion system (WECS) includes wind turbines, generators, control systems, interconnection apparatus. The blades convert the kinetic energy of the wind into mechanical energy. The latter is converted into electrical energy by a synchronous or asynchronous type of electric generator. Figure 5.6 shows the block diagram of the WECS. Most generators need to run at high speed to generate electricity. The power output goes to the grid by using a transformer, there is also a proper controller to avoid disturbances and to protect the electrical system [165]. The wind farm can be distributed in many areas such as offshore, onshore, hilly, etc.

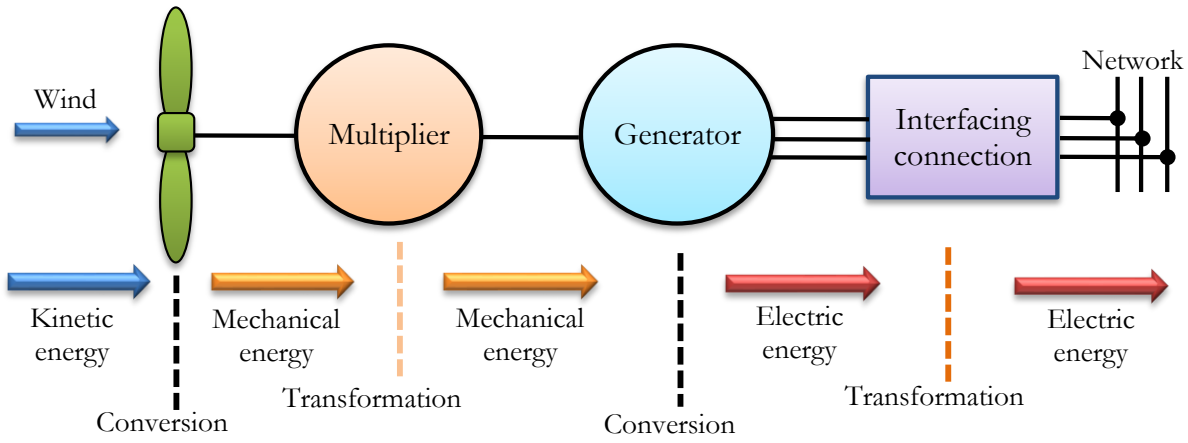

Figure 5.6 The wind energy conversion system (WECS)

5.4.1. Wind turbine generators technology

Two main types of generators used in the wind turbine industry are synchronous generators and asynchronous generators. The synchronous generator of the wind turbine can be a wound rotor synchronous generator (WRSG) and a permanent magnet synchronous generator (PMSG). The asynchronous generator of the wind turbine can be a squirrel-cage induction generator (SCIG), doubly fed induction generator (DFIG), wound rotor induction generator (WRIG), etc [168], [169].

5.4.1.1. Synchronous Generator

The synchronous generator operates at the synchronous speed, dictated by the frequency of the connected grid. The advantage of the synchronous generator over the asynchronous generator is the absence of a reactive magnetizing current. The magnetic field of the synchronous generator can be obtained by magnets or by a conventional field winding. If the generator has a sufficient number of poles, it can be used for direct-drive applications that do not require a gearbox (multiplier). the synchronous generator is more expensive and complex than an asynchronous generator of equivalent size [168]. There two types of the synchronous generator are used in the wind turbine industry:

- ***Permanent magnet synchronous generator (PMSG):***

PMSG has a wound stator, while its rotor is provided with a permanent magnet pole system. The auto-excitation feature of this generator allows it to operate with a high power factor and a high efficiency, it is suitable for application to wind generation systems. In fact, in the small turbine category, its reduced cost and simplicity make it the most used generator. However, in higher power applications, the materials used for producing permanent magnets are expensive and they are difficult to manufacture make them the least competitive.

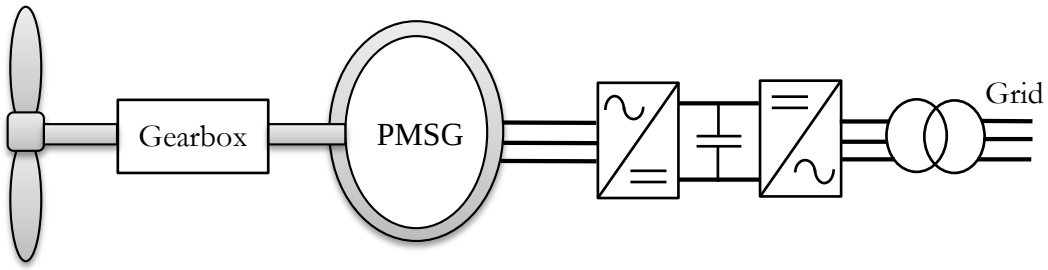

Figure 5.7 WECS with permanent magnet synchronous generator (PMSG)

- ***Wound rotor synchronous generator (WRSG):***

WRSG is the workhorse of the electrical power industry [168]. The direct connection to the power grid implies that the synchronous generator runs at a constant speed, which is fixed by the frequency of the grid. Excitation is provided by the rotor winding, through which direct current

(DC) flows. The implementation of a converter in a multipolar system without gears allows direct drive at variable speed. However, this solution involves the use of an oversized generator and a power converter sized for the total system power.

5.4.1.2. Asynchronous Generator

The asynchronous generator is widely used in medium and large wind turbines due to its robustness, mechanical simplicity and reduced cost. Its major disadvantage is the consumption of a reactive current of magnetization to the stator.

- ***Squirrel-cage induction generator (SCIG):***

  The SCIG is an important choice used by the industry because of its simplicity, good performance and reduced maintenance. There are many solutions to cover the demand of reactive power through of connection of a group of capacitors in parallel with the generator, or by the implementation of a static power converter as shown in Fig. 5.8.

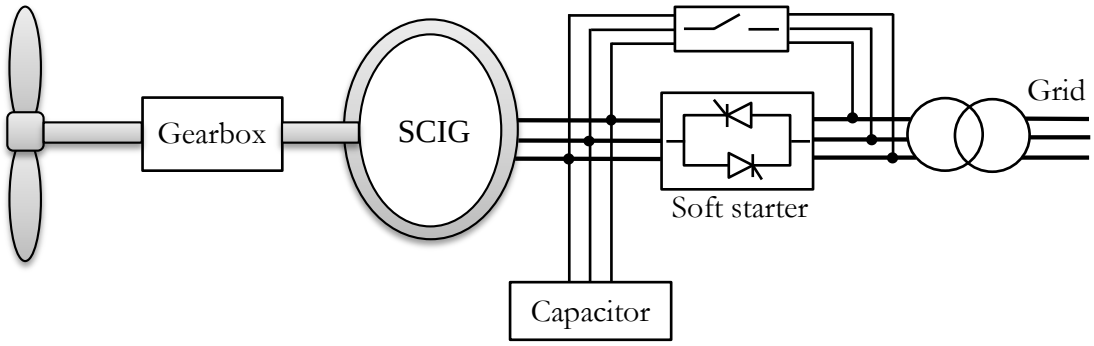

Figure 5.8 WECS with squirrel-cage induction generator (SCIG)

- ***Doubly fed induction generator (DFIG):***

  The DFIG has attracted particular interest especially as a generator in the field of wind energy. DFIG has the stator is directly connected to the grid through an interface consisting of two static converters, and while the rotor is connected to the grid through a voltage source converter (VSC) technology. Dual Power refers to the stator voltage taken from the network and the rotor voltage supplied by the inverter. This system allows variable speed operation over a specific operating range. The converter compensates for the difference in mechanical and electrical frequencies by injecting a variable frequency current into the rotor. A drawback of the DFIG is the inevitable need for slip rings [168]. The general structure of the control block diagram in the DFIG-WECS having two levels of control is shown in Fig. 5.9.

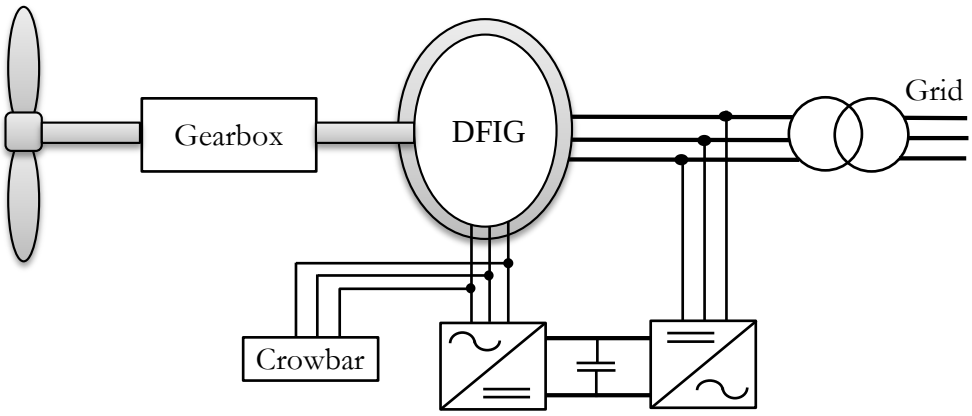

Figure 5.9 WECS with doubly fed induction generator (DFIG)

5.4.2. Fixed-Speed and Variable-Speed WECS

Many different types of WECSs are classified based on their features and drive train types [170]. The wind turbines can also be classified according to their speed control ability into two significant classes such as fixed-speed wind turbines and variable-speed wind turbines [168].

5.4.2.1. Fixed-speed wind turbines

Fixed-speed wind turbines rotate at an almost constant speed which is determined by the no of poles of the electrical generator, grid frequency and the gear ratio. The characteristic of these wind turbines is that they are equipped with a SCIG connected directly to the electrical grid. This machine is driven by a multiplier and its speed is kept approximately constant by a mechanical blade orientation system (pitch control). A capacitor battery is often combined to compensate for the reactive power needed to magnetize the asynchronous cage machine. wind turbines of this type are equipped with an aerodynamic control (stall control or pitch control) to regulate the power above the rated wind speed and protect them during high wind speeds [168]. The rotor speed of the FSWT is almost fixed regardless of the wind speed and it's stuck to the electrical grid frequency and cannot be changed. The advantages of FSWT are the simple, robust and low cost of construction parts [168]. In small wind turbines, FSWTs seem to be the most competitive concept in terms of cost. In large wind turbines and particularly in wind farms, the problems with fixed-speed operation become more and more significant [171]. This configuration has the following disadvantages [168], [172]:

- A reactive energy-consuming device necessary for magnetizing the asynchronous machine;
- Noisy, due to the modification of the highly stressed blade orientation system;
- Frequent variations in mechanical torque due to the movement of the blades to maintain a constant speed, resulting in rapid variations in the current in the array;
- Inability to adjust the generated power.
- limited power quality control and uncontrollable reactive power consumption

5.4.2.2. Variable-speed wind turbines

During the past decade, variable-speed wind turbine technology has become the dominant type among the installed wind turbines. The generators most commonly used for high-power variable speed wind turbines are doubly-fed induction generators (DFIG) because their characteristics allow for a variable mechanical force. The characteristic of these wind turbines is that the variable-speed operation can only be achieved by decoupling the electrical grid frequency and mechanical rotor frequency through a power electronic interface [168]. Within variable-speed operation, it is possible to continuously adapt (accelerate or decelerate) the rotational speed of the wind turbine to the wind speed, in such a way that the turbine operates continuously at its highest level of aerodynamic efficiency. The main advantages of variable speed wind turbines compared to fixed speed generators are [168]:

- For low wind speeds where the maximum power is converted, this increases the power generated in the system;
- The possibility to control the generator speed via electromagnetic torque. In particular, it reduces the role of the blade orientation system.
- The active and reactive power can be easily controlled
- It reduces mechanical effort by the fact that when the wind changes, the turbine speed is adapted.
- Noise during low power operation is reduced because the speed is low.
- It adapts the large wind turbine's integration into the electricity grid.

This configuration contains the only disadvantages associated with:

- Increased cost and power losses due to power electronics
- The control system more complex

5.5. Modeling of wind turbine

In the WECS principle, the kinetic energy of the wind resource is transformed into mechanical energy through a wind turbine and hence it is converted into electrical energy. The kinetic energy (E_k) can be expressed in terms of air mass m moving at speed v_{wind} as follow:

$$E_k = \frac{1}{2} m v_{wind}^2 \quad \textbf{(5.1)}$$

During a period t, the mass of air m passing through a given area "A" at a speed with a density of air mass ρ. The air mass per second can be expressed as:

$$m = \rho A v_{wind} \quad \textbf{(5.2)}$$

By substituting Eq. (5.2) in Eq. (5.1), the power transferred to a wind turbine is given as follows:

$$P_{wt} = \frac{1}{2}\rho A v_{wind}^3 \quad \textbf{(5.3)}$$

As per Betz limit, the mechanical energy captured by the wind turbine depends on the power efficiency of the rotor C_P, and is demonstrated by using the following equation:

$$P_m = \frac{1}{2}\rho A C_p(\lambda,\beta) v_{wind}^3 \quad \textbf{(5.4)}$$

where ρ is the air density, A is the area swept out by turbine blades (m^2), C_p is the power coefficient of the rotor, λ (or TSR) is defined as the tip-speed ratio, β is the angle of pitch and v_{wind} is the wind speed (m/s).

The tip-speed ratio λ is defined as the ratio between the linear speed of the turbine Ω_t at the tip of the blade and the wind speed, its expression is given as follows:

$$\lambda = \frac{\Omega_t R_{blade}}{v_{wind}} \quad \textbf{(5.5)}$$

where Ω_t is the angular speed (m/s) and R_{blade} is the rotor blade radius (m).

The power efficiency of the rotor C_P or called the power coefficient of the rotor is the function of the blade tip speed ratio λ and blade pitch angle β, Cp is maximum at β = 0. The theoretical maximum value of the power coefficient is given as 0.59. In practical designs, for high-speed, two-blade turbines, the maximum achievable $C_P$is between 0.4 and 0.5, and for low-speed turbines with more blades, it's between 0.2 and 0.4. The power coefficient of the rotor C_P is defined by the following formula:

$$C_P(\lambda,\beta) = C_1\left(\frac{C_2}{\lambda_i} - C_3\beta - C_4\right)\exp\left(\frac{-C_5}{\lambda_i}\right) + C_6\lambda \quad \textbf{(5.6)}$$

With the reduced specific speed

$$\frac{1}{\lambda_i} = \left(\frac{1}{\lambda + 0.08\beta} - \frac{0.035}{\beta^3 + 1}\right) \quad \textbf{(5.7)}$$

For the example studied, the coefficients C1 to C6 are as follows: C1 to C6 are C1= 0.5176, C2 = 116, C3 = 0.4, C4 = 5, C5 = 21 and C6=0.0068.

Figure 5.10 shows a typical relationship between the power coefficient and the tip speed ratio λ. It can be noted that the maximum value of the power coefficient C_p is equal to 0.48 for β = 0° and λ = 7.8.

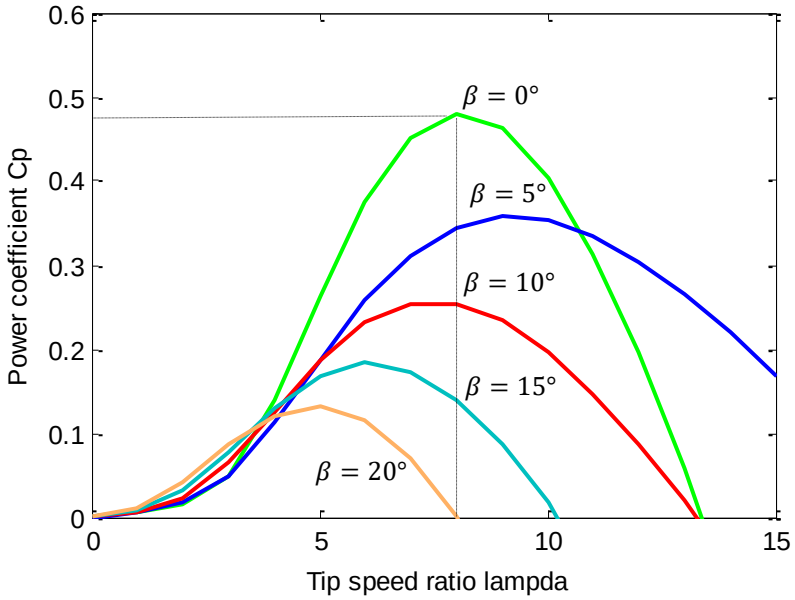

Figure 5.10 Power coefficient of the wind turbine model

5.6. Stochastic modeling of wind power

The distribution function was used in this work to model and characterize the distributions of wind speed variations known as the Weibull probability density function (PDF) [107], this functi on makes it possible to characterize the frequency distribution of wind speeds over a given time: a year, a month or a day for example. The wind industry needs to be able to differentiate between wind speeds [173]. The Weibull distribution PDF for wind speed is given by Eq. (5.8) [174]:

$$f_V(V) = \frac{k}{c}\left(\frac{v}{c}\right)^{k-1} e^{\left[\left(-\frac{v}{c}\right)^k\right]} \tag{5.8}$$

where f_V is the PDF of wind speed, k and c respectively the shape factor and scale factor (m/s), v is the wind speed.

The mean of Weibull distribution is expressed as:

$$M_{wbl} = c^m * \Gamma\left(1+\frac{m}{k}\right), \quad m = 1,2,\ldots..n \tag{5.9}$$

where gamma function Γ is given by Eq. (5.10) as follow:

$$\Gamma(x) = \int_0^\infty exp^{-t} t^{x-1} dt \tag{5.10}$$

The Weibull distribution is known as the Rayleigh distribution when the shape factor k is equal to 2 and is used for most land-based wind turbine sites. Figure 5.11 shows the Weibull PDF of wind speed curves for shape factors k=2, and three different values of scale factor c are indicated; c = 5 m/s, c =15 m/s, and c =25 m/s.

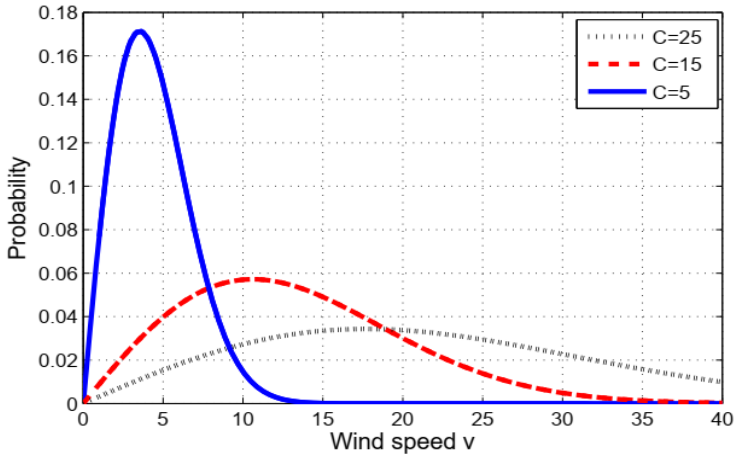

Figure 5.11 Weibull PDF characteristic for different values of *c* [175]

The cumulative distribution function (CDF) of the Weibull distribution expressed in Eq. (5.11), is obtained by integration of Weibull PDF [37], [176], whose most literature adopts this Weibull distribution which is very close to the reality of wind speed.

$$f_{CDF_v}(v) = \int_0^v f_v(v)\,dv = 1 - e^{-\left(\frac{v}{c}\right)^k} \tag{5.11}$$

where f_{CDF_v} is Weibull cumulative distribution function (CDF).

5.6.1. The power output of the wind generator

The output wind power curve of a wind generator is shown in Fig. 5.12. The wind power output can be represented in four regions depending on the wind speeds as expressed in the following equation:

$$P_w = \begin{cases} 0 & if\ v < v_{cut\_in} \quad and\ v > v_{cut\_off} \\ P_{wr}\left(\dfrac{v - v_{cut\_in}}{v_{rated} - v_{cut\_in}}\right) & if\ \ v_{cut\_in} < v < v_{v_{rated}} \\ P_{wr} & if\ v_{rated} < v < v_{cut\_off} \end{cases} \tag{5.12}$$

where P_{wr} is the rated power of the wind generator, $v_{cut\text{-}in}$ is the wind speed at which wind turbine starts to generate power, $v_{cut\text{-}off}$ is the wind speed at which the wind turbine is disconnected, v_{rated} is the wind speed at which the mechanical power output will be the rated power.

In the first region, no power will be produced due to the very low speeds. In the second region, wind turbines are started to generate power when the wind speed exceeds v_{cut-in} and the power generated increases with the wind speed grows until the rated power of the turbine is reached at the rated speed v_{rated} . In the third region, at wind speeds from v_{cut-in} to $v_{cut-off}$, the power generation

remains constant until cut-off wind speed ($v_{cut-off}$ in the figure). In the fourth region, to avoid high mechanical damage, the wind turbine is stopped when wind speeds exceed the cut-out wind speed limit.

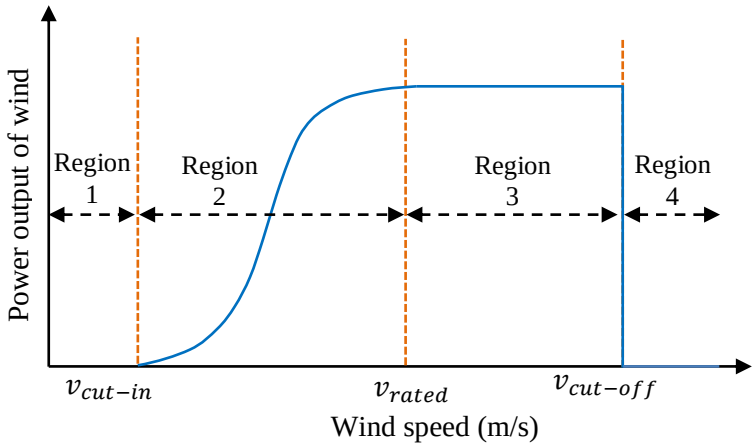

Figure 5.12 The wind power output curve

5.6.2. Wind power probabilities for different wind speeds

The probability of the wind turbine power output for the Weibull distribution function will lead to discrete and continuous portions. These two portions are explained as follows:

The probability for the discrete portion of the wind power output is expressed by Eq. (5.13) and Eq. (5.14), respectively [177]. According to Eq. (5.12), when wind speed v is below v_{cut-in} and above $v_{cut-off}$, the output wind power is zero. Also, the wind power is equal to the rated power P_{wr} when the wind speed is between v_{rated} and $v_{cut-off}$. The two probabilities can be calculated as follows:

$$f_w(P_w)\{P_w = 0\} = 1 - exp\left(-\left(\frac{v_{cut-in}}{c}\right)^k\right) + exp\left(-\left(\left(\frac{v_{cut-off}}{c}\right)^k\right)\right) \quad \textbf{(5.13)}$$

$$f_w(P_w)\{P_w = P_{wr}\} = exp\left(-\left(\frac{v_{rated}}{c}\right)^k\right) - exp\left(-\left(\frac{v_{cut-off}}{c}\right)^k\right) \quad \textbf{(5.14)}$$

On the other hand, the power output of the wind turbine for the continuous portion is being between v_{cut-in} and v_{rated} and can be expressed as follows:

$$f_w(P_w) = \frac{klv_{cut-in}}{c}\left(\frac{(1+\rho*1)v_{cut-in}}{c}\right)^{k-1} * exp\left(-\left(\frac{(1+\rho*1)v_{cut-in}}{c}\right)^k\right) \quad \textbf{(5.15)}$$

where $\rho = P_w/P_{wr}$ is the ration of linear range wind speed to cut-in wind speed, $l = (v_{rated} - v_{cut-in})/v_{cut-in}$ is the ratio of wind power output to rated wind power.

5.7. OPF formulation considering stochastic wind power

The objective function in this section is to minimize the total generation cost (TGC) to meet the load demands in the system. The TGC is obtained through the optimal scheduling of thermal and wind units subject to operating constraints. The objective function consisting of fuel and wind costs is given in Eq. (5.16):

$$\mathrm{F}_{\mathrm{tot}} = \sum_{i=1}^{N} F_i\left(P_i\right) + \sum_{i=1}^{NW} \mathrm{C}_{wr}\left(P_{wr}\right) + \sum_{i=1}^{NW} \mathrm{C}_{p.wr}\left(P_{wr.av} - P_{wr}\right) + \sum_{i=1}^{NW} C_{r.wr}\left(P_{wr} - P_{wr.av}\right) \tag{5.16}$$

In the above expression, the first term denotes thermal power generation cost, the second, third, and last term of the objective function presented the costs due to available wind power, respectively.

Subject to:

- **Equality constraints:**

In the case of incorporating wind power, the equality constraints which represents the load balance equation for real and reactive powers are expressed as follow:

$$P_{G_i} + P_{WS_i} - P_{d_i} = V_i \sum_{j=1}^{N} V_j \left(g_{ij} \cos\delta_{ij} + z_{ij} \sin\delta_{ij}\right) \tag{5.17}$$

$$Q_{G_i} + Q_{WS_i} - Q_{d_i} = V_i \sum_{j=1}^{N} V_j \left(g_{ij} \sin\delta_{ij} + z_{ij} \cos\delta_{ij}\right) \tag{5.18}$$

- **Inequality constraints:**

The inequality constraints which represents the limiting of the power system operation in the case of incorporating wind power are described as follow:

$$\begin{cases} P_{Gi}^{min} \le P_{Gi} \le P_{Gi}^{max} \\ P_{WSi}^{min} \le P_{WSi} \le P_{WSi}^{max} \\ Q_{Gi}^{min} \le Q_{Gi} \le Q_{Gi}^{max} \\ Q_{WSi}^{min} \le Q_{WSi} \le Q_{WSi}^{max} \\ V_{Gi}^{min} \le V_{Gi} \le V_{Gi}^{max} \\ T_{NTi}^{min} \le T_{NTi} \le T_{NTi}^{max} \\ \left|S_{Li}\right| \le S_{Li}^{max} \end{cases} \tag{5.19}$$

The wind power model integrated into the OPF formulation is divided into three parts, the direct cost, the penalty cost due to the underestimation and the reserve cost due to the overestimation of available wind power. The details of all terms described in Eq. (5.16) are explained as below:

❖ ***Cost of thermal power generation***

The cost function of the thermal generators can be expressed with the same function given in Eq. (3.4):

❖ ***The direct cost of wind power***

The system operator (SO) pays the cost of purchasing wind power from a wind power producer based on the power purchase agreement. This cost is termed as the direct cost and is defined as follows [124]:

$$C_{wr}(P_{wr}) = d_r * P_{wr} \quad \textbf{(5.20)}$$

where d_r is the direct cost coefficient for the jth wind generator and P_{wr} is the scheduled power output.

❖ ***Cost due to the underestimation of wind power***

The underestimation situation is due to when the actual wind power is higher than the estimated value. So, the utility operator needs to pay a penalty cost for not using the surplus amount of available wind power [109], [124]. The penalty cost function due to the underestimation of available wind power can be represented by Eq. (5.21) as follows [177]:

$$C_{p.wr}\left(P_{wr,av} - P_{wr}\right) = k_p\left(P_{w,av} - P_{wr}\right) = k_p \int_{P_{wr}}^{P_{r.0}} \left(W - P_{wr}\right) f_W\left(W\right) \quad \textbf{(5.21)}$$

where $C_{p.wr}$ the cost associated with wind power surplus (underestimation), $P_{p.wr}$ the actual available power output, k_p is the penalty cost coefficient due to underestimation, and $f_W(W)$ represent the probability density function (PDF).

❖ ***Cost due to the overestimation of wind power***

On contrary to the underestimation situation, the overestimation situation is due when the actual wind power is less than the estimated value. So, a spinning reserve is needed for grid operators [124]. The penalty cost function due to the overestimation of available wind power can be represented by Eq. (5.22) as follows [125]:

$$P_{r.wr}\left(P_{wr} - W_{wr.av}\right) = k_r\left(P_{wr} - W_{w.av}\right) = k_r \int_{0}^{P_{wr}} \left(P_{wr} - W\right) f_W\left(W\right) \quad \textbf{(5.22)}$$

where $C_{r.wr}$ the cost associated with wind power shortage (overestimation) and k_r is the reserve cost coefficient due to overestimation.

- **Control variables**

The set of control variables in the case to solve the OPF problem considering stochastic wind power can be represented by vector *u* as follows:

$$u = \left[P_{G_2} \ldots P_{G_{NG}}, P_{WS_1} \ldots P_{WS_{NW}}, V_{G1} \ldots V_{GNG}, Q_{C1} \ldots Q_{C_{NC}}, T_1 \ldots T_{NT} \right] \quad \textbf{(5.23)}$$

where P_G is the thermal generator active power, P_{WS} is the wind active power, V_G is the generator voltage, Q_C is the reactive power injected by the shunts compensator, T is the tap setting of transformers, SVC is the static VAR compensator device, NG is the number of thermal generators unit, NW is the number of wind farms, NC is the number of shunts compensators units and NT is the number of regulating transformers.

- **State variables**

The vector of the state variables, in this case, comprises the active power generation at the slack bus, the reactive power outputs of the generators Q_G, the reactive power outputs of the wind farms Q_{WS}, the voltage magnitude at load bus V_L and the apparent power flow S_l. The vector of the state variables x can be obtained as follow:

$$x = \left[P_{G_{slack}}, Q_{G_1} \ldots Q_{G_{NG}}, Q_{WS_1} \ldots Q_{WS_{NW}}, V_{L_1} \ldots V_{L_{NL}}, S_{l_1} \ldots S_{l_{nl}} \right] \quad \textbf{(5.24)}$$

where NG is the total number of generator buses, NW is the number of wind farms, NL is the total number of load buses or PQ buses, and nl is the total number of transmission lines.

5.8. OPF solution considering stochastic wind power

This part of the study is dedicated to solve the OPF problem considering stochastic wind power in the system and demonstrate the effectiveness of the proposed algorithms to solve this stochastic optimization problem. The main objective here is to minimize the total costs of conventional power generation and wind power generation. The function of wind power cost includes the direct cost, the penalty cost due to the underestimation and the reserve cost due to the overestimation of available wind power. In this work, the function of Weibull probability density is used to model and characterize the distributions of wind speed. This model is generally recognized by the scientific community as it has demonstrated good results. SMA and ALO algorithms are adopted in this study to deal with the OPF problem integrating stochastic wind power with conventional thermal units in the system. The simulation studies are carried out on the standard IEEE-30 bus system and a large Algerian electrical power system ALG 114-bus.

5.8.1. Application on the IEEE 30-bus system

To verify the performance and efficiency of the proposed algorithms to solve the OPF problem in a small power system considering stochastic wind power, the standard IEEE 30-bus system is considered by including two wind farms located at busses numbers 10 and 24 as shown in Fig. 5.13. The optimal locations of the wind farm in the standard IEEE 30-bus system have been determined by [178].

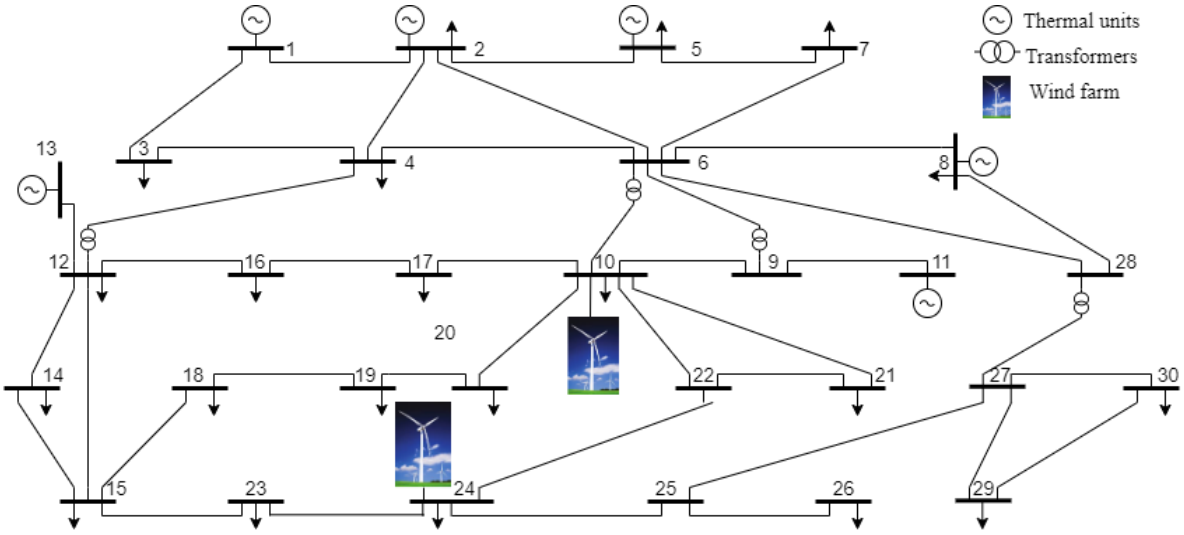

Figure 5.13 IEEE 30-bus electrical network with two wind farms at busses10 and 24

Both wind farms (WFs) consist of 30 units of wind turbine with a nominal power rating of each wind turbine is 2 MW. So each wind farm has a total capacity of 30 MW. Table 5.3 details the specification of wind turbine characteristics used in all optimization cases in this study concern with incorporating wind farms for the IEEE 30-bus system [179].

Table 5.2 The wind turbine characteristics used for a wind system

Parameters	**Value**
k	2
c	3
dr	1.3
P_{rated}	2000 KW
V_{rated}	12 m/s
V_{cut-in}	4 m/s
$V_{cut-off}$	25 m/s
$k_{p.j}$ (penalty factor)	1 $\$/MWh$
$k_{r.j}$ (reserve factor)	4 $\$/MWh$

In this section, OPF has been performed for two different cases studies based on the active power loading:

- **Case 1**: OPF solution considering stochastic wind power under nominal load;
- **Case 2**: OPF solution considering stochastic wind power under heavy load;

5.8.1.1. OPF solution considering stochastic wind power under nominal load

In this case, the proposed algorithms are applied to solve the OPF problem considering stochastic wind power under a normal operating regime with a total load of 283.4 MW (base case). The optimal results obtained by SMA and ALO are presented in Table 5.3.

Table 5.3 Comparison of results obtained by SMA and ALO for IEEE 30-bus system considering wind power: Under nominal load

Control variables	Limits		Active power loading 283.4 MW		
	Min	Max	Without wind	SMA	ALO
P_{G1}	50	200	177.5784	139.3865	138.0336
P_{G2}	20	80	48.6770	39.6216	38.2920
P_{G5}	15	50	21.2668	18.6332	18.2313
P_{G8}	10	35	21.2316	10.0000	12.9977
P_{G11}	10	30	12.0890	10.0000	10.0024
P_{G13}	12	40	12.0000	12.0000	12.0008
P_{WS1}	0.95	1.1	-	30.0000	30.0000
P_{WS2}	0.9	1.1	-	30.0000	30.0000
V_{G1}	0.9	1.1	1.1000	1.1000	1.1000
V_{G2}	0.9	1.1	1.0879	1.0894	1.0891
V_{G5}	0.9	1.1	1.0618	1.0644	1.0646
V_{G8}	0.9	1.1	1.0701	1.0760	1.0760
V_{G11}	0.9	1.1	1.1000	1.0539	1.0377
V_{G13}	0.9	1.1	1.1000	1.0183	1.0099
V_{WS1}	0.9	1.1	///	1.0000	1.0000
V_{WS2}	0.9	1.1	///	1.0000	1.0000
T_{11}	0.9	1.1	1.0259	1.0903	1.0870
T_{12}	0.9	1.1	0.9010	1.0286	1.0614
T_{15}	0.9	1.1	0.9803	1.0980	1.0935
T_{36}	0.9	1.1	0.9568	1.0594	1.0363
Q_{C10}	0	5	4.3806	0.0139	0.3427
Q_{C12}	0	5	4.7790	2.8581	4.2142
Q_{C15}	0	5	4.8272	0	2.4251
Q_{C17}	0	5	4.9942	2.2721	1.6994
Q_{C20}	0	5	2.5651	2.7844	1.5542
Q_{C21}	0	5	2.8396	5.0000	3.6144
Q_{C23}	0	5	3.4609	4.8785	3.7560
Q_{C24}	0	5	4.9957	0.2167	4.7245
Q_{C29}	0	5	1.1562	0.9389	1.0789
Total generation cost ($/h)			798.9709	725.7113	726.4565
Power losses (MW)			8.5752	6.2413	6.1579
Voltage deviation (p.u)			1.4494	0.6285	0.5829
Reserved real power			-	53.5074	53.5074

Table 5.3 presents the results obtained by the proposed algorithms to minimize the total generation cost (TGC), which are the total fuel and wind costs. The sizing of the two wind farms can

be referred to in the same table. According to this Table, it appears clear that all control variables are within the admissible limits. In addition, the results obtained show that the total generation cost with considering wind power is different and better than the results obtained without considering wind power. Furthermore, the active power losses obtained have also been reduced from 8.5752 MW to 6.2413 MW by SMA, and to 6.1579 MW by ALO, which is lowered by 27.21 % and 28.19 %, respectively. On the other hand, the SMA algorithm leads to a total generation cost of 725.7113 $/h, while ALO provides 726.4565 $/h. Thus, SMA provides the best solution value to minimize the TGC in the IEEE 30-bus test system by incorporating wind power compared to the ALO algorithm. Moreover, the implementation of wind farms in the system has significantly improved the power system operation.

The convergence curves of the SMA and ALO to minimize the total generation cost are shown in Fig. 5.14. Based on the convergence curves presented in this Figure, it can be seen that the SMA converges towards the global optimum value in only 50th iteration, compared to the ALO, in which the convergence towards the optimal solution is reached at iteration 145.

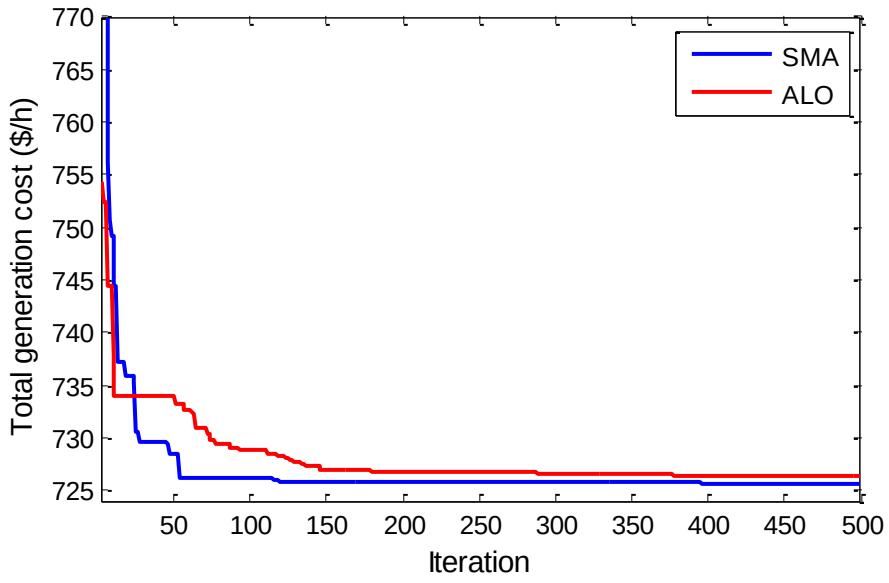

Figure 5.14 Convergence characteristics of SMA and ALO for IEEE 30-bus system considering wind power: Under normal operation

5.8.1.2. OPF solution considering stochastic wind power under heavy load

In the second part, the proposed algorithms are applied to solve the OPF problem considering stochastic wind power under heavy load. The goal is to illustrate and highlight the effect of the load variation on the quality of the results. In this test, the rate of increase of the load is 45% compared to the nominal load, so the active power loading is 410.93 MW. The optimal results obtained by SMA and ALO algorithms are presented in Table 5.4.

Table 5.4 Comparison of results obtained by SMA and ALO for IEEE 30-bus system considering wind power: Under heavy load.

Control variables	Limits		Active power loading 410.90 MW		
	Min	Max	Without wind	SMA	ALO
P_{G1}	50	200	199.9977	195.2207	188.5134
P_{G2}	20	80	78.8218	57.6992	60.5925
P_{G5}	15	50	42.4211	32.9495	31.8857
P_{G8}	10	35	34.9915	34.9999	32.1378
P_{G11}	10	30	29.9997	21.9266	27.1867
P_{G13}	12	40	38.2946	20.3897	22.6480
P_{WS1}	0.9	1.1	-	30.0000	30.0000
P_{WS2}	0.9	1.1	-	30.0000	30.0000
V_{G1}	0.9	1.1	1.1000	1.1000	1.1000
V_{G2}	0.9	1.1	1.0843	1.0804	1.0861
V_{G5}	0.9	1.1	1.0286	1.0264	1.0313
V_{G8}	0.9	1.1	1.0616	1.0669	1.0795
V_{G11}	0.9	1.1	1.1000	1.1000	1.1000
V_{G13}	0.9	1.1	1.1000	1.0516	1.0580
V_{WS1}	0.9	1.1	-	1.0000	1.0000
V_{WS2}	0.9	1.1	-	1.0000	1.0000
T_{11}	0.9	1.1	1.0189	1.0896	1.1000
T_{12}	0.9	1.1	1.0211	1.0991	1.0397
T_{15}	0.9	1.1	1.0511	1.0997	1.0893
T_{36}	0.9	1.1	0.9609	1.0272	1.0767
Q_{C10}	0	5	4.8813	4.1783	4.6406
Q_{C12}	0	5	1.9164	4.8901	4.4111
Q_{C15}	0	5	3.1109	3.1556	1.3437
Q_{C17}	0	5	4.9727	4.9617	1.1743
Q_{C20}	0	5	1.3915	1.1554	4.1730
Q_{C21}	0	5	4.9937	0.0066	3.4722
Q_{C23}	0	5	2.9808	2.7736	4.8212
Q_{C24}	0	5	4.6307	1.3769	1.2927
Q_{C29}	0	5	1.1981	1.2900	1.4034
Total generation cost ($/h)			1339.4776	1198.1826	1201.3418
Power losses (MW)			13.5964	12.2555	12.0342
Voltage deviation (p.u)			0.7413	0.6066	0.7167
Reserved real power			-	53.5074	53.5074

Table 5.4 summarizes the results achieved using SMA and ALO considering stochastic wind power with a higher active power loading of 410.90 MW. From this table, the active power generated values obtained by the proposed algorithms are modified and distributed of optimal values after the integration of two wind farms. Moreover, SMA and ALO provide 1198.1826 $/h and 1201.3418 $/h, respectively, satisfying all system constraints. These values are considered as the best values of total generation cost compared to the value obtained in a case without incorporating wind power. On the other hand, the total generation cost obtained by SMA is 1198.1826 $/h, which is better than provides by the ALO algorithm (1201.3418 $/h). In general, the implementation of wind farm installation to the system has significantly reduced the total generation cost and the active power loss value in the case of higher active power loadings.

The convergence characteristics of the total generation cost obtained by SMA and ALO are shown in Fig. 5.15. This figure demonstrates that the SMA algorithm can converge to the global optimum at iteration 170, while ALO towards the optimal solution is reached at iteration 230.

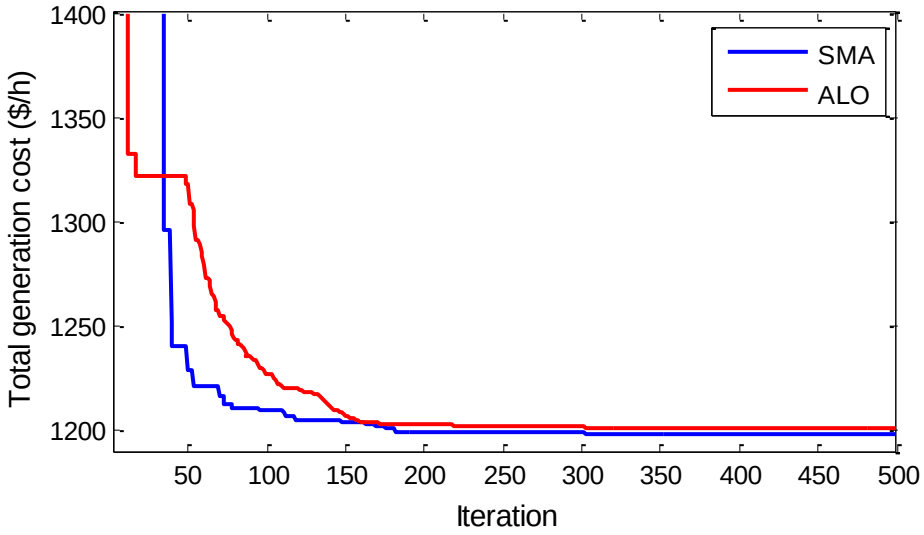

Figure 5.15 Convergence characteristics of SMA and ALO: Under heavy load

5.8.2. Application on the Algerian 114-bus system

In order to verify the performance and efficiency of the proposed methods to solve nonlinear problems in a larger-scale electrical power system considering stochastic wind power, OPF is performed on the practical Algerian electrical network system ALG 114-bus. The Algerian power system ALG 114-bus is considered by including two wind farms located at busses 99 (Setif) and 107 (Djelfa) as shown in Fig. 5.16. The two wind farms (WF) consist of 40 units of wind turbine generation (WTG), with a nominal power rating of each WTG is 1.5 MW.

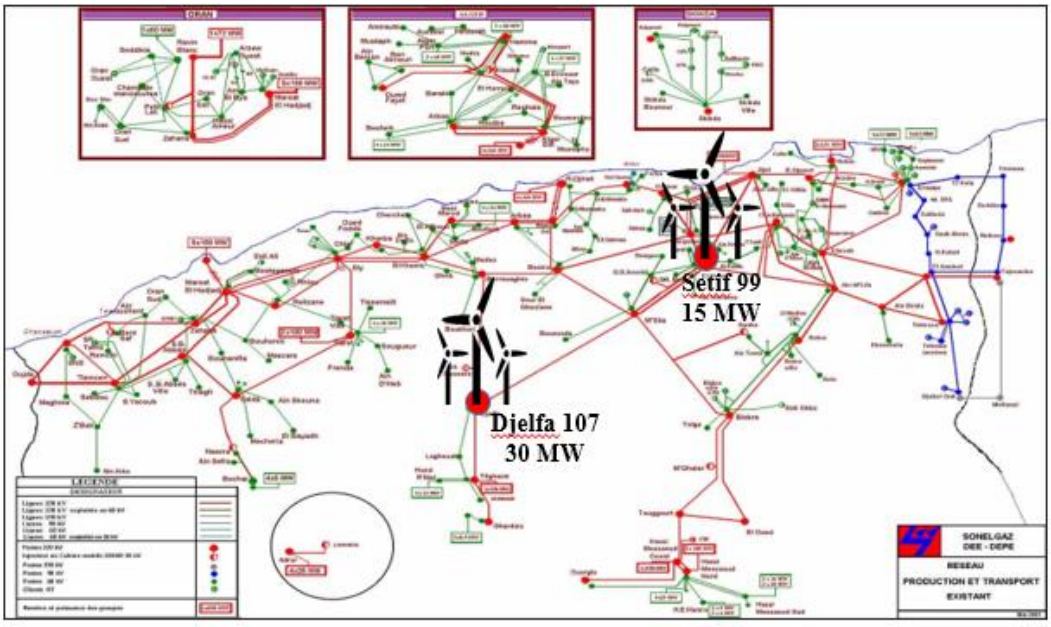

Figure 5.16 Algerian power system with including two wind farms

The choice of the turbine has been set for General Electric GE 1.5-77 machines. The characteristics of this wind turbine are shown in Table 5.5.

Table 5.5 The wind turbine characteristics used for a wind system

Parameters	**Wind turbine1**	**Wind turbine 2**
dr	1.75	2
P_{rated}	15 MW	30 MW
V_{cut-in}	3.5 m/s	3.5 m/s
V_{rated}	12 m/s	12 m/s
$V_{cut-off}$	25 m/s	25 m/s
$k_{p.j}$ (penalty factor)	1.5 $/MWh	1.5 $/MWh
$k_{r.j}$ (reserve factor)	3 $/MWh	3 $/MWh

Table 5.6 Comparison of results obtained by SMA and ALO for ALG 114-bus system considering wind power

Control variables	**Min**	**Max**	**Without wind**	**SMA**	**ALO**
P_{G4}	135	1350	451.3078	444.8246	427.0616
P_{G5}	135	1350	451.1405	446.1754	430.3228
P_{G11}	10	100	99.9998	99.9992	100.0000
P_{G15}	30	300	193.3981	190.5629	192.9336
P_{G17}	135	1350	446.9078	439.3309	419.9720
P_{G19}	34,5	345	194.8571	190.8661	194.5118
P_{G22}	34,5	345	191.8038	190.0866	198.5462
P_{G52}	34,5	345	188.5324	186.9000	182.8298
P_{G80}	34,5	345	190.4592	184.5212	204.6103
P_{G83}	30	300	187.8661	181.9296	188.0060
P_{G98}	30	300	188.6026	183.2775	205.6290
P_{G100}	60	600	600.0000	599.9998	600.0000
P_{G101}	20	200	200.0000	200.0000	200.0000
P_{G109}	10	100	100.0000	99.9995	99.9938
P_{G111}	10	100	99.9976	100.0000	100.0000
P_{WS1}	0	15		15.0000	12.3210
P_{WS2}	0	30		30.0000	29.1603
V_{G4}	0.9	1.1	1.0997	1.1000	1.0993
V_{G5}	0.9	1.1	1.1000	1.1000	1.0991
V_{G11}	0.9	1.1	1.0954	1.0990	1.0998
V_{G15}	0.9	1.1	1.1000	1.1000	1.1000
V_{G17}	0.9	1.1	1.1000	1.1000	1.0983
V_{G19}	0.9	1.1	1.0599	1.0523	1.0864
V_{G22}	0.9	1.1	1.0620	1.0589	1.0946
V_{G52}	0.9	1.1	1.0661	1.0622	1.0881
V_{G80}	0.9	1.1	1.1000	1.1000	1.1000
V_{G83}	0.9	1.1	1.1000	1.1000	1.0996
V_{G98}	0.9	1.1	1.1000	1.1000	1.1000
V_{G100}	0.9	1.1	1.1000	1.1000	1.1000
V_{G101}	0.9	1.1	1.1000	1.1000	1.1000
V_{G109}	0.9	1.1	1.1000	1.1000	1.1000
V_{G111}	0.9	1.1	1.0701	1.0650	1.0995
Total generation cost ($/h)			18914.105	18624.9978	18685.7284
Power losses (MW)			57.8726	56.4733	58.8981
Voltage deviation (p.u.)			4.9714	4.8197	5.3991
Reserved real power cost			-	41.0227	43.8776

Table 5.6 summarizes the best results reached by the proposed algorithms to minimize total generation cost (TGC) by incorporating two wind farms in ALG 114-bus system. Based on the results achieved with considering wind energy, the SMA and ALO algorithms lead to TGC of 18624.9978 \$/h and 18685.7284 \$/h, respectively. The incorporation of wind farms gave more significant profit in TGC and reducing active power losses. The convergence characteristics of the SMA and ALO are shown in Fig. 5.17. The convergence of the SMA is reached in the first 170 iterations, while the convergence of the ALO towards the optimal solution is reached at iteration 230.

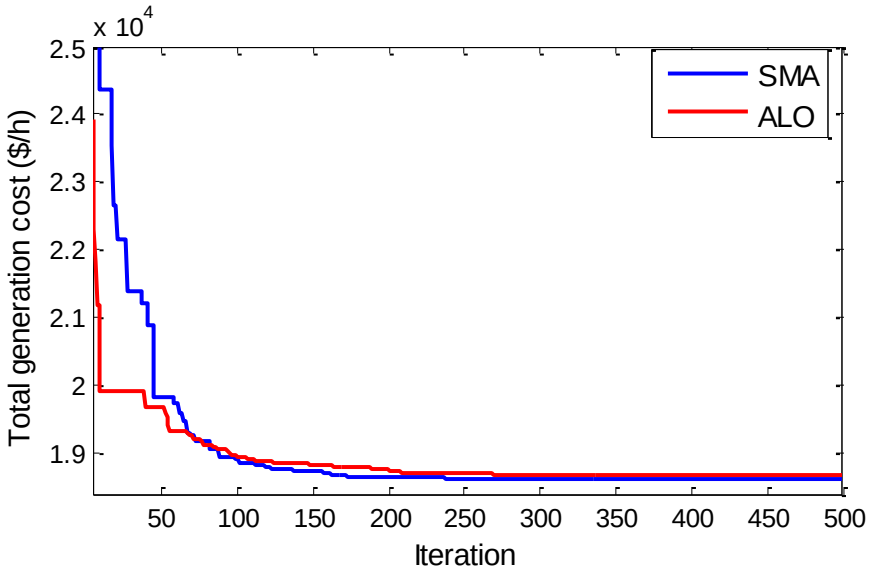

Figure 5.17 Convergence characteristics of SMA and ALO considering wind power

5.9. OPF solution considering stochastic wind power and SVC devices

This part is dedicated to demonstrate the effectiveness of the proposed algorithms to solve the OPF problem considering stochastic wind power with the presence of FACTS systems, in particular, static VAR compensator (SVC). In this problem, the total generation cost is used as the objective function to be minimized. The proposed algorithm was examined on the IEEE-30 bus and Algerian 114-bus power systems.

5.9.1. Application on the IEEE 30-bus system

In this case study, the proposed algorithm SMA is applied to solve the OPF problem by incorporating stochastic wind power and SVC devices under heavy load. To verify the performance and effectiveness of SMA, the active power loading are considered, is the active power loading equal 410.93 MW. The optimal location of the SVC found by SMA is bus N° 30. Table 5.7 summarizes the results obtained with higher active power loading. From this table, it can be seen also that the voltage deviation is reduced from 0.6066 p.u to 0.5465 p.u. Fig. 5.18 represents the effect of the SVC to improve the voltage profile under higher loading. SVC has a great effect in controlling and maintaining voltages within their acceptable limits.

Table 5.7 Comparison of results obtained by SMA for IEEE 30-bus system considering wind power and SVC

Control variables	Limits		Active power loading 410.93 MW	
	Min	Max	Without SVC	With SVC
P_{G1}	50	200	195.2207	195.2576
P_{G2}	20	80	57.6992	57.8394
P_{G5}	15	50	32.9495	32.7988
P_{G8}	10	35	34.9999	34.9896
P_{G11}	10	30	21.9266	23.1781
P_{G13}	12	40	20.3897	19.1394
P_{WS1}	0	40	30.0000	30.0000
P_{WS2}	0	40	30.0000	30.0000
V_{G1}	0.95	1.1	1.1000	1.1000
V_{G2}	0.9	1.1	1.0804	1.0818
V_{G5}	0.9	1.1	1.0264	1.0263
V_{G8}	0.9	1.1	1.0669	1.0694
V_{G11}	0.9	1.1	1.1000	1.0964
V_{G13}	0.9	1.1	1.0516	1.0371
T_{11}	0.9	1.1	1.0896	1.1000
T_{12}	0.9	1.1	1.0991	1.0993
T_{15}	0.9	1.1	1.0997	1.0974
T_{36}	0.9	1.1	1.0272	1.0455
Q_{C10}	0	5	4.1783	3.8886
Q_{C12}	0	5	4.8901	0.8560
Q_{C15}	0	5	3.1556	1.6088
Q_{C17}	0	5	4.9617	5.0000
Q_{C20}	0	5	1.1554	4.1684
Q_{C21}	0	5	0.0066	4.9944
Q_{C23}	0	5	2.7736	4.7325
Q_{C24}	0	5	1.3769	0.0423
Q_{C29}	0	5	1.2900	4.8493
Q_{WS1}	-15	40	4.7442	57.8394
Q_{WS2}	-15	40	10.3240	32.7988
Q_{SVC_30}	-25	25	-	6.6716
Total generation cost ($/h)			1198.1826	1198.2092
Power losses (MW)			12.2555	12.2729
Voltage deviation (p.u.)			**0.6066**	**0.5465**
Reserved real power			53.5074	53.5074

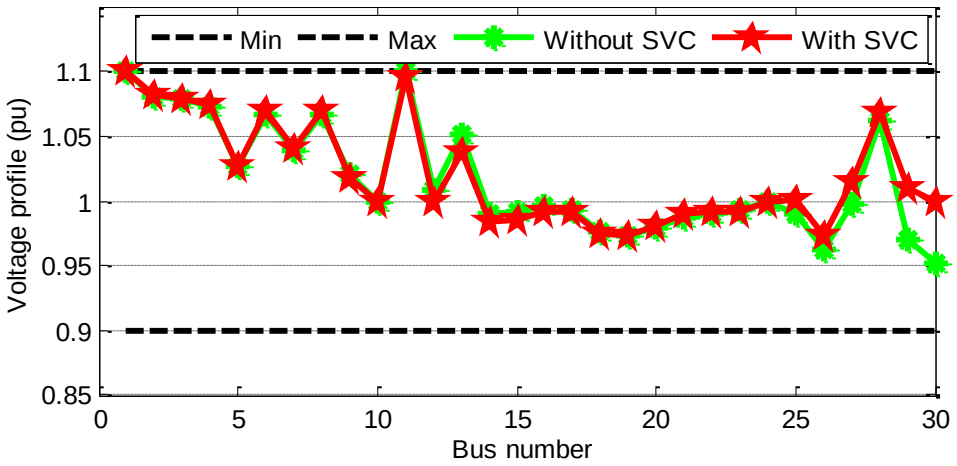

Figure 5.18 The effect of SVC on voltage profile with considering wind power: Higher loading

5.9.2. Application on the Algerian 114-bus system

In order to illustrate the effectiveness of the SMA in presence of SVC devices on the power system, the ALG 114-bus is considered by including two SVC devices at busses N°68 (Sedjerara) and bus N°89 (Souk Ahras). These locations of SVC devices are considered the optimal placement in the Algerian 114-bus system found by the SMA algorithm. The optimization results are given in Table 5.8. After the results of the simulation, the installation of the SVC improved considerably the total generation cost, the active power loss. Figure 5.19 represents that the effect of SVC devices is significant in the Algerian 114-bus system to maintain the voltages within acceptable limits.

Table 5.8 Comparison of results obtained by SMA for ALG 114-bus system considering wind power and SVC

Control variables	Min	Max	**Without SVC**	**SVC**
P_{G4}	135	1350	444.8246	446.5335
P_{G5}	135	1350	446.1754	443.8411
P_{G11}	10	100	99.9992	99.9993
P_{G15}	30	300	190.5629	188.6959
P_{G17}	135	1350	439.3309	441.6877
P_{G19}	34,5	345	190.8661	189.4341
P_{G22}	34,5	345	190.0866	186.7558
P_{G52}	34,5	345	186.9000	185.9111
P_{G80}	34,5	345	184.5212	186.0970
P_{G83}	30	300	181.9296	183.6420
P_{G98}	30	300	183.2775	184.3464
P_{G100}	60	600	599.9998	600.0000
P_{G101}	20	200	200.0000	200.0000
P_{G109}	10	100	99.9995	99.9985
P_{G111}	10	100	100.0000	100.0000
P_{WS1}	0	15	15.0000	15.0000
P_{WS2}	0	30	30.0000	29.9999
V_{G4}	0.9	1.1	1.1000	1.0999
V_{G5}	0.9	1.1	1.1000	1.1000
V_{G11}	0.9	1.1	1.0990	1.0993
V_{G15}	0.9	1.1	1.1000	1.0993
V_{G17}	0.9	1.1	1.1000	1.1000
V_{G19}	0.9	1.1	1.0523	1.0590
V_{G22}	0.9	1.1	1.0589	1.0683
V_{G52}	0.9	1.1	1.0622	1.0668
V_{G80}	0.9	1.1	1.1000	1.0998
V_{G83}	0.9	1.1	1.1000	1.1000
V_{G98}	0.9	1.1	1.1000	1.1000
V_{G100}	0.9	1.1	1.1000	1.1000
V_{G101}	0.9	1.1	1.1000	1.1000
V_{G109}	0.9	1.1	1.1000	1.0998
V_{G111}	0.9	1.1	1.0650	1.0792
Q_{SVC_68}	-25	+25	-	22.000
Q_{SVC_89}	-25	+25	-	32.800
Fuel cost ($/h)			18624.9978	18610.7234
Power losses (MW)			56.4733	54.9422
Voltage deviation (p.u.)			4.8197	4.5968
Reserved real power cost ($/h)			41.0227	41.0227

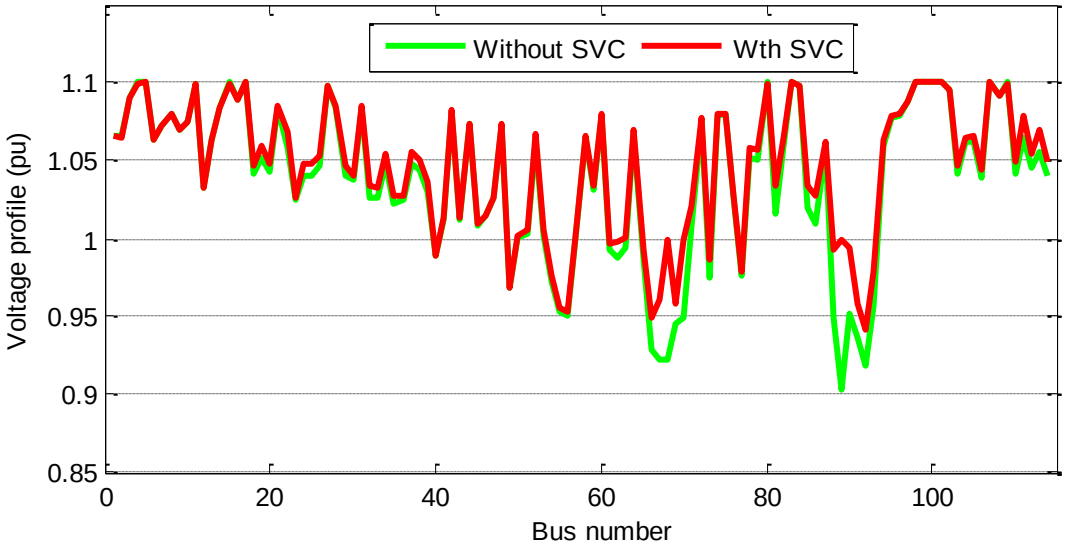

Figure 5.19 The effect of SVC on voltage profile in ALG 114-bus system considering wind power

5.10. OPF solution considering stochastic wind power and VSC-MTDC

The wind energy merging by HVDC technology is proposed in this part to improve the electrical power system quality. The simulation study will be devoted to the application of the proposed algorithms to solve the OPF problem by incorporating wind energy via voltage source converter-based multi-terminal DC (VSC-MTDC) system. The simulations are carried out on the IEEE 30-bus and Algerian 114-bus power systems to verify the efficiency and performance of the proposed algorithms and to demonstrate the influence of the Wind-VSC-MTDC system.

5.10.1. Application on the IEEE 30-bus system

In order to illustrate the effectiveness of the proposed algorithms to solve the OPF problem with incorporating wind farms by a multi-terminal VSC-HVDC (VSC-MTDC or DC grid), the standard IEEE 30-bys system is modified by incorporating two wind farms by a mesh system of 4-terminal VSC-HVDC (VSC-MTDC) as shown in Figure 5.20. The VSC-MTDC system, in this case, contains four converters VSCs, which the VSC1 Converter Station (Reference bus in the DC grids) is connected to the AC system at bus 10, the VSC3 is connected to the AC system at bus 24. VSC1 and VSC3 convert serve as an inverter and can also provide reactive power and participate it to AC system in order to control of AC bus voltage. Also, the VSC2 and VSC4 conversion stations are connected to the two wind farms 1 and 2, respectively, to capture the maximum power from both farms. VSC2 and VSC4 convert serve as a rectifier and controlled using standard torque and speed control methods. On the other hand, the total capacity of both offshore wind farms (OWFs) is 60 MW. Both of them consist of 30 wind turbine units with a nominal power rating of each wind turbine is 2 MW. Each wind farm contains 15 wind turbine units with a total capacity of 30 MW.

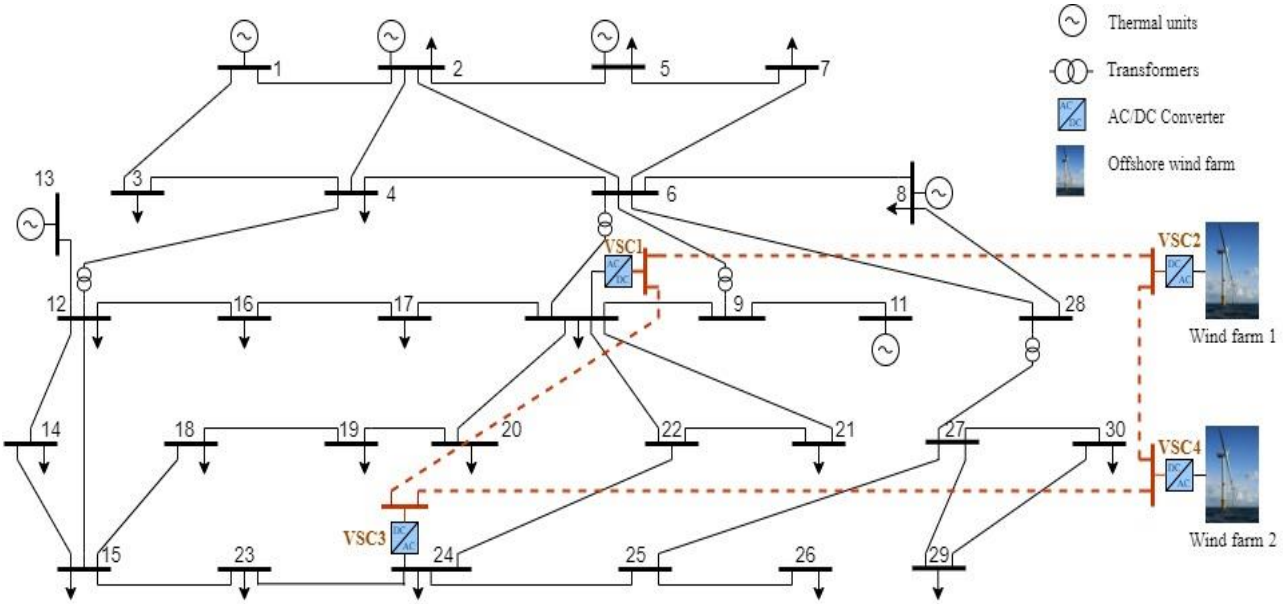

Figure 5.20 Modified IEEE-30 bus system with two wind farms and 4-terminal VSC-MTDC

The parameters at the conversion stations are given in Table 5.9, and the detailed operating modes of the VSC station are given in Table 5.10.

Table 5.9 The parameters of the converters stations

Converter parameters		**Voltage & Converter loss data 1 and 2**	
$X_{tr}(p.u)$	0.1121	$\pm V_{dc}$	400
$R_{tr}\ (p.u)$	0.0015	a	1.103
$B_f\ (p.u)$	0.0887	b	0.887
$X_c\ (p.u)$	0.1642	c_{rec}	2.885
$R_c\ (p.u)$	0.0001	c_{inv}	4.371

Table 5.10 The operating mode of the VSC station

VSC stations	**V_{DC} (Kv)**	**Type**	**AC bus**
$VSC1$	± 400	Slack	Bus 10
$VSC2$	± 400	PV	OWF 1
$VSC3$	± 400	PV	Bus 24
$VSC4$	± 400	PV	OWF 2

In this section, two objective functions have been considered to verify the efficiency and performance of the proposed algorithms to solve the OPF problem considering offshore wind farms (WFs) and VSC-MTDC with the rate of increase of the load is 45% compared to the nominal load:

- **Case 1**: Minimization of total generation cost;
- **Case 2**: Minimization of active power transmission losses;

Detail optimal results of control variables obtained by the proposed algorithms for both cases are tabulated in Table 5.11.

Table 5.11 Comparison of results obtained by SMA and ALO for IEEE 30-bus system considering wind power and VSC-MTDC

Control variables	Limits		Without OWFs and VSC-MTDC	With OWFs and VSC-MTDC			
				Case 1		Case 2	
	Min	Max		SMA	ALO	SMA	ALO
P_{G1}	50	200	199.9977	194.8481	195.1997	124.2018	125.6619
P_{G2}	20	80	78.8218	56.8858	58.1712	79.9995	78.6194
P_{G5}	15	50	42.4211	33.1844	34.2656	50.0000	50.0000
P_{G8}	10	35	34.9915	35.0000	27.7347	35.0000	35.0000
P_{G11}	10	30	29.9997	22.3789	23.3367	30.0000	29.9989
P_{G13}	12	40	38.2946	21.1717	25.1287	39.9945	40.0000
P_{w1}	0.9	1.1	-	30.0000	30.0000	30.0000	30.0000
P_{w2}	0.9	1.1	-	30.0000	30.0000	30.0000	30.0000
V_{G1}	0.9	1.1	1.1000	1.1000	1.1000	1.1000	1.1000
V_{G2}	0.9	1.1	1.0843	1.0849	1.0855	1.0907	1.0918
V_{G5}	0.9	1.1	1.0286	1.0370	1.0436	1.0582	1.0681
V_{G8}	0.9	1.1	1.0616	1.0743	1.0757	1.0737	1.0833
V_{G11}	0.9	1.1	1.1000	1.1000	1.1000	1.1000	1.0999
V_{G13}	0.9	1.1	1.1000	1.0999	1.0466	1.1000	1.0793
V_{w1}	0.9	1.1	-	1.0000	1.0000	1.0000	1.0000
V_{w2}	0.9	1.1	-	1.0000	1.0000	1.0000	1.0000
T_{11}	0.9	1.1	1.0189	1.0211	1.0439	1.0038	1.0426
T_{12}	0.9	1.1	1.0211	1.0033	1.0881	0.9001	1.0801
T_{15}	0.9	1.1	1.0511	1.0353	1.0969	0.9951	1.0773
T_{36}	0.9	1.1	0.9609	0.9730	1.0981	0.9506	1.0324
Q_{C10}	0	5	4.8813	4.8717	4.8963	4.6100	2.3939
Q_{C12}	0	5	1.9164	3.9231	1.3278	3.1471	4.6907
Q_{C15}	0	5	3.1109	3.9855	3.4503	0	1.3239
Q_{C17}	0	5	4.9727	5.0000	4.4812	0.2908	3.6984
Q_{C20}	0	5	1.3915	4.0802	1.7452	0.0000	3.5172
Q_{C21}	0	5	4.9937	2.8416	3.7568	1.9905	3.9591
Q_{C23}	0	5	2.9808	1.8055	4.0174	4.9893	3.2586
Q_{C24}	0	5	4.6307	3.8042	4.5021	1.0841	5.0000
Q_{C29}	0	5	1.1981	3.3885	4.5657	1.5014	4.9463
Total generation cost ($/h)			1339.4776	**1200.0611**	**1204.7789**	1292.40	1290.50
Power losses (MW)			13.5964	12.5390	12.9066	**8.2657**	**8.3502**
Voltage deviation (p.u)			0.7413	0.6066	0.7103	2.7633	0.7767
Reserved real power			-	53.5074	53.5074	53.5074	53.5074

Table 5.12 DC bus data for two cases studied

VSC stations	Voltage limits (p.u)		Voltage (p.u)	Active power (MW)
	Min	Max		
VSC1	0.9	1.1	1.000	39.372
VSC2	0.9	1.1	1.007	-29.904
VSC3	0.9	1.1	1.003	20.013
VSC4	0.9	1.1	1.009	-29.904

Table 5.11 summarize the results obtained by SMA and ALO algorithms to solve the OPF problem considering VSC-based MTDC system for stochastic offshore wind energy transmission for two different objective functions. From this table, the output of the generator power is modified and

reduced after the integration of the offshore wind farm by VSC-MTDC technology, which leads to fewer costs for the operation. Also, each wind farm generates at its maximum power point during the increase of the load at 45%. Moreover, it can be seen that the total generation cost and active power losses are considerably reduced after connecting the offshore wind farm into the AC system, which reduced from the values of 1198.1826 $/h and 12.2555 MW in the case without the presence of wind farms to 1198.1826 $/h, 12.2555 MW obtained by SMA, and reduced to 1198.1826 $/h and 12.2555 MW obtained by ALO. These results showed that the impact of offshore wind power is highly to reduce the total generation cost and active power.

For case 1, the total fuel cost and active power loss provided by the SMA are 1328.0798 $/h and 12.2720, respectively, which are minimum than obtained by the ALO (1330.3884 $/h and 12.4143 MW). The convergence curve of total generation cost obtained via the SMA and ALO algorithms for case 1 is shown in Figure 5.21. From this figure, the convergence of the SMA is reached in the first 300 iterations, while the convergence of the ALO towards the optimal solution is reached at iteration 190. In this case, The ALO algorithm rapidly converges towards the global optimal solution than the SMA algorithm.

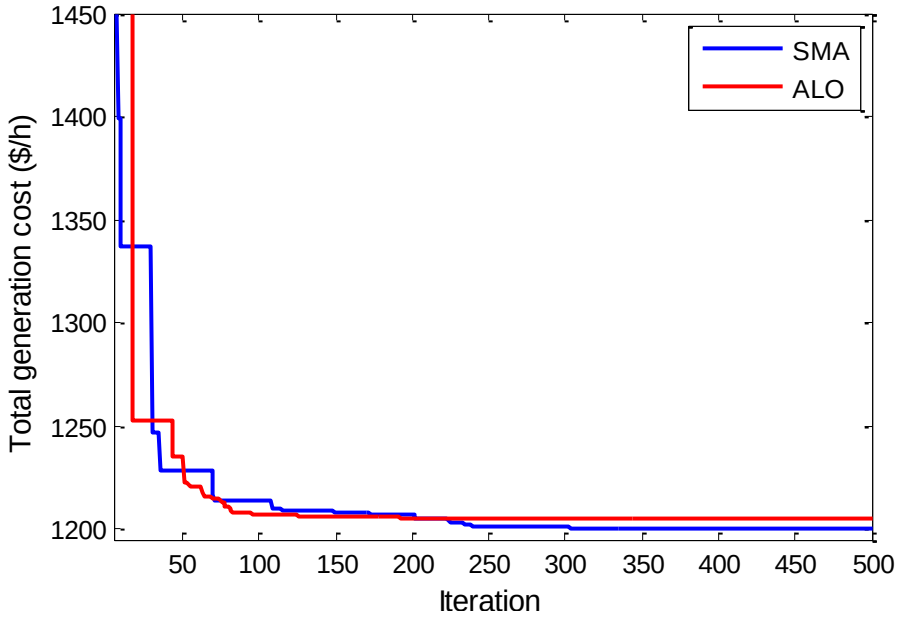

Figure 5.21 Convergence characteristics of SMA and ALO for IEEE 30-bus in the case 1

For case 2, the convergence curve of active power loss obtained via the SMA and ALO algorithms for case 2 is shown in Figure 5.22. In this case, the SMA algorithm provides 10.8684 MW and 1359.10 $/h, respectively, for the active power loss total fuel cost, these values are better compared to results achieved by the ALO algorithm (11.0052 MW and 1359.60 $/h). As result, connecting the offshore wind farms to AC grids through the VSC-MTDC system will be a better option in terms of transforming wind energy for long-distance, which leads to a more stable operation

of the electrical grid.

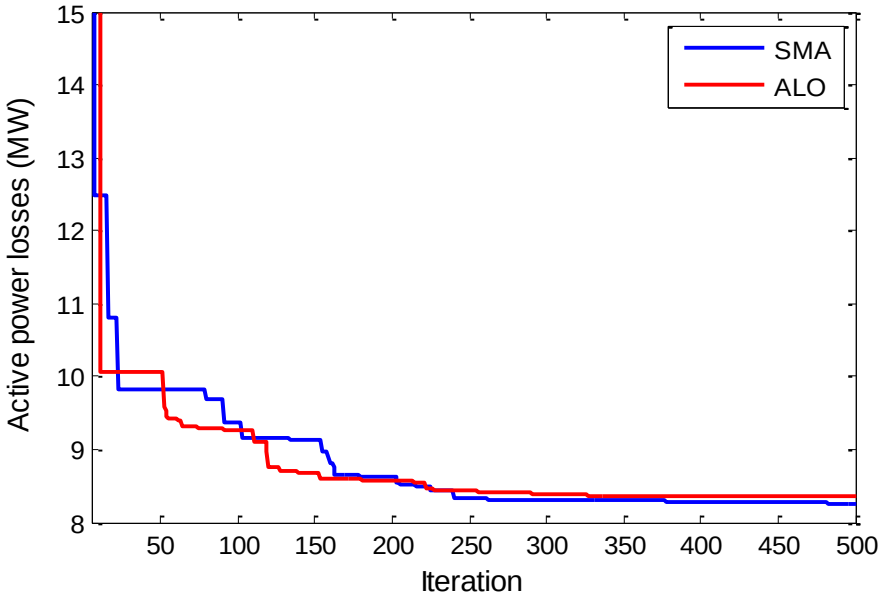

Figure 5.22 Convergence characteristics of SMA and ALO for IEEE 30-bus system in the case 2

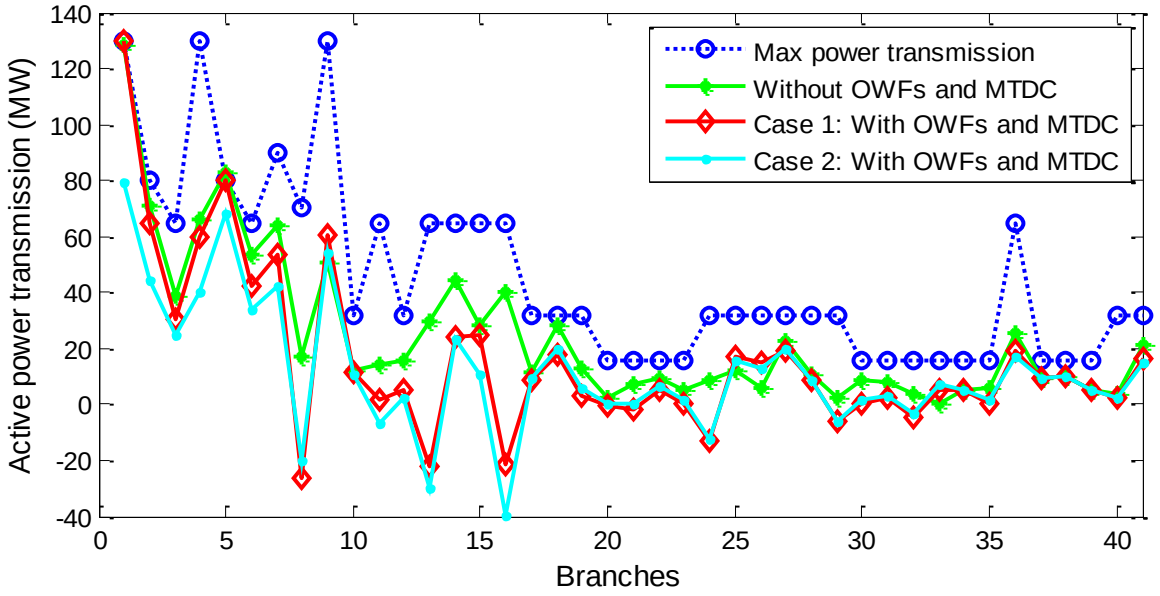

Figure 5.23 The effect of OWFs and VSC-MTDC on the transmission power line in IEEE 30-bus system

Figure 5.23 shows the active power transmitted for different cases studied in this part According to this figure, it is noted that some of the lines close to the maximum limit for the case without the integration of wind energy through the VSC-MTDC system such as line 1 (between the busses N°1 and N°2), line 5 (between the busses N°2 and N°5) and line 18 (between busses N°12 and N°15), these overload lines is a risk on the electrical system. So, the integration of wind energy by the MTDC system allows reducing the overload in all the lines concerned especially in case 2 which the objective is to minimize the active power loss. Thus, the integration of wind power by VSC-MTDC allows reducing the problem of overloading power lines.

5.10.2. Application on the Algerian 114-bus system

This part presents the application of the proposed methods to solve OPF problems in a larger-scale electrical power system considering stochastic wind power and VSC-MTDC system. The Algerian power system ALG 114-bus is considered by including two wind farms located in the Saharan region by a VSC-MTDC system of 4-terminal as shown in the Fig 5.24.

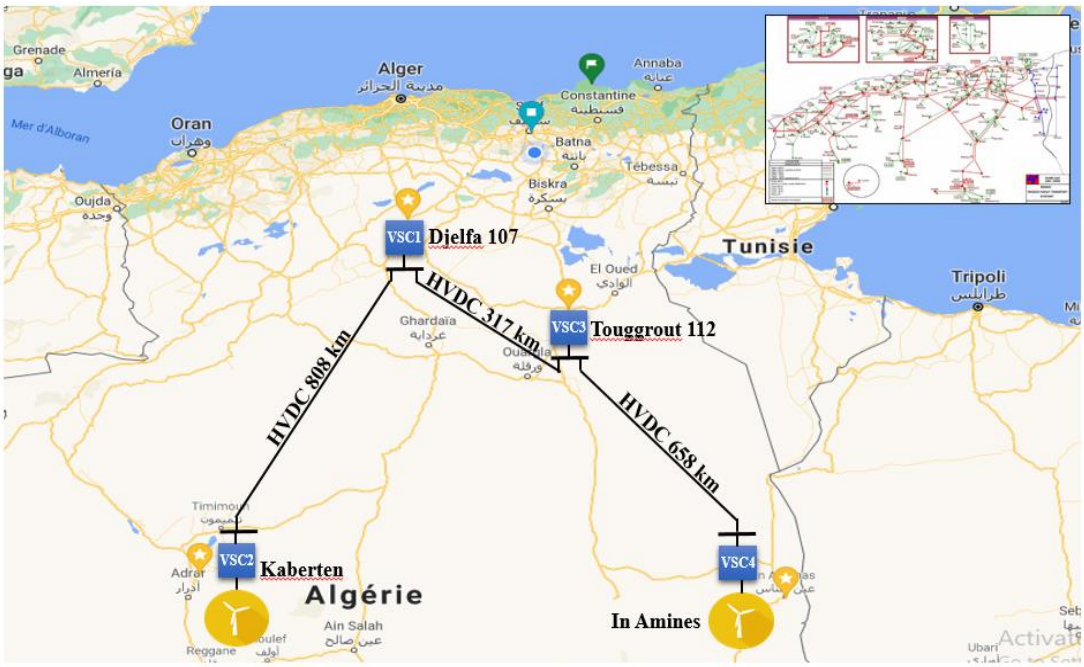

Figure 5.24 Algerian power system with including two wind farms by SVC-MTDC

The first wind farm located at the site of Kaberten (75 km north of Adrar), and the second wind farm is located in In Amines (265 Km north of Ilizi). The two sites connected with the Algerian power system ALG 114-bus system at busses 107 (Djelfa) and 112 (Touggrout) by a VSC-MTDC system. The two wind farms (WFs) consist of 40 units of wind turbine generators with a rated capacity of each WTG is 2 MW. The choice of the turbine has been set for Gamesa G80/2000 machines with a rated capacity of 2 MW. The wind turbine characteristics are given in Table 5.13.

Table 5.13 The wind turbine characteristics used for a wind system

Parameters	**Wind turbine**
dr	1.75
P_{rated}	15 MW
V_{cut-in}	3.5 m/s
V_{rated}	12 m/s
$V_{cut-off}$	25 m/s
$k_{p.j}$ (penalty factor)	1.5 $/MWh
$k_{r.j}$ (reserve factor)	3 $/MWh

In the VSC-MTDC system, the converters station VSC1 and VSC3 are connected to the ALG

114-bus system at busses 107 and 112, respectively. Also, the VSC2 and VSC4 conversion stations are connected to the two offshore wind farms 1 and 2, respectively, to capture the maximum power from both farms. The detailed operating modes of the VSC station are given in Table 5.14.

Table 5.14 The operating mode of the VSCs station

VSC stations	V_{DC} (KV)	Type	AC bus
$VSC1$	± 400	Slack	Bus 107 (Djelfa)
$VSC2$	± 400	PV	WF 1 (Adrar)
$VSC3$	± 400	PV	Bus 112 (Touggourt)
$VSC4$	± 400	PV	WF 2 (In Amines)

Table 5.15 Comparison of results obtained by SMA and ALO for ALG 114-bus system considering wind power and VSC-MTDC

Control Variables	Limits		Without WFs	With WFs and VSC-MTDC	
	Min	Max		SMA	ALO
P_{G4}	135	1350	451.3078	430.8214	413.0737
P_{G5}	135	1350	451.1405	434.2790	416.6631
P_{G11}	10	100	99.9998	100.0000	100.0000
P_{G15}	30	300	193.3981	182.2214	227.2429
P_{G17}	135	1350	446.9078	422.3410	411.4394
P_{G19}	34,5	345	194.8571	180.4350	176.7809
P_{G22}	34,5	345	191.8038	180.3468	212.4519
P_{G52}	34,5	345	188.5324	177.5660	175.2274
P_{G80}	34,5	345	190.4592	174.3634	154.5194
P_{G83}	30	300	187.8661	173.1213	190.0370
P_{G98}	30	300	188.6026	168.7981	159.2114
P_{G100}	60	600	600.0000	600.0000	599.9999
P_{G101}	20	200	200.0000	200.0000	199.9999
P_{G109}	10	100	100.0000	100.0000	89.3308
P_{G111}	10	100	99.9976	99.9982	99.9999
P_{WS1}	0	80	-	80.0000	80.0000
P_{WS2}	0	80	-	80.0000	80.0000
V_{G4}	0.9	1.1	1.0997	1.0971	1.0944
V_{G5}	0.9	1.1	1.1000	1.0983	1.0961
V_{G11}	0.9	1.1	1.0954	1.0961	1.0950
V_{G15}	0.9	1.1	1.1000	1.1000	1.0980
V_{G17}	0.9	1.1	1.1000	1.1000	1.0997
V_{G19}	0.9	1.1	1.0599	1.0628	1.0882
V_{G22}	0.9	1.1	1.0620	1.0665	1.0975
V_{G52}	0.9	1.1	1.0661	1.0593	1.0920
V_{G80}	0.9	1.1	1.1000	1.1000	1.0938
V_{G83}	0.9	1.1	1.1000	1.1000	1.0977
V_{G98}	0.9	1.1	1.1000	1.1000	1.0981
V_{G100}	0.9	1.1	1.1000	1.1000	1.1000
V_{G101}	0.9	1.1	1.1000	1.0773	1.0926
V_{G109}	0.9	1.1	1.1000	1.0056	1.0967
V_{G111}	0.9	1.1	1.0701	1.1000	1.0969
Fuel cost ($/h)			18914.105	17944.5766	18060.6608
Power losses (MW)			57.8726	57.2915	58.9776
Voltage deviation (p.u)			4.9714	5.1262	5.6014
Reserved real power COST			-	41.0227	41.0227

Table 5.16 DC bus data of VSC-MTDC system

VSC stations	Voltage Limites (p.u)		Voltage (p.u)	Active power (MW)
	Min	Max		
VSC1	0.9	1.1	1.000	57.061
VSC2	0.9	1.1	1.016	-79.914
VSC3	0.9	1.1	0.994	100.136
VSC4	0.9	1.1	1.009	-79.914

Table 5.15 summarized the obtained results reached by SMA and ALO algorithms considering VSC-based MTDC systems for wind energy transmission. From this table, it can be seen that the total generation cost and active power losses are considerably reduced after connecting the offshore wind farm into the AC system. The obtained results demonstrate the effectiveness of the VSC-based MTDC system in order to transport wind energy over a long distance. Moreover, the total fuel cost and active power loss provide by the SMA algorithm are 17944.5766 $/h and 57.2915 MW, respectively, which are minimum than obtained by the ALO algorithm (18060.6608 $/h and 58.9776 MW). The convergence curve of the total generation cost for the best run of both algorithms is shown in Fig. 5.25.

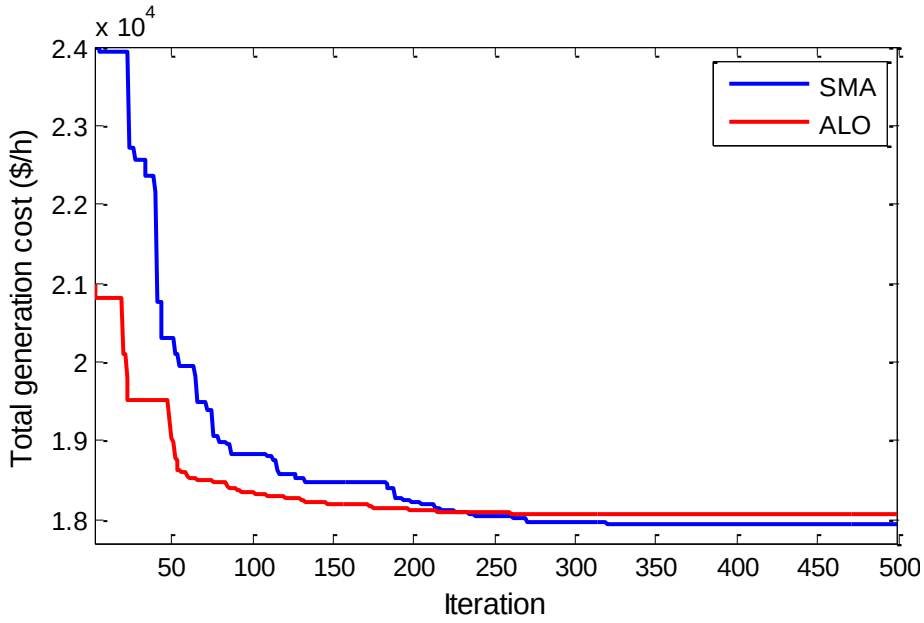

Figure 5.25 Convergence characteristics of SMA and ALO for ALG 114-bus system

5.11. Conclusion

This chapter is focused on minimizing the total generation cost according to the optimal scheduling of thermal and wind units, which allows the system to operate safely even with the uncertainty of wind power. The cost function of operating wind power in this part is divided into three

parts, the direct cost, the underestimated cost, and the overestimated cost. The OPF problem considering stochastic wind power with and without SVC-HVDC system has been formulated and solved by using the proposed algorithms SMA and ALO. These proposed algorithms have been tested and proven on the IEEE 30-bus and Algerian electrical 114-bus systems, and different scenarios are considered. The VSC-MTDC is used to transport offshore wind energy located over a long distance. The integration of wind power has significantly reduced the values of the total generation cost and the active power losses. With the incorporation of SVC-HVDC technology, the system operation has been improved by ensuring a good wind farm integration, avoiding the overload transmission line, reduce the active power losses as well as improve the voltage deviation. Moreover, the comparative of obtained results in all cases show that SMA produces very competitive performance and outperformed the ALO algorithm.

Chapter 06: General conclusion and Future Works

6.1. General Conclusion

The increase in energy consumption in recent years has led grid operators to search for renewable and environmentally friendly sources to cover this consumption. Incorporating renewable energy sources (RESs) into the electrical grid is a suitable solution to mitigate the increasing energy demand. The stochastic nature of RESs creates new challenges for grid operators. Hence, it is necessary to meet these challenges through optimal analysis of the planning and operation of modern power systems for the economic integration of this type of energy.

In this research work, the problem of optimal power flow (OPF) considering stochastic renewable energy sources has been analyzed and solved using advanced metaheuristic optimization techniques. These stochastic RESs are characterized as intermittent, variable as well as limited predictability. Implementation of flexible AC transmission systems (FACTS) and high voltage direct current (HVDC) systems are considered in this thesis, which opens new perspectives to ensure better performance and improve the operating of a transmission system. There are three parts to this thesis: application of advanced artificial intelligence techniques based on metaheuristic optimization algorithms to solve OPF problems, OPF solution incorporating FACTS-HVDC technology, and an OPF solution considering stochastic wind power.

The first part of this thesis addressed solving the OPF problem in small, practical, and large-scale power systems with three different single objective functions i.e., minimize the fuel cost, reduce the active power transmission losses and improve the voltage deviation. To reach a globally optimal solution to these objectives, two nature-inspired optimization algorithms called the slime mould algorithm (SMA) and ant lion optimization (ALO) are presented and applied to solve the OPF problem. The simulations have been carried out on the IEEE 14-bus, IEEE 57-bus, and practical Algerian electric 114-bus systems to examine the performances and effectiveness of the proposed algorithms. The obtained results prove the capability and efficiency of the proposed algorithms to solve the OPF problem according to the best values of control variables. To verify the effectiveness of the proposed algorithms, an analysis is done by comparing the results obtained between the proposed algorithms and other existing algorithms in the literature is performed. This comparison proved that the proposed algorithms significantly outperformed the techniques mentioned in Chapter 3. The comparative analysis of the proposed algorithms was performed and shows that the SMA has

better and robust performance compared to the ALO algorithm in solving the OPF problem.

The second part of this thesis deals with the implementation of FACTS-HVDC systems to improve the efficiency of electrical power grids, especially with the important growth of power demand. As a result of this important growth, voltage regulation and active power control are some of the most important concerns in power systems. Therefore, the FACTS system, in particular static VAR compensator (SVC), and HVDC transmission line have been implemented to regulate the voltage and control the active power. In this context, the OPF problem has been adopted considering SVC and HVDC transmission lines in order to improve the behavior of the electricity grid under contingency conditions (load variation and line outage). To further improve the power efficiency of the system, the proposed algorithms SMA and ALO are employed to find the optimal setting and location of SVC and HVDC transmission lines in electric power systems. The simulations have been carried out on the IEEE 30-bus and Algerian 114-bus systems with the objective function are the minimization of total fuel cost. To illustrate the effect of the SVC and HVDC transmission line on the technical parameters of the electrical network under contingency conditions, a comparison of results between the case without and with the SVC and HVDC transmission line is performed. The application of the SVC and HVDC transmission line improved considerably the fuel cost, reduce the active power loss, maintain the load bus voltages within acceptable limits as well as reduce line power transmission overloads. The proposed algorithms have been successfully applied to solve the OPF problem considering SVC devices and HVDC transmission lines in contingency conditions.

The last part of this thesis has been focused on the solve the problem of OPF considering stochastic wind power with the presence of FACTS-HVDC systems in the normal and contingency conditions. Among the important points addressed by this thesis is the incorporation of remotely located large wind farms by a multi-terminal DC (VSC-MTDC) system, which is considered one of the most attractive options to connect these wind farms to the onshore AC grids. This topology has a range of technological and economic advantages to provide a more robust network. In this work, the function of Weibull probability density (PDF) has been used to model and characterize the distributions of variable wind speed. The OPF problem considering stochastic wind power has been formulated with the objective function is to minimize the total generation cost (TGC) according to the optimal scheduling of thermal and wind units. This generation schedule provides an optimal analysis of the planning and operation of modern power systems. The wind power model integrated into the OPF formulation is divided into three parts, the direct cost, the penalty cost due to the underestimation and the reserve cost due to the overestimation of available wind power. The proposed algorithms SMA and ALO are applied on the IEEE 30-bus and Algerian electrical 114-bus systems,

and different scenarios are considered. The results obtained indicate that the integration of wind farms either directly to the system or by VSC-MTDC has significantly reduced the total generation cost, the active power losses as well as improve the voltage deviation compared to the results obtained in case when the system is operating without wind power. Moreover, the optimal use of wind power can also contribute to reducing load demand and, as a result, emissions from thermal generation plants. In most of the optimization problems that were made in this part, a comparative study demonstrates that SMA produces very competitive performance and outperformed ALO in terms of convergence rate towards the global optimum solution.

6.2. Scope for future research

Many perspectives of the optimal integration of renewable energies with the presence of FACTS-HVDC systems can be addressed in future research. These are some of the perspectives:

- The problem of optimal power flow considering stochastic wind power and FACTS-HVDC systems can be performed using hybrid advanced metaheuristic optimization techniques to improve the convergence speed.
- The OPF problem considering hybrid stochastic renewable energy sources such as solar energy, tidal energy,...etc, can be solved using single or hybrid advanced metaheuristic optimization techniques and could be studied as future work.
- This work has been concentrate on the solving of OPF problem under steady-state, the OPF problem under the dynamic state may be studied using single or hybrid metaheuristic optimization techniques.

References

[1] S. C. Bhatia, "Energy resources and their utilisation," in *Advanced Renewable Energy Systems*, Woodhead Publishing India, 2014, pp. 1–31.

[2] BP PLC, "BP Statistical Review of World Energy," *Technical report*, 2019.

[3] A. McCrone, U. Moslener, F. D'Estais, and C. Grüning, "Global Trends in Renewable Energy Investment 2019," *Technical report*, Frankfurt School-UNEP Centre/BNEF, 2019.

[4] A. Alassi, S. Bañales, O. Ellabban, G. Adam, and C. MacIver, "HVDC Transmission: Technology Review, Market Trends and Future Outlook," *Renew. Sustain. Energy Rev.*, vol. 112, pp. 530–554, 2019, doi: 10.1016/j.rser.2019.04.062.

[5] D. Gielen, F. Boshell, D. Saygin, M. D. Bazilian, N. Wagner, and R. Gorini, "The role of renewable energy in the global energy transformation," *Energy Strateg. Rev.*, vol. 24, pp. 38–50, 2019, doi: 10.1016/j.esr.2019.01.006.

[6] BloombergNEF, "Energy transition investment trends 2021," *Technical report*, 2021.

[7] J. K. Kaldellis, D. Apostolou, M. Kapsali, and E. Kondili, "Environmental and social footprint of offshore wind energy . Comparison with onshore counterpart," *Renew. Energy*, vol. 92, pp. 543–556, 2016, doi: 10.1016/j.renene.2016.02.018.

[8] International Renewable Energy Agency (IRENA), "Renewable capacity statistics 2021," *Technical report*, 2021.

[9] Global Wind energy council (GWEC), "Global Wind Report 2021," *Technical report*, p. 75, 2021.

[10] U. Zafar, "Literature review of wind turbines," *Special Project*, Bauhaus Universität, Weimar, 2018.

[11] Adnan Durakovic, "World's Largest Offshore Wind Farm Fully Up and Running," 2020. [Online]. Available: https://www.offshorewind.biz/2020/01/30/worlds-largest-offshore-wind-farm-fully-up-and-running/.

[12] Nadja Skopljak, "Highlights of the Month–January 2020," 2020. [Online]. Available: https://www.offshorewind.biz/2020/02/03/highlights-of-the-month-january-2020/.

[13] "Greater Changhua Offshore Wind Projects," *NS Energy*, 2019. [Online]. Available: https://www.nsenergybusiness.com/projects/greater-changhua-offshore-wind-projects/.

[14] D. Naimi, T. Bouktir, and A. Salhi, "Improvement of transient stability of Algerian power system network with wind farm," in *Proceedings of International Renewable and Sustainable Energy Conference, IRSEC 2013*, 2013, pp. 251–256, doi: 10.1109/IRSEC.2013.6529658.

[15] G. Hocine, L. Fatiha, G. F. Zohra, and A. Tayeb, "The Interest of the Wind Farm of Adrar to the Southwest Network of Algeria," *Iran. J. Energy Environ.*, vol. 10, no. 3, pp. 165–170, 2019, doi: 10.5829/ijee.2019.10.03.01.

[16] A. Abderrahim, M. M. Boudia, N. Ghellai, Y. Menni, and H. Ameur, "Determination of Wind Potential in some Regions of Algeria," *Iran. (Iran.) J. Energy Environ.*, vol. 11, no. 3, pp. 193–197, 2020, doi: 10.5829/ijee.2020.11.03.03.

[17] D. Abdeslame, N. Kasbadji Merzouk, S. Mekhtoub, M. Abbas, and M. Dehmas, "Estimation of power generation capacities of a wind farms installed in windy sites in Algerian high plateaus," *Renew. Energy*, vol. 103, pp. 630–640, 2017, doi: 10.1016/j.renene.2016.10.075.

[18] A. Derai, A. Kaabeche, and S. Diaf, "Etude de faisabilité technico-économique de fermes éoliennes en Algérie," *Rev. des Energies Renouvelables*, vol. 20, no. 4, pp. 693–712, 2017.

[19] Y. Zahraoui, M. R. Basir Khan, I. AlHamrouni, S. Mekhilef, and M. Ahmed, "Current Status, Scenario, and Prospective of Renewable Energy in Algeria: A Review," *Energies*, vol. 14, no. 9, p. 2354, 2021, doi: 10.3390/en14092354.

[20] N. H. Daaou, "L'énergie éolienne en Algérie," *Bulletin des Energies Renouvelables*, Division Energie Eolienne - CDER, pp. 7–9, 2018.

[21] P. Sharma and A. Kumar, "Thevenin's equivalent based P–Q–V voltage stability region visualization and enhancement with FACTS and HVDC," *Electr. Power Energy Syst.*, vol. 80, pp. 119–127, 2016, doi: 10.1016/j.ijepes.2016.01.026.

[22] P. Prabhakar and A. Kumar, "Voltage stability boundary and margin enhancement with FACTS and HVDC," *Electr. Power Energy Syst.*, vol. 82, pp. 429–438, 2016, doi: 10.1016/j.ijepes.2016.03.038.

[23] D. Sen, S. R. Ghatak, and P. Acharjee, "Optimal allocation of static VAR compensator by a hybrid algorithm," *Energy Syst.*, vol. 10, no. 3, pp. 677–719, 2017, doi: 10.1007/s12667-017-0247-7.

[24] W. Long and S. Nilsson, "Introduction to Flexible AC Transmission Systems (FACTS) Controllers: A Chronology," in *CIGRE Green Books*, Springer International Publishing Switzerland, 2020, pp. 1–11.

[25] P. Kumar, "Enhancement of power quality by an application FACTS devices," *Int. J. Power Electron. Drive Syst.*, vol. 6, no. 1, pp. 10–17, 2015, doi: 10.11591/ijpeds.v6.i1.pp10-17.

[26] J. Beerten, "Modeling and Control of DC Grids," University of Leuven, 2013.

[27] J. Setreus and L. Bertling, "Introduction to HVDC technology for reliable electrical power systems," in *Proceedings of the 10th International Conference on Probabilistic Methods Applied to Power Systems, PMAPS 2008*, 2008, pp. 560–567.

[28] J. Beerten, D. Van Hertem, and R. Belmans, "VSC MTDC systems with a distributed DC voltage control - A power flow approach," in *2011 IEEE Trondheim PowerTech, Trondheim*, 2011, pp. 1–6, doi: 10.1109/PTC.2011.6019434.

[29] E. Acha, P. Roncero-Sánchez, A. de la Villa-Jaén, L. M. Castro, and B. Kazemtabrizi, *VSC-FACTS-HVDC: analysis, modelling and simulation in power grids*, First Edit. John Wiley & Sons Ltd, 2019.

[30] S. Hocine and L. Djamel, "Optimal number and location of UPFC devices to enhence voltage profile and minimizing losses in electrical power systems," *Int. J. Electr. Comput. Eng.*, vol. 9, no. 5, pp. 3981–3992, 2019, doi: 10.11591/ijece.v9i5.pp3981-3992.

[31] J. M. Maza-Ortega, E. Acha, S. García, and A. Gómez-Expósito, "Overview of power electronics technology and applications in power generation transmission and distribution," *J. Mod. Power Syst. Clean Energy*, vol. 5, no. 4, pp. 499–514, 2017, doi: 10.1007/s40565-017-0308-x.

[32] M. Saravanan, S. M. R. Slochanal, P. Venkatesh, and S. A. J. Prince, "Application of PSO technique for optimal location of FACTS devices considering system loadability and cost of installation," in *7th International Power Engineering Conference, IPEC2005*, 2005, pp. 276–283, doi: 10.1109/ipec.2005.207001.

[33] T. V. Nguyen, P. Petit, F. Maufay, M. Aillerie, and J. P. Charles, "Power-line communication between parallel DC-DC optimizers on a high voltage direct current bus," in *WIT Transactions on Ecology and The Environment, Energy Production and Management in the 21st Century*, 2014, vol. 190, pp. 1297–1308, doi: 10.2495/EQ141202.

[34] Gunnar Herzig, "Global Offshore Wind Report 2019," Technical report, World Forum Offshore (WFO) wind, 2020.

[35] EWEA, "Delivering offshore wind power in Europe," *Technical report, European Wind Energy Association*, 2007.

[36] M. J. Carrizosa, F. D. Navas, G. Damm, and F. Lamnabhi-Lagarrigue, "Optimal power flow in multi-terminal HVDC grids with offshore wind farms and storage devices," *Int. J. Electr. Power Energy Syst.*, vol. 65, pp. 291–298, 2015, doi: 10.1016/j.ijepes.2014.10.016.

[37] H. T. Jadhav and R. Roy, "Stochastic optimal power flow incorporating offshore wind farm and electric vehicles," *Int. J. Electr. Power Energy Syst.*, vol. 69, pp. 173–187, 2015, doi: 10.1016/j.ijepes.2014.12.060.

[38] N. R. Chaudhuri, *Integrating Wind Energy to Weak Power Grids using High Voltage Direct Current*

Technology. Springer, 2019.

[39] D. Van Hertem, O. Gomis-Bellmunt, and J. Liang, *HVDC Grids: For Offshore and Supergrid of the Future*. New Jersey: John Wiley & Sons, 2016.

[40] J. carpentier, "Contribution à l'étude du dispatching économique," *Bull. La Société Française Des Electr.*, vol. 3, pp. 431–447, 1962.

[41] M. Ebeed, S. Kamel, and F. Jurado, "Optimal power flow using recent optimization techniques," in *Classical and Recent Aspects of Power System Optimization*, Ahmed F. Zobaa, Shady H.E. Abdel Aleem, and A. Y. Abdelaziz, Eds. Elsevier Inc., 2018, pp. 157–183.

[42] K. Teeparthi and D. M. Vinod Kumar, "Multi-objective hybrid PSO-APO algorithm based security constrained optimal power flow with wind and thermal generators," *Eng. Sci. Technol. an Int. J.*, vol. 20, no. 2, pp. 411–426, 2017, doi: 10.1016/j.jestch.2017.03.002.

[43] J.C. Das, *Load Flow Optimization and Optimal Power Flow*, Volume 2. Georgia, USA: CRC Press, 2018.

[44] A. Mukherjee and V. Mukherjee, "Solution of optimal power flow with FACTS devices using a novel oppositional krill herd algorithm," *Int. J. Electr. Power Energy Syst.*, vol. 78, pp. 700–714, 2016, doi: 10.1016/j.ijepes.2015.12.001.

[45] H. W. Dommel and W. F. Tinney, "Optimal power flow solutions," *IEEE Trans. Power Appar. Syst.*, vol. 87, no. 10, pp. 1866–1876, 1968, doi: 10.1109/TPAS.1968.292150.

[46] S. A.-H. Soliman and A.-A. H. Mantawy, *Modern Optimization Techniques with Applications in Electric Power Systems*, Energy Sys. Springer Science, 2012.

[47] F. Glover, "Future paths for integer programming and links to artificial intelligence," *Comput. Oper. Res.*, vol. 13, no. 5, pp. 533–549, 1986, doi: 10.1016/0305-0548(86)90048-1.

[48] J. Radosavljevic, *Metaheuristic Optimization in Power Engineering*. The Institution of Engineering and Technology, 2018.

[49] S. Mirjalili and A. Lewis, "The Whale Optimization Algorithm," *Adv. Eng. Softw.*, vol. 95, pp. 51–67, 2016, doi: 10.1016/j.advengsoft.2016.01.008.

[50] Nikolaos E. Karkalos, A. P. Markopoulos, and J. Paulo Davim, *Computational Methods for Application in Industry 4.0*. Springer, 2019.

[51] A. Biswas, K. K. Mishra, S. Tiwari, and A. K. Misra, "Physics-Inspired Optimization Algorithms: A Survey," *J. Optim.*, pp. 1–16, 2013, doi: 10.1155/2013/438152.

[52] A. A. El-Fergany and H. M. Hasanien, "Salp swarm optimizer to solve optimal power flow comprising voltage stability analysis," *Neural Comput. Appl.*, vol. 32, no. 3, pp. 1–17, 2019, doi: 10.1007/s00521-019-04029-8.

[53] A.-A. A. Mohamed, Y.S. Mohamed, A. A. El-Gaafary, and A.M. Hemeida, "Optimal power flow using moth swarm algorithm," *Electr. Power Syst. Res*, vol. 142, pp. 190–206, 2017.

[54] P. P. Biswas, P. N. Suganthan, R. Mallipeddi, and G. A. J. Amaratunga, "Optimal power flow solutions using differential evolution algorithm integrated with effective constraint handling techniques," *Eng. Appl. Artif. Intell.*, vol. 68, pp. 81–100, 2018, doi: 10.1016/j.engappai.2017.10.019.

[55] S. Surender Reddy and C. Srinivasa Rathnam, "Optimal Power Flow using Glowworm Swarm Optimization," *Int. J. Electr. Power Energy Syst.*, vol. 80, pp. 128–139, 2016, doi: 10.1016/j.ijepes.2016.01.036.

[56] K. Abaci and V. Yamacli, "Differential search algorithm for solving multi-objective optimal power flow problem," *Int. J. Electr. Power Energy Syst.*, vol. 79, pp. 1–10, 2016, doi: 10.1016/j.ijepes.2015.12.021.

[57] H. Pulluri, R. Naresh, and V. Sharma, "A solution network based on stud krill herd algorithm for optimal power flow problems," *Soft Comput.*, vol. 22, no. 1, pp. 159–176, 2018, doi: 10.1007/s00500-

016-2319-3.

[58] S. S. Jadon, J. C. Bansal, R. Tiwari, and H. Sharma, "Artificial bee colony algorithm with global and local neighborhoods," *Int. J. Syst. Assur. Eng. Manag.*, vol. 9, no. 3, pp. 589–601, 2018, doi: 10.1007/s13198-014-0286-6.

[59] M. Rezaei Adaryani and A. Karami, "Artificial bee colony algorithm for solving multi-objective optimal power flow problem," *Int. J. Electr. Power Energy Syst.*, vol. 53, no. 1, pp. 219–230, 2013, doi: 10.1016/j.ijepes.2013.04.021.

[60] S. Duman, "Symbiotic organisms search algorithm for optimal power flow problem based on valve-point effect and prohibited zones," *Neural Comput. Appl.*, vol. 28, no. 11, pp. 3571–3585, 2017, doi: 10.1007/s00521-016-2265-0.

[61] H. R. E. H. Bouchekara, A. E. Chaib, M. A. Abido, and R. A. El-Sehiemy, "Optimal power flow using an Improved Colliding Bodies Optimization algorithm," *Appl. Soft Comput. J.*, vol. 42, pp. 119–131, 2016, doi: 10.1016/j.asoc.2016.01.041.

[62] T. Hariharan and K. M. Sundaram, "Optimal Power Flow Using Firefly Algorithm with Unified Power Flow Controller," *Circuits Syst.*, vol. 07, no. 08, pp. 1934–1942, 2016, doi: 10.4236/cs.2016.78168.

[63] H. R. E. H. Bouchekara, "Optimal power flow using black-hole-based optimization approach," *Appl. Soft Comput. J.*, vol. 24, pp. 879–888, 2014, doi: 10.1016/j.asoc.2014.08.056.

[64] Z. Hasan and M. E. El-Hawary, "Optimal power flow by black hole optimization algorithm," *Proc. - 2014 Electr. Power Energy Conf. EPEC 2014*, pp. 134–141, 2014, doi: 10.1109/EPEC.2014.43.

[65] A. Ramesh Kumar and L. Premalatha, "Optimal power flow for a deregulated power system using adaptive real coded biogeography-based optimization," *Int. J. Electr. Power Energy Syst.*, vol. 73, pp. 393–399, 2015, doi: 10.1016/j.ijepes.2015.05.011.

[66] H. R. E. H. Bouchekara, M. A. Abido, A. E. Chaib, and R. Mehasni, "Optimal power flow using the league championship algorithm: A case study of the Algerian power system," *Energy Convers. Manag.*, vol. 87, pp. 58–70, 2014, doi: 10.1016/j.enconman.2014.06.088.

[67] M. Ghasemi, S. Ghavidel, E. Akbari, and A. A. Vahed, "Solving non-linear, non-smooth and non-convex optimal power flow problems using chaotic invasive weed optimization algorithms based on chaos," *Energy*, vol. 73, pp. 340–353, 2014, doi: 10.1016/j.energy.2014.06.026.

[68] Tarek Bouktir, Linda Slimani, and M. Belkacemi, "A Genetic Algorithm for Solving Optimal Power Flow Problem," *Leonardo J. Sci.*, pp. 44–58, 2004.

[69] T. M. Mohan and T. Nireekshana, "A Genetic Algorithm for Solving Optimal Power Flow Problem," *Proc. 3rd Int. Conf. Electron. Commun. Aerosp. Technol. ICECA 2019*, pp. 1438–1440, 2019, doi: 10.1109/ICECA.2019.8822090.

[70] B. Bentouati, S. Chettih, P. Jangir, and I. N. Trivedi, "A solution to the optimal power flow using multi-verse optimizer," *J. Electr. Syst.*, vol. 12, no. 4, pp. 716–733, 2016.

[71] P. Ren and N. Li, "Optimal power flow solution using the Harmony search algorithm," *Appl. Mech. Mater.*, pp. 1938–1941, 2014, doi: 10.4028/www.scientific.net/AMM.599-601.1938.

[72] I. Ghosh and P. K. Roy, "Application of earthworm optimization algorithm for solution of optimal power flow," *2019 Int. Conf. Opto-Electronics Appl. Opt. Optronix 2019*, vol. 1, no. 1, pp. 1–6, 2019, doi: 10.1109/OPTRONIX.2019.8862335.

[73] I. N. Trivedi, P. Jangir, S. A. Parmar, and N. Jangir, "Optimal power flow with voltage stability improvement and loss reduction in power system using Moth-Flame Optimizer," *Neural Comput. Appl.*, vol. 30, no. 6, pp. 1889–1904, 2018, doi: 10.1007/s00521-016-2794-6.

[74] A. Attia, R. A. El, and H. M. Hasanien, "Electrical Power and Energy Systems Optimal power fl ow solution in power systems using a novel Sine-Cosine algorithm," *Electr. Power Energy Syst.*, vol. 99, pp. 331–343, 2018, doi: 10.1016/j.ijepes.2018.01.024.

[75] R. Kouadri, L. Slimani, T. Bouktir, and I. Musirin, "Optimal power flow solution for wind integrated

power in presence of VSC-HVDC using ant lion optimization," *Indones. J. Electr. Eng. Comput. Sci.*, vol. 12, no. 2, pp. 625–633, 2018, doi: 10.11591/ijeecs.v12.i2.pp625-633.

[76] E. Naderi, M. Pourakbari-Kasmaei, and H. Abdi, "An efficient particle swarm optimization algorithm to solve optimal power flow problem integrated with FACTS devices," *Appl. Soft Comput. J.*, vol. 80, pp. 243–262, 2019, doi: 10.1016/j.asoc.2019.04.012.

[77] S. Li, H. Chen, M. Wang, A. A. Heidari, and S. Mirjalili, "Slime Mould Algorithm : A New Method for Stochastic Optimization," *Futur. Gener. Comput. Syst.*, 2020, doi: https://doi.org/10.1016/j.future.2020.03.055.

[78] S. Mirjalili, "The ant lion optimizer," *Adv. Eng. Softw.*, vol. 83, pp. 80–98, 2015, doi: 10.1016/j.advengsoft.2015.01.010.

[79] J. de A. B. Júnior, M. H. R. Nascimento, C. A. O. de Freitas, J. C. Leite, and T. L. R. Carvajal, "Approach of economic-emission load dispatch using Ant Lion Optimizer," *Int. J. Adv. Eng. Res. Sci.*, vol. 5, no. 7, pp. 184–190, 2018, doi: 10.22161/ijaers.5.7.26.

[80] E. S. Ali, S. M. Abd Elazim, and A. Y. Abdelaziz, "Ant Lion Optimization Algorithm for renewable Distributed Generations," *Energy*, vol. 116, pp. 445–458, 2016, doi: 10.1016/j.energy.2016.09.104.

[81] E. S. Ali, S. M. Abd Elazim, and A. Y. Abdelaziz, "Ant Lion Optimization Algorithm for optimal location and sizing of renewable distributed generations," *Renew. Energy*, vol. 101, pp. 1311–1324, 2017, doi: 10.1016/j.renene.2016.09.023.

[82] P. D. P. Reddy, V. V. Reddy, and T. G. Manohar, "Ant Lion optimization algorithm for optimal sizing of renewable energy resources for loss reduction in distribution systems," *J. Electr. Syst. Inf. Technol.*, vol. 5, no. 3, pp. 663–680, 2018, doi: 10.1016/j.jesit.2017.06.001.

[83] H. M. Dubey, M. Pandit, and B. K. Panigrahi, "Hydro-thermal-wind scheduling employing novel ant lion optimization technique with composite ranking index," *Renew. Energy*, vol. 99, pp. 18–34, 2016, doi: 10.1016/j.renene.2016.06.039.

[84] H. M. Dubey, M. Pandit, and B. K. Panigrahi, "Ant lion optimization for short-term wind integrated hydrothermal power generation scheduling," *Int. J. Electr. Power Energy Syst.*, vol. 83, pp. 158–174, 2016, doi: 10.1016/j.ijepes.2016.03.057.

[85] D. Ramavath and M. Sharma, "Optimal Power Flow Using Modified Ant Lion Optimizer," in *International Conference on Renewable Energy Integration into Smart Grids-2020*, 2020, pp. 14–15, doi: 10.1109/ICREISG49226.2020.9174551.

[86] S. Ahmed, N. Djemai, and T. Bouktir, "Optimal Power Flow Solution using Ant Lion Optimizer Algorithm," in *International Conference on Recent Advances in Electrical Systems*, 2016, vol. 1, no. 13, pp. 13–18.

[87] V. K. Kamboj, A. Bhadoria, and S. K. Bath, "Solution of non-convex economic load dispatch problem for small-scale power systems using ant lion optimizer," *Neural Comput. Appl.*, vol. 28, no. 8, pp. 2181–2192, 2017, doi: 10.1007/s00521-015-2148-9.

[88] I. N. Trivedi, P. Jangir, and S. A. Parmar, "Optimal power flow with enhancement of voltage stability and reduction of power loss using ant-lion optimizer," *Cogent Eng.*, vol. 3, no. 1, 2016, doi: 10.1080/23311916.2016.1208942.

[89] Enrique Acha, Claudio R. Fuerte-Esquivel, Hugo Ambriz-Pérez, and César Angeles-Camacho, *FACTS: Modelling and Simulation in Power Networks*. John Wiley & Sons Ltd, 2004.

[90] Z. Lu, M. S. Li, W. J. Tang, and Q. H. Wu, "Optimal location of FACTS devices by a Bacterial Swarming Algorithm for reactive power planning," in *07 IEEE Evolutionary Computing. CEC 2007*, 2007, pp. 2344–2349, doi: 10.1109/CEC.2007.4424764.

[91] W. Shao and V. Vittal, "LP-based OPF for corrective FACTS control to relieve overloads and voltage violations," *IEEE Trans. Power Syst.*, vol. 21, no. 4, pp. 1832–1839, 2006, doi: 10.1109/TPWRS.2006.881127.

[92] K. Y. Lee, M. M. Farsangi, and H. Nezamabadi-pour, "Hybrid of analytical and heuristic techniques for FACTS devices in transmission systems," in *IEEE Power Engineering Society General Meeting, PES*, 2007, pp. 1–8, doi: 10.1109/PES.2007.386180.

[93] A. K. Mohanty and A. K. Barik, "Power System Stability Improvement Using FACTS Devices," *Int. J. Mod. Eng. Res.*, vol. 1, no. 2, pp. 666–672, 2011.

[94] A. AL Ahmad and R. Sirjani, "Optimal placement and sizing of multi-type FACTS devices in power systems using metaheuristic optimisation techniques: An updated review," *Ain Shams Eng. J.*, vol. 63, 2019, doi: 10.1016/j.asej.2019.10.013.

[95] M. Taleb, A. A. Ali, A. Salem, and M. Abouazma, "Advanced Method for Optimal Allocation of FACTS Devices Using Line Stability Index Combined with Meta-Heuristic Optimization Techniques," in *21st International Middle East Power Systems Conference, MEPCON 2019*, 2019, pp. 324–329, doi: 10.1109/MEPCON47431.2019.9008163.

[96] T. Duong, Y. Jiangang, and V. Truong, "Application of min cut algorithm for optimal location of FACTS devices considering system loadability and cost of installation," *Int. J. Electr. Power Energy Syst.*, vol. 63, pp. 979–987, 2014, doi: 10.1016/j.ijepes.2014.06.072.

[97] K. Y. Lee, M. M. Farsangi, and H. Nezamabadi-pour, "Hybrid of Analytical and Heuristic Techniques for FACTS Devices," in *Applications of Modern Heuristic Optimization Methods in Power and Energy*, K. Y. Lee and Z. Vale, Eds. Wiley-IEEE Press, 2020.

[98] D. Mondal, A. Chakrabarti, and A. Sengupta, "Optimal placement and parameter setting of SVC and TCSC using PSO to mitigate small signal stability problem," *Int. J. Electr. Power Energy Syst.*, vol. 42, no. 1, pp. 334–340, 2012, doi: 10.1016/j.ijepes.2012.04.017.

[99] M. K. Mohamad Zamani, I. Musirin, S. A. S. Mustaffa, and S. I. Suliman, "Optimal SVC allocation via symbiotic organisms search for voltage security improvement," *Telkomnika*, vol. 19, no. 3, pp. 1267–1274, 2017, doi: 10.12928/TELKOMNIKA.v17i3.9905.

[100] T. N. V. L. N. Kumar and R. V. S. Satyanarayana, "A Modified BFOA Approach for Optimal Location and Sizing of Facts for Enhancing Power System Security," *i-manager's J. Power Syst. Eng.*, vol. 5, no. 3, pp. 24–33, 2017, doi: 10.26634/jps.5.3.13669.

[101] T. N. V. L. N. Kumar and R. V. S. Satyanarayana, "Enhancing Power System Security: A Multi-Objective Optimal Approach to Identify the Location and Size of SVC.," *IUP J. Electr. Electron. Eng.*, vol. XI, no. 1, pp. 45–58, 2018.

[102] S. A. Jumaat and I. Musirin, "Σ-multi-objective evolutionary particle swarm optimization approach for transmission loss and cost minimization with svc installation," *J. Fundam. Appl. Sci.*, vol. 10, no. 3S, pp. 715–728, 2018, doi: http://dx.doi.org/10.4314/jfas.v10i3s.61.

[103] E. R. Sanseverino *et al.*, "Optimal Placements of SVC Devices in Low Voltage Grids with High Penetration of PV Systems," in *9th IEEE International Symposium on Power Electronics for Distributed Generation Systems, PEDG 2018*, 2018, pp. 1–6, doi: 10.1109/PEDG.2018.8447619.

[104] B. Bhattacharyya and S. Kumar, "Loadability enhancement with FACTS devices using gravitational search algorithm," *Int J Electr Power Energy Syst*, vol. 78, pp. 470–479, 2016, doi: 10.1016/j.ijepes.2015.11.114.

[105] A. Rezaee Jordehi, "Brainstorm optimisation algorithm (BSOA): An efficient algorithm for finding optimal location and setting of FACTS devices in electric power systems," *Int. J. Electr. Power Energy Syst.*, vol. 69, pp. 48–57, 2015, doi: 10.1016/j.ijepes.2014.12.083.

[106] A. Panda and M. Tripathy, "Security constrained optimal power flow solution of wind-thermal generation system using modified bacteria foraging algorithm," *Energy*, vol. 93, pp. 816–827, 2015, doi: 10.1016/j.energy.2015.09.083.

[107] A. Panda and M. Tripathy, "Optimal power flow solution of wind integrated power system using modified bacteria foraging algorithm," *Int. J. Electr. Power Energy Syst.*, vol. 54, pp. 306–314, 2014, doi: 10.1016/j.ijepes.2013.07.018.

[108] R. Roy and H. T. Jadhav, "Optimal power flow solution of power system incorporating stochastic wind power using Gbest guided artificial bee colony algorithm," *Int. J. Electr. Power Energy Syst.*, vol. 64, pp. 562–578, 2015, doi: 10.1016/j.ijepes.2014.07.010.

[109] E. E. Elattar, "Optimal Power Flow of a Power System Incorporating Stochastic Wind Power Based on Modified Moth Swarm Algorithm," *IEEE Access*, vol. 7, pp. 89581–89593, 2019, doi: 10.1109/ACCESS.2019.2927193.

[110] S. Duman, J. Li, L. Wu, and U. Guvenc, "Optimal power flow with stochastic wind power and FACTS devices: a modified hybrid PSOGSA with chaotic maps approach," *Neural Comput. Appl.*, vol. 32, no. 12, pp. 8463–8492, 2019, doi: 10.1007/s00521-019-04338-y.

[111] M. Ahmad, N. Javaid, I. A. Niaz, S. Shafi, O. U. Rehman, and H. M. Hussain, "Application of Bird Swarm Algorithm for Solution of Optimal Power Flow Problems," in *Complex, Intelligent, and Software Intensive Systems*, vol. 772-AISC, Springer International Publishing, 2019, pp. 280–291.

[112] S. Shafiq, N. Javaid, S. Asif, F. Ali, N. H. Chughtai, and N. Khurshid, "An optimal power flow approach for stochastic wind and solar energy integrated power systems," in *Advances in Intelligent Systems and Computing*, vol. AISC 772, Springer International Publishing, 2019, pp. 292–304.

[113] S. Surender Reddy, "Multi-objective optimal power flow for a thermal-wind-solar power system," *J. Green Eng.*, vol. 7, no. 4, pp. 451–476, 2017, doi: 10.13052/jge1904-4720.741.

[114] A. Panda, "A Computational Framework for Wind Power Integration in Stochastic Optimal Power Flow Analysis," *Am. Int. J. Res. Sci. Technol. Eng. Math.*, pp. 17–23, 2018.

[115] M. H. Sulaiman and Z. Mustaffa, "Solving optimal power flow problem with stochastic wind–solar–small hydro power using barnacles mating optimizer," *Control Eng. Pract.*, vol. 106, p. 104672, 2021, doi: doi.org/10.1016/j.conengprac.2020.104672.

[116] M. Abdullah, N. Javaid, I. U. Khan, Z. A. Khan, A. Chand, and Noman Ahmad, "Optimal Power Flow with Uncertain Renewable Energy Sources Using Flower Pollination Algorithm," in *Advances in Intelligent Systems and Computing*, vol. AISC 926, Springer International Publishing, 2020, pp. 95–107.

[117] S. Duman, L. Wu, and J. Li, "Moth Swarm Algorithm Based Approach for the ACOPF Considering Wind and Tidal Energy," in *Artificial Intelligence and Applied Mathematics in Engineering Problems*, no. LNDECT 43, Springer Nature Switzerland, 2020, pp. 830–843.

[118] T. Samakpong, W. Ongsakul, and M. N. Madhu, "Optimal Power Flow Considering Cost of Wind and Solar Power Uncertainty Using Particle Swarm Optimization," in *Intelligent Computing and Optimization*, Springer Nature Switzerland, 2020, pp. 190–203.

[119] S. B. Pandya and H. R. Jariwala, "Renewable Energy Resources Integrated Multi-Objective Optimal Power Flow using Non-Dominated Sort Grey Wolf Optimizer," *J. Green Eng.*, vol. 10, no. 1, pp. 180–205, 2020.

[120] S. B. Pandya and H. R. Jariwala, "Stochastic wind-thermal power plants integrated multi-objective optimal power flow," *Majlesi J. Electr. Eng.*, vol. 14, no. 2, pp. 93–110, 2020.

[121] A. Abdollahi, A. A. Ghadimi, M. R. Miveh, F. Mohammadi, and F. Jurado, "Optimal Power Flow Incorporating FACTS Devices and Stochastic Wind Power Generation using Krill Herd Algorithm," *Electronics*, vol. 9, p. 1043, 2020, doi: 10.3390/electronics9061043.

[122] M. H. Sulaiman and Z. Mustaffa, "Optimal power flow incorporating stochastic wind and solar generation by metaheuristic optimizers," *Microsyst. Technol.*, vol. 7, no. 2004, p. 5046, 2020, doi: doi.org/10.1007/s00542-020-05046-7.

[123] E. Kaymaz, S. Duman, and U. Guvenc, "Optimal power flow solution with stochastic wind power using the Lévy coyote optimization algorithm," *Neural Comput. Appl.*, vol. 9, 2020, doi: 10.1007/s00521-020-05455-9.

[124] P. P. Biswas, P. N. Suganthan, and G. A. J. Amaratunga, "Optimal power flow solutions incorporating

stochastic wind and solar power," *Energy Convers. Manag.*, vol. 148, pp. 1194–1207, 2017, doi: 10.1016/j.enconman.2017.06.071.

[125] S. Makhloufi, A. Mekhaldi, and M. Teguar, "Three powerful nature-inspired algorithms to optimize power flow in Algeria's Adrar power system," *Energy*, vol. 116, pp. 1117–1130, 2016, doi: 10.1016/j.energy.2016.10.064.

[126] M. Ebeed, S. Kamel, and F. Jurado, "Optimal power flow using recent optimization techniques," in *Classical and Recent Aspects of Power System Optimization*, Elsevier Inc., 2018, pp. 157–183.

[127] "IEEE 57-bus power system," *College of Engineering, Electrical Engineering, University of Washington*. [Online]. Available: http://www.ee.washington.edu/research/pstca.

[128] G. Chen, Z. Lu, Z. Zhang, and Z. Sun, "Optimal Power Flow Using an Improved Hybrid Differential Evolution Algorithm," *Open Electr. Electron. Eng. J.*, vol. 11, pp. 177–192, 2017, doi: 10.2174/1874129001711010177.

[129] M. Ghasemi, S. Ghavidel, M. M. Ghanbarian, and M. Gitizadeh, "Multi-objective optimal electric power planning in the power system using Gaussian bare-bones imperialist competitive algorithm," *Inf. Sci. (Ny).*, vol. 294, pp. 286–304, 2015, doi: 10.1016/j.ins.2014.09.051.

[130] H. R. El-Hana Bouchekara, M. A. Abido, and A. E. Chaib, "Optimal Power Flow Using an Improved Electromagnetism-like Mechanism Method," *Electr. Power Components Syst.*, vol. 44, no. 4, pp. 434–449, 2016, doi: 10.1080/15325008.2015.1115919.

[131] P. Chinta, K. R. Subhashini, and J. K. Satapathy, "Optimal Power Flow Using A New Evolutionary Approach : Animal Migration Optimization," in *International Conference on Innovative Technologies in Engineering*, 2018.

[132] X. He, W. Wang, J. Jiang, and L. Xu, "An improved artificial bee colony algorithm and its application to multi-objective optimal power flow," *Energies*, vol. 8, no. 4, pp. 2412–2437, 2015, doi: 10.3390/en8042412.

[133] A. A. El-Fergany and H. M. Hasanien, "Tree-seed algorithm for solving optimal power flow problem in large-scale power systems incorporating validations and comparisons," *Appl. Soft Comput. J.*, vol. 64, pp. 307–316, 2018, doi: 10.1016/j.asoc.2017.12.026.

[134] L. Slimani and T. Bouktir, "Optimal power flow solution of the algerian electrical network using differential evolution algorithm," *Telkomnika*, vol. 10, no. 2, pp. 199–210, 2012, doi: 10.12928/telkomnika.v10i2.778.

[135] R. Kouadri, I. Musirin, L. Slimani, T. Bouktir, and A. Info, "OPF for large scale power system using ant lion optimization : a case study of the Algerian electrical network," vol. 9, no. 2, pp. 252–260, 2020, doi: 10.11591/ijai.v9.i2.pp252-260.

[136] B. Mahdad and K. Srairi, "Solving practical economic dispatch using hybrid GA-DE-PS method," *Int. J. Syst. Assur. Eng. Manag.*, vol. 5, no. 3, pp. 391–398, 2014, doi: 10.1007/s13198-013-0180-7.

[137] O. Herbadji, L. Slimani, and T. Bouktir, "Optimal power flow with four conflicting objective functions using multiobjective ant lion algorithm: A case study of the algerian electrical network," *Iran. J. Electr. Electron. Eng.*, vol. 15, no. 1, pp. 94–113, 2019, doi: 10.22068/IJEEE.15.1.94.

[138] V. Beiranvand, W. Hare, and Y. Lucet, "Best practices for comparing optimization algorithms," *Optim. Eng.*, vol. 18, no. 4, pp. 815–848, 2017, doi: 10.1007/s11081-017-9366-1.

[139] N. G. Hingorani, "Power Electronics in Electric Utilities: Role of Power Electronics in Future Power Systems," *Proc. IEEE*, vol. 76, no. 4, pp. 481–482, 1988, doi: 10.1109/5.4432.

[140] T. Kang, J. Yao, T. Duong, S. Yang, and X. Zhu, "A hybrid approach for power system security enhancement via optimal installation of flexible ac transmission system (FACTS) devices," *Energies*, vol. 10, no. 9, 2017, doi: 10.3390/en10091305.

[141] H. I. Shaheen, G. I. Rashed, and S. J. Cheng, "Application and comparison of computational intelligence techniques for optimal location and parameter setting of UPFC," *Eng. Appl. Artif. Intell.*,

vol. 23, no. 2, pp. 203–216, 2010, doi: 10.1016/j.engappai.2009.12.002.

[142] R. K. Khadanga, "Performance Analysis of Flexible A . C . Transmission System Devices for Stability Improvement of Power System," PhD Thesis. National Institute of Technology. Rourkela, 2016.

[143] A. Oukennou, A. Sandali, and S. Elmoumen, "Coordinated Placement and Setting of FACTS in Electrical Network based on Kalai-smorodinsky Bargaining Solution and Voltage Deviation Index," *Int. J. Electr. Comput. Eng.*, vol. 8, no. 6, p. 4079, 2018, doi: 10.11591/ijece.v8i6.pp4079-4088.

[144] A. Korompili, Q. Wu, and H. Zhao, "Review of VSC HVDC connection for offshore wind power integration," *Renew. Sustain. Energy Rev.*, vol. 59, pp. 1405–1414, 2016, doi: 10.1016/j.rser.2016.01.064.

[145] D. Van Hertem and M. Delimar, "High Voltage Direct Current (HVDC) electric power transmission systems," in *Electricity Transmission, Distribution and Storage Systems*, Ziad Melhem, Ed. Abingdon, Oxfordshire, UK: Woodhead Publishing Limited, 2013, pp. 143–173.

[146] A. Kalair, N. Abas, and N. Khan, "Comparative study of HVAC and HVDC transmission systems," *Renew. Sustain. Energy Rev.*, vol. 59, pp. 1653–1675, 2016, doi: 10.1016/j.rser.2015.12.288.

[147] V. K. Sood, *HVDC and FACTS Controllers: Applications of Static Converters in Power Systems*. New York USA: Kluwer Academic Publishers, 2004.

[148] K. Hafeez, A. B. Awan, S. Z. Uddin, I. Yousaf, M. N. Ullah, and Z. A. Khan, "To Investigate Environmental effects of HVDC versus HVAC Transmission Systems," *J. Basic Appl. Sci. Res.*, vol. 3, no. 8, pp. 840–843, 2013.

[149] M. P. Bahrman and B. K. Johnson, "The ABCs of HVDC transmission technology," *Ieee Power & Energy Magazine*, pp. 32–44, 2007.

[150] R. L. Sellick and M. Åkerberg, "Comparison of HVDC Light (VSC) and HVDC Classic (LCC) site aspects, for a 500MW 400kV HVDC transmission scheme," in *IET Conference Publications*, 2012, pp. 1–6, doi: 10.1049/cp.2012.1945.

[151] O. Anaya-Lara, D. Campos-Gaona, E. Moreno-Goytia, and G. Adam, *Offshore Wind Energy Generation: Control, Protection, and Integration to Electrical Systems*. John Wiley & Sons, 2014.

[152] L. Teppoz, "Commande d'un système de conversion de type VSC-HVDC. Stabilité - Contrôle des perturbations," PhD Thesis. Institut National Polytechnique of Grenoble - INPG, 2005.

[153] M. Eremia, C. C. Liu, and A. A. Edris, "VSC–HVDC TRANSMISSION," in *Advanced Solutions in Power Systems: HVDC, FACTS, and AI Techniques*, John Wiley & Sons, 2016, pp. 125–270.

[154] J. Setréus and L. B. Tjernberg, "Introduction to HVDC Technology for Reliable Electrical Power Systems," in *Proceedings of the 10th International Conference on Probabilistic Methods Applied to Power Systems, PMAPS 2008*, 2008, pp. 560–567.

[155] C. Du, "VSC-HVDC for Industrial Power Systems," Doctoral Thesis, Department of Energy and Environment, Chalmers University of Technology, 2007.

[156] R. Grünbaum, B. Halvarsson, and A. Wilk-Wilczynski, "FACTS and HVDC Light for Power System Interconnections," in *Power Delivery Confrerence*, 1999, pp. 1–18.

[157] P. A. Owusu and S. Asumadu-sarkodie, "A review of renewable energy sources , sustainability issues and climate change mitigation," *Cogent Eng.*, pp. 1–14, 2016, doi: 10.1080/23311916.2016.1167990.

[158] N. L. Panwar, S. C. Kaushik, and S. Kothari, "Role of renewable energy sources in environmental protection : A review," *Renew. Sustain. Energy Rev.*, vol. 15, no. 3, pp. 1513–1524, 2011, doi: 10.1016/j.rser.2010.11.037.

[159] I. Yahyaoui, *Advances in Renewable Energies and Power Technologies*. Madrid, Spain: Elsevier Inc., 2018.

[160] J. Khan and M. H. Arsalan, "Solar power technologies for sustainable electricity generation – A review," *Renew. Sustain. Energy Rev.*, vol. 55, pp. 414–425, 2016, doi: 10.1016/j.rser.2015.10.135.

[161] O. Erdinc, *Optimization in Renewable Energy Systems: recent perspectives*. Istanbul, Turkey: Butterworth-Heinemann, 2017.

[162] I. Komusanac, G. Brindley, and D. Fraile, "Wind energy in Europe in 2019: Trends and statistics," *Technical report, WindEurope Business Intelligence*, 2020.

[163] M. A. HYAMS, "Wind energy in the built environment," in *Metropolitan Sustainability*, Woodhead Publishing, 2012, pp. 457–499.

[164] A. Hosseini and N. Goudarzi, "Design and CFD study of a hybrid vertical-axis wind turbine by employing a combined Bach-type and H-Darrieus rotor systems," *Energy Convers. Manag.*, vol. 189, pp. 49–59, 2019, doi: 10.1016/j.enconman.2019.03.068.

[165] N. R. Babu and P. Arulmozhivarman, "Wind Energy Conversion Systems-A Technical Review," *J. Eng. Sci. Technol.*, vol. 8, no. 4, pp. 493–507, 2013.

[166] A. E. Craig, J. O. Dabiri, and J. R. Koseff, "Low order physical models of vertical axis wind turbines," *J. Renew. Sustain. Energy*, vol. 9, no. 1, 2017, doi: 10.1063/1.4976983.

[167] S. Mertens, "Wind Energy in the Built Environment: Concentrator Effects of Buildings," Doctoral Thesis, Technische Universiteit Delft, 2006.

[168] A. D. Hansen, "Wind Turbine Technologies," in *Wind Energy Engineering*, 1st ed., T. Letcher, Ed. Elsevier Inc., 2017, pp. 145–160.

[169] T. Funabashi, "Introduction," in *Integration of Distributed Energy Resources in Power Systems*, Elsevier, 2016, pp. 1–14.

[170] M. Cheng and Y. Zhu, "The state of the art of wind energy conversion systems and technologies : A review," *Energy Convers. Manag.*, vol. 88, pp. 332–347, 2014, doi: 10.1016/j.enconman.2014.08.037.

[171] L. Helle and F. Blaabjerg, "Wind Turbine Systems," in *Control in Power Electronics*, Academic Press Series in Engineering, 2002, pp. 483–509.

[172] Å. LARSSON, "The Power Quality of Wind Turbines," Doctoral Thesis, Chalmers University of Technology, Goteborg, 2000.

[173] A. S. A. Badawi *et al.*, "Weibull Probability Distribution of Wind Speed for Gaza Strip for 10 Years," *Appl. Mech. Mater.*, vol. 892, pp. 284–291, 2019, doi: 10.4028/www.scientific.net/AMM.892.284.

[174] I. Y. F. Lun and J. C. Lam, "A study of Weibull parameters using long- term wind observations," *Renew. energy*, vol. 20, no. 2, pp. 145–153, 2000, doi: 10.1016/S0960-1481(99)00103-2.

[175] M. A. Abuella, "Study of Particle Swarm for Optimal Power Flow in IEEE Benchmark Systems Including Wind Power Generators," Thesis, Southern Illinois University Carbondale, 2012.

[176] A. Pacheco, E. Gorbeña, C. Sequeira, and S. Jerez, "An evaluation of offshore wind power production by floatable systems: A case study from SW Portugal," *Energy*, vol. 131, pp. 239–250, 2017, doi: 10.1016/j.energy.2017.04.149.

[177] J. Hetzer, D. C. Yu, and K. Bhattarai, "An economic dispatch model incorporating wind power," *IEEE Trans Energy Convers*, vol. 23, no. 2, pp. 603–611, 2008, doi: 10.1109/TEC.2007.914171.

[178] L. Slimani and T. Bouktir, "Application of Differential Evolution Algorithm to Optimal Power Flow with High Wind Energy Penetration," vol. 53, no. 1, pp. 59–68, 2012.

[179] S. Haddi, O. Bouketir, and T. Bouktir, "Improved optimal power flow for a power system incorporating wind power generation by using Grey Wolf Optimizer algorithm," *Adv. Electr. Electron. Eng.*, vol. 16, no. 4, pp. 471–488, 2018, doi: 10.15598/aeee.v16i4.2883.

Appendix A- MAs for OPF considering stochastic wind

The applied metaheuristic algorithms (MAs) in the literature for OPF solutions considering stochastic wind power are listed in Table A.1.

Table A.1 Literature review regarding applied metaheuristic algorithms for OPF considering stochastic wind power

Algorithm	OPF Incorporating	Objective Function Fuel	System	Year	Ref
BMO	wind–solar–small hydro power	Fuel- wind–solar–small hydro costs & power loss & combined generation cost and emission	Modified IEEE-30 bus IEEE 57-bus	2021	[115]
FPO	Wind-Solar and combined wind-hydro	Fuel-Wind-Solar and combined wind and hydro costs	modified IEEE 30-bus	2020	[116]
MSA	Wind and tidal power	Fuel-Wind-Tidal costs	IEEE 30-bus	2020	[117]
PSO	Wind and solar power	Fuel-Wind-Solar costs	IEEE New England 39-bus	2020	[118]
GWO	Wind and solar power	Fuel-Wind-Solar costs	modified IEEE 30-bus	2020	[119]
MFA	Wind power	Fuel-Wind costs & emission & Voltage deviation & power losses & voltage stability index	Modified IEEE 30-bus	2020	[120]
KHA	Wind power and FACTS	Fuel-Wind costs & power losses & emission & combined economic and environmental costs	Modified IEEE-30 bus IEEE 57-bus	2020	[121]
GOA, BWO GWO, ALO, PSO, GSA, MFO and BMO	Wind and solar power	Fuel-Wind-Solar costs & power loss & combined generation cost and emission	Modified IEEE 30-bus	2020	[122]
LCOA	Wind power	Single and multiple of Fuel-Wind costs & fuel cost with valve effect & emissions & voltage stability & voltage deviation & power loss	IEEE-30 bus IEEE 57-bus IEEE 118-bus	2020	[123]
MMSA	Wind power	Fuel-Wind costs & power loss & voltage deviation	Modified IEEE 30-bus Modified IEEE 118-bus	2019	[109]
MPSOGSA	Wind power and FACTS	Fuel-Wind costs and emission	IEEE 30-bus IEEE 57-bus	2019	[110]
BSA	Wind and solar power	Fuel-Wind-Solar costs	Modified IEEE 30-bus	2019	[111]
GA	Wind and solar power	Fuel-Wind-Solar costs & emission	IEEE-30 bus	2019	[112]

PSO	Wind and solar power	Fuel-Wind-Solar costs & power loss & voltage stability	Modified IEEE 30-bus	2018	[113]
MBFA and GA	Wind power	Fuel-Wind costs with power loss	IEEE 30-bus	2018	[114]
DE	Wind and solar power	Fuel-Wind-Solar costs & emission	IEEE-30 bus	2017	[124]
CSA, FA and FPA	Wind power	Fuel-Wind-Solar costs & emission	Isolated Adrar Algerian power system	2016	[125]
GGABC	Wind power	Fuel-Wind costs and emission	IEEE 30-bus	2015	[108]
MBFA	Wind power and FACTS	Fuel-Wind costs	Modified IEEE 30-bus	2015	[106]
MBFA	Wind power	Fuel-Wind costs	Modified IEEE 30-bus	2014	[107]

Appendix B- IEEE 30-bus test system data

The bus data and line data of the IEEE 30-bus test system are represented in Table B.1 and Table B.2, respectively.

Table B.1 Bus data of the IEEE 30-bus test system

Bus N°	Bus voltage		load		Generation	
	Magnitude (pu)	Phase angle (°)	Real power (MW)	Reactive power (MVar)	Real power (MW)	Reactive power (MVar)
1	1.0060	0	0.00	0.00	175.86	0
2	1.0450	0	21.7	12.7	48.64	0
3	1.0000	0	2.40	1.20	0	0
4	1.0000	0	7.60	1.60	0	0
5	1.0100	0	94.2	19.0	21.19	0
6	1.0000	0	0.00	0.00	0	0
7	1.0000	0	22.8	10.9	0	0
8	1.0100	0	30.0	30.0	22.51	0
9	1.0000	0	0.00	0.00	0	0
10	1.0000	0	5.80	2.00	0	0
11	1.0820	0	0.00	0.00	12.33	0
12	1.0000	0	11.2	7.50	0	0
13	1.0710	0	0.00	0.00	12.00	0
14	1.0000	0	6.20	1.60	0	0
15	1.0000	0	8.20	2.5	0	0
16	1.0000	0	3.50	1.80	0	0
17	1.0000	0	9.00	5.80	0	0
18	1.0000	0	3.20	0.90	0	0
19	1.0000	0	9.50	3.40	0	0
20	1.0000	0	2.20	0.70	0	0
21	1.0000	0	17.5	11.2	0	0
22	1.0000	0	0.00	0.00	0	0
23	1.0000	0	3.20	1.60	0	0
24	1.0000	0	8.70	6.70	0	0
25	1.0000	0	0.00	0.00	0	0
26	1.0000	0	3.50	2.30	0	0
27	1.0000	0	0.00	0.00	0	0
28	1.0000	0	0.00	0.00	0	0
29	1.0000	0	2.40	0.90	0	0
30	1.0000	0	10.6	1.90	0	0

Table B.2 Line data of the IEEE 30-bus test system

From bus	To bus	Resistance	Reactance	Susceptance
1	2	0.0192	0.0575	0.0264
1	3	0.0452	0.1852	0.0204
2	4	0.0570	0.1737	0.0184
3	4	0.0132	0.0379	0.0042
2	5	0.0472	0.1983	0.0209

2	6	0.0581	0.1763	0.0187
4	6	0.0119	0.0414	0.0045
5	7	0.0460	0.1160	0.0102
6	7	0.0267	0.0820	0.0085
6	8	0.0120	0.0420	0.0045
6	9	0	0.2080	0
6	10	0	0.5560	0
9	11	0	0.2080	0
9	10	0	0.1100	0
4	12	0	0.2560	0
12	13	0	0.1400	0
12	14	0.1231	0.2559	0
12	15	0.0662	0.1304	0
12	16	0.0945	0.1987	0
14	15	0.2210	0.1997	0
16	17	0.0824	0.1923	0
15	18	0.1073	0.2185	0
18	19	0.0639	0.1292	0
19	20	0.0340	0.0680	0
10	20	0.0936	0.2090	0
10	17	0.0324	0.0845	0
10	21	0.0348	0.0749	0
10	22	0.0727	0.1499	0
21	22	0.0116	0.0236	0
15	23	0.1000	0.2020	0
22	24	0.1150	0.1790	0
23	24	0.1320	0.2700	0
24	25	0.1885	0.3292	0
25	26	0.2544	0.3800	0
25	27	0.1093	0.2087	0
28	27	0	0.3960	0
27	29	0.2198	0.4153	0
27	30	0.3202	0.6027	0
29	30	0.2399	0.4533	0
8	28	0.0636	0.2000	0.0214
6	28	0.0169	0.0599	0.0650

Table B.1 presents the fuel cost function parameter for the IEEE 30-bus test system

Table B.3 Fuel cost function parameter for the IEEE 30-bus test system

JB N°	P_i^{max}	P_i^{min}	A_i ($/h$)	B_i($/MW * h$)	C_i($/MW^2 * h$)
1	200	50	0	2.00	0.00375
2	80	20	0	1.75	0.01750
3	50	15	0	1.00	0.06250
4	35	10	0	3.25	0.00830
5	30	10	0	3.00	0.02500
6	40	12	0	3.00	0.02500

Appendix C- IEEE 57-bus test system data

The bus data of the IEEE 57-bus system are represented in Table C.1.

Table C.1 Bus data of the IEEE 57-bus test system

Bus N°	Bus voltage		load		Generation	
	Magnitude (p.u)	Phase angle (°)	Real power (MW)	Reactive power (MVar)	Real power (MW)	Reactive power (MVar)
1	1.0060	0	55	17	128.9	-16.1
2	1.0450	0	3	88	0	-0.8
3	1.0000	0	41	21	40	-1
4	1.0000	0	0	0	0	0
5	1.0100	0	13	4	0	0
6	1.0000	0	75	2	0	0.8
7	1.0000	0	0	0	0	0
8	1.0100	0	150	22	450	62.1
9	1.0000	0	121	26	0	0
10	1.0000	0	5	0	0	0
11	1.0820	0	0	0	0	2.2
12	1.0000	0	377	24	310	128.5
13	1.0710	0	18	2.3	0	0
14	1.0000	0	10.5	5.3	0	0
15	1.0000	0	22	5	0	0
16	1.0000	0	43	3	0	0
17	1.0000	0	42	8	0	0
18	1.0000	0	27.2	9.8	0	0
19	1.0000	0	3.3	0.6	0	0
20	1.0000	0	2.3	1	0	0
21	1.0000	0	0	0	0	0
22	1.0000	0	0	0	0	0
23	1.0000	0	6.3	2.1	0	0
24	1.0000	0	0	0	0	0
25	1.0000	0	6.3	3.2	0	0
26	1.0000	0	0	0	0	0
27	1.0000	0	9.3	0.5	0	0
28	1.0000	0	4.6	2.3	0	0
29	1.0000	0	17	2.6	0	0
30	1.0000	0	3.6	1.8	0	0
31	1.0710	0	5.8	2.9	0	0
32	1.0000	0	1.6	0.8	0	0
33	1.0000	0	3.8	1.9	0	0
34	1.0000	0	0	0	0	0
35	1.0000	0	6	3	0	0
36	1.0000	0	0	0	0	0
37	1.0000	0	0	0	0	0
38	1.0000	0	14	7	0	0
39	1.0000	0	0	0	0	0
40	1.0000	0	0	0	0	0

41	1.0000	0	6.3	3	0	0
42	1.0000	0	7.1	4.4	0	0
43	1.0000	0	2	1	0	0
44	1.0000	0	12	1.8	0	0
45	1.0000	0	0	0	0	0
46	1.0000	0	0	0	0	0
47	1.0000	0	29.7	11.6	0	0
48	1.0000	0	0	0	0	0
49	1.0710	0	18	8.5	0	0
50	1.0000	0	21	10.5	0	0
51	1.0000	0	18	5.3	0	0
52	1.0000	0	4.9	2.2	0	0
53	1.0000	0	20	10	0	0
54	1.0000	0	4.1	1.4	0	0
55	1.0000	0	6.8	3.4	0	0
56	1.0000	0	7.6	2.2	0	0
57	1.0000	0	6.7	2	0	0

Appendix D- Algerian 114-bus power system data

The bus data of the Algerian 114-bus power system are represented in Table D.1.

Table D.1 Bus data of the Algerian 114-bus power system

Bus N°	Bus voltage		load		Generation	
	Magnitude (p.u)	Phase angle (°)	Real power (MW)	Reactive power (MVar)	Real power (MW)	Reactive power (MVar)
1	1	0	0	0	0	0
2	1	0	36	17	0	0
3	1	0	64	31	0	0
4	1.0773	0	125	94	750	400
5	1	0	335	250	300	160
6	1	0	78	37	0	0
7	1	0	55	26	0	0
8	1	0	50	24	0	0
9	1	0	40	19	0	0
10	1	0	42	21	0	0
11	1	0	96	47	160	30
12	1	0	31	15	0	0
13	1	0	13	6	0	0
14	1	0	136	65	0	0
15	1	0	0	0	60	30
16	1	0	0	0	0	0
17	1.0682	0	0	0	640	400
18	1	0	0	0	0	0
19	1	0	11	5	100	60
20	1	0	14	9	0	0
21	1	0	70	52	0	0
22	1	0	42	25	60	40
23	1	0	23	11	0	0
24	1	0	60	36	0	0
25	1	0	17	8	0	0
26	1	0	55	26	0	0
27	1	0	0	0	0	0
28	1	0	0	0	0	0
29	1	0	37	18	0	0
30	1	0	30	15	0	0
31	1	0	0	0	0	0
32	1	0	40	24	0	0
33	1	0	29	14	0	0
34	1	0	29	14	0	0
35	1	0	33	16	0	0
36	1	0	17	8	0	0
37	1	0	11	5	0	0
38	1	0	20	10	0	0
39	1	0	20	10	0	0

40	1	0	21	10	0	0
41	1	0	53	32	0	0
42	1	0	0	0	0	0
43	1	0	31	18	0	0
44	1	0	0	0	0	0
45	1	0	12	6	0	0
46	1	0	0	0	0	0
47	1	0	21	10	0	0
48	1	0	0	0	0	0
49	1	0	13	6	0	0
50	1	0	4	2	0	0
51	1	0	1	1	0	0
52	1	0	56	27	80	50
53	1	0	16	8	0	0
54	1	0	21	10	0	0
55	1	0	18	9	0	0
56	1	0	33	20	0	0
57	1	0	35	21	0	0
58	1	0	0	0	0	0
59	1	0	36	17	0	0
60	1	0	0	0	0	0
61	1	0	27	13	0	0
62	1	0	22	11	0	0
63	1	0	49	29	0	0
64	1	0	0	0	0	0
65	1	0	11	5	0	0
66	1	0	35	21	0	0
67	1	0	10	5	0	0
68	1	0	11	5	0	0
69	1	0	20	10	0	0
70	1	0	7	3	0	0
71	1	0	36	22	0	0
72	1	0	0	0	0	0
73	1	0	36	22	0	0
74	1	0	0	0	0	0
75	1	0	0	0	0	0
76	1	0	12	6	0	0
77	1	0	7	3	0	0
78	1	0	13	7	0	0
79	1	0	14	7	0	0
80	1	0	157	107	100	56
81	1	0	0	0	0	0
82	1	0	75	36	0	0
83	1	0	70	51	230	120
84	1	0	46	34	0	0
85	1	0	45	22	0	0
86	1	0	0	0	0	0
87	1	0	32	15	0	0
88	1	0	46	22	0	0
89	1	0	34	17	0	0

90	1	0	18	9	0	0
91	1	0	44	21	0	0
92	1	0	10	5	0	0
93	1	0	0	0	0	0
94	1	0	48	23	0	0
95	1	0	35	17	0	0
96	1	0	0	0	0	0
97	1	0	42	20	0	0
98	1	0	13	6	100	30
99	1	0	105	50	0	0
100	1.0773	0	33	16	550	50
101	1.0818	0	50	24	360	50
102	1	0	34	16	0	0
103	1	0	66	32	0	0
104	1	0	18	9	0	0
105	1	0	0	0	0	0
106	1	0	64	31	0	0
107	1	0	65	37	0	0
108	1	0	22	11	0	0
109	1.0818	0	37	18	180	85
110	1	0	13	6	0	0
111	1.0909	0	94	56	200	85
112	1	0	24	12	0	0
113	1	0	23	11	0	0
114	1	0	24	12	0	0

ملـخص:

مع زيادة استهلاك الطاقة وأسعار الوقود في السنوات الأخيرة، دعمت العديد من الحكومات مشاريع تطبيقات الطاقة المتجددة في بلدانها. تخلق الطبيعة العشوائية لهذه الموارد تحديات جديدة لمشغلي الشبكة. وبالتالي، من الضروري مواجهة هذه التحديات من خلال التحليل الأمثل لتخطيط وتشغيل أنظمة الطاقة الحديثة من أجل التكامل الاقتصادي لهذا النوع من الطاقة. في هذه الأطروحة، يركز العمل المنجز بشكل أساسي على حل مشكلة تدفق الطاقة الأمثل (OPF) مع الأخذ في الاعتبار طاقة الرياح العشوائية، نظام نقل التيار المتردد المرن (FACTS) وكذلك تقنية النقل بالتيار المباشرعالي الجهد (HVDC). من بين النقاط المهمة التي تناولتها هذه الأطروحة دمج مزارع الرياح الكبيرة الموجودة عن بعد بواسطة نظام DC متعدد المحطات (VSC-MTDC). في هذا العمل، تم اعتماد تقنيتين متقدمتين للذكاء الاصطناعي، أي خوارزمية قوالب الوحل (SMA) و خوارزمية أسد النمل (ALO) لحل مشكلة تدفق الطاقة الأمثل. في حالة عدم وجود طاقة الرياح، تم استخدام العديد من الدراسات لتوضيح فعالية الخوارزميات المقترحة. أثبتت النتائج المتحصل عليها أن الخوارزميات المقترحة تفوقت بشكل كبير على التقنيات الأخرى الموجودة في الأدبيات. في مشكلة تدفق الطاقة الأمثل مع مراعاة طاقة الرياح العشوائية مع او بدون دمج نظام VSC-FACTS-HVDC، تتمثل الوظيفة الموضوعية في تقليل تكلفة التوليد الإجمالية وفقًا للجدولة المثلى لوحدات الحرارة والرياح. تم فحص الخوارزميات المقترحة على النظام القياسي 30عقدة ونظام الطاقة الجزائري 114عقدة. أظهرت النتائج التي تم الحصول عليها بواسطة الخوارزميات المقترحة SMA و ALO أن دمج مزارع الرياح قد ساهم بشكل كبير في تحسين نظام الطاقة مقارنة بالنتائج التي تم الحصول عليها بدون دمج طاقة الرياح.

كلمـات مفتاحيـــة: الطاقة المتجددة، التدفق الأمثل للطاقة، طاقة الرياح العشوائية، أنظمة مرنة للنقل بالتيار المتناوب، تقنية النقل بالتيار المباشر عالي الجهد، VSC-MTDC ، الذكاء الاصطناعي، SMA، ALO.

Résumé

Avec l'augmentation de la consommation d'énergie et des prix des carburants ces dernières années, de nombreux gouvernements ont soutenu des projets d'application d'énergies renouvelables dans leurs pays. La nature stochastique de ces ressources crée de nouveaux défis pour les gestionnaires de réseau. Par conséquent, il est nécessaire de relever ces défis grâce à une analyse optimale de la planification et de l'exploitation des systèmes électriques modernes pour l'intégration économique de ce type d'énergie. Dans cette thèse, le travail effectué se concentre principalement sur la résolution du problème de l'écoulement de puissance optimal (OPF) en tenant compte de l'énergie éolienne stochastique, des dispositifs de système de transmission CA flexible (FACTS) ainsi que la technologie à courant continu haute tension (HVDC). Parmi les points importants abordés par cette thèse, il y a l'incorporation de grands parcs éoliens éloignés par un système multi-terminal DC (VSC-MTDC). Dans ce travail, deux techniques avancées d'intelligence artificielle, à savoir, l'algorithme de moule visqueux (SMA) et l'algorithme optimisation de fourmis (ALO) ont été adoptés pour résoudre le problème OPF. Dans le cas sans énergie éolienne, des études numériques sont utilisées pour illustrer l'efficacité des algorithmes proposés. Les résultats obtenus ont prouvé que les algorithmes proposés surpassaient considérablement par rapport à les autres méthodes existantes dans la littérature. Dans le problème de l'OPF considérant l'énergie éolienne stochastique avec et sans VSC-FACTS-HVDC, la fonction objectif est de minimiser le coût total de production en fonction de la planification optimale des unités thermiques et éoliennes. Les algorithmes proposés ont été examinés sur le réseau IEEE 30 jeux de barres et le réseau Algérien 114 jeux de barres. Les résultats obtenus par les algorithmes proposés SMA et ALO ont montré que l'intégration du parc éolien a considérablement amélioré le système électrique par rapport aux résultats obtenus sans énergie éolienne.

Mots Clés : Energies renouvelables, écoulement de puissance optimal, énergie éolienne stochastique, dispositifs FACTS, technologie HVDC, VSC-MTDC, intelligence artificielle, SMA, ALO.

Abstract

With the increase in energy consumption and fuel prices in recent years, many governments have supported renewable energy application projects in their countries. The stochastic nature of these resources creates new challenges for grid operators. Hence, it is necessary to meet these challenges through optimal analysis of the planning and operation of modern power systems for the economic integration of this type of energy. In this thesis, the work done focuses mainly on solving the optimal power flow (OPF) problem considering stochastic wind power, flexible AC transmission system (FACTS) and high voltage direct current (HVDC) technology. Among the important points addressed by this thesis is the incorporation of remotely located large wind farms by a multi-terminal DC (VSC-MTDC) system. In this work, two advanced artificial intelligence (AI) techniques i.e., slime mould algorithm (SMA) and ant lion optimization (ALO) have been adopted to solve the OPF problem. In the case without wind power, numerical cases have been studied to illustrate the effectiveness of the proposed algorithms. The obtained results proved that the proposed algorithms significantly outperformed other existing techniques in the literature. In the problem of OPF considering stochastic wind power with and without incorporating the VSC-FACTS-HVDC system, the objective function is to minimize the total generation cost according to the optimal scheduling of thermal and wind units. The proposed algorithms were examined on the IEEE-30 bus and Algerian with 114-bus systems. The results obtained showed that the integration of wind farms has significantly improved the power system compared to the results obtained without wind power.

Key Words: Renewable energy, optimal power flow, stochastic wind power, FACTS devices, HVDC technology, VSC-MTDC, artificial intelligence, SMA, ALO.